Dissertation

submitted to the

Combined Faculties for the Natural Sciences and for Mathematics

of the Ruperto-Carola University of Heidelberg, Germany

for the degree of

Doctor of Natural Sciences

presented by

M.Sc. Tobias Speck

born in: Pforzheim, Germany

Oral examination: 27.02.2018

BiTE-armed oncolytic measles viruses for cancer immunovirotherapy

Referees: Prof. Dr. Ralf Bartenschlager

Prof. Dr. Christof von Kalle

Abstract

Attenuated measles virus (MV) vaccine strains preferentially infect, replicate in and thus destruct cancerous cells. In recent years, it has become evident that therapeutic success of oncolytic virotherapy largely depends on the modulation of the immune system. MV-mediated oncolysis induces an immunogenic cell death (ICD), which provides the basis to enhance or reinitiate a sustained antitumor immune response. In clinical testing, salvage therapy with oncolytic MV has led to complete tumor resolutions, demonstrating its therapeutic potential. However, extensive therapeutic efficacy is limited to a minority of patients. Thus, efforts are put into preclinical research to generate more potent MV vectors.

Many strategies in cancer immunotherapy aim to augment T cell responses against tumor cells. Bispecific T cell engagers (BiTEs) simultaneously engage T cells and tumor cells. BiTE-mediated T cell engagement activates the engaged T cell and specifically directs its cytotoxic potential towards the crosslinked tumor cell. BiTE therapy has achieved compelling clinical success in the treatment of B cell malignancies. However, BiTEs have failed to demonstrate efficacy against solid tumors so far. Moreover, short terminal half-life of BiTEs requires continuous intravenous infusion and systemic administration of BiTEs can cause severe or even fatal side effects.

We hypothesize that tumor-targeted expression of BiTEs by oncolytic MV enhances therapeutic efficacy, as compared to either monotherapy alone. Furthermore, we hypothesize that tumor-restricted BiTE-expression reduces systemic exposure to BiTEs and thus increases safety of BiTE therapy. To test these hypotheses, MVs encoding BiTEs were generated (MV-BiTE). MV-BiTE vectors were characterized *in vitro* in terms of replication kinetics, oncolytic activity and BiTE expression. BiTEs produced by MV-BiTE-infected cells were purified to evaluate binding specificity and BiTE-mediated T cell cytotoxicity *in vitro*. Therapeutic efficacy of MV-BiTE in terms of survival was demonstrated using syngeneic and xenogeneic tumor models. For all studies, no signs of MV-BiTE-related toxicities were observed and BiTE plasma levels of MV-BiTE-treated mice remained below detection limit.

Conclusively, tumor-targeted expression of BiTEs by oncolytic MV is feasible and prevented systemic exposure to BiTEs. Moreover, MV-BiTE treatment demonstrated therapeutic efficacy in different models of solid tumors *in vivo*. The MV-BiTE constructs constitute a modular vector platform that can be adapted to target any tumor antigen of choice. Thus, MV-BiTE therapy represents a promising approach for individualized cancer immunovirotherapy.

Zusammenfassung

Abgeschwächte Viren des Masernvirus-Impfstammes infizieren und replizieren präferentiell in Krebszellen, was zur Zerstörung der infizierten Krebszelle führt. In den vergangenen Jahren wurde bewiesen, dass der Erfolg der onkolytischen Virustherapie zu einem Großteil von der Modulation des Immunsystems abhängt. Masernvirus-vermittelte Onkolyse induziert einen immunogenen Zelltod, welcher die Grundlage für die Verstärkung oder Reinitialisierung einer anhaltenden Anti-Tumor-Immunantwort bereitet. In klinischen Studien mit onkolytischen Masernviren konnten Tumore in austherapierten Krebspatienten vollständig zurückentwickelt werden, was das therapeutische Potential von Masernviren eindrucksvoll demonstriert. Jedoch werden solch umfangreiche therapeutische Effekte nur bei wenigen Patienten erzielt. Aus diesem Grund sind Wissenschaftler in der präklinischen Forschung darum bemüht potentere Masernviren zu entwickeln.

Viele Strategien in der Krebsimmuntherapie versuchen gezielt die T-Zell-Antworten gegen Krebszellen zu verstärken. BiTE-Antikörper (bispecific T cell engager) sind bispezifische Antikörper, die T-Zellen und Krebszellen miteinander verbinden können. Die BiTE-vermittelte T-Zell-Bindung aktiviert die T-Zelle und richtet ihr zytotoxisches Potential spezifisch gegen die verbundene Krebszelle. Die BiTE-Therapie hat überzeugende klinische Erfolge in der Behandlung von bösartigen B-Zell-Erkrankungen erzielt. Jedoch haben BiTE-Therapien bisher keine Wirksamkeit gegen solide Krebserkrankungen gezeigt. Darüber hinaus erfordert die kurze Halbwertszeit von BiTE-Antikörpern eine kontinuierliche intravenöse Infusion und die systemische Gabe von BiTE-Antikörpern kann ernsthafte oder sogar tödliche Nebenwirkungen verursachen.

Wir stellen die Hypothese auf, dass die Expression von BiTE-Antikörpern in Krebszellen durch das onkolytische Masernvirus die therapeutische Wirksamkeit im Vergleich zu den jeweiligen Einzeltherapien verbessert. Des Weiteren nehmen wir an, dass die lokale Expression von BiTE-Antikörpern die systemische Belastung verringert und dadurch die Sicherheit der BiTE-Therapie verbessert. Um diese Hypothesen zu überprüfen wurden Masernviren hergestellt, die BiTE-Antikörper kodieren (MV-BiTE). Die MV-BiTE-Vektoren wurden *in vitro* bezüglich ihrer Replikationskinetiken, ihrer onkolytischen Aktivität und der BiTE-Antikörper-Expression charakterisiert. BiTE-Antikörper, hergestellt von MV-BiTE-infizierten Zellen, wurden aufgereinigt, um ihre Bindungsspezifität und die BiTE-vermittelte T-Zell-Zytotoxizität *in vitro* zu untersuchen. Die therapeutische Wirksamkeit von MV-BiTE in Bezug auf die Überlebensdauer von Mäusen wurde in syngenen und xenogenen Tumormodellen demonstriert.

In allen Studien wurden keine Anzeichen einer MV-BiTE-verursachten Toxizität beobachtet und die BiTE-Plasma-Level von MV-BiTE-behandelten Mäusen blieben unterhalb der Nachweisgrenze.

Zusammenfassend kann gesagt werden, dass die Expression von BiTE-Antikörpern in Krebszellen durch onkolytische Masernviren realisierbar ist und eine systemische Belastung mit BiTE-Antikörpern verringert. Darüber hinaus demonstrierte MV-BiTE therapeutische Wirksamkeit in verschiedenen Modellen solider Tumore *in vivo*. Die MV-BiTE-Konstrukte stellen eine modulare Vektor-Plattform dar, die wahlweise an jedes beliebige Tumorantigen angepasst werden kann. Dadurch verkörpert die MV-BiTE-Therapie einen vielversprechenden Ansatz in der individualisierten Krebs-Immunvirustherapie.

Table of Contents

Abbreviations

AA	Amino acid
ABAM	Antibiotic-antimycotic
ADC	Antibody-drug conjugate
ADCC	Antibody-dependent cell-mediated cytotoxicity
AE	Adverse event
ALL	Acute lymphoblastic leukemia
APC	Allophycocyanin
APC	Antigen-presenting cell
APC-Cy7	Allophycocyanin-cyanine dye 7
ATP	Adenosine triphosphate
ATU	Additional transcription unit
BC	Before Christ
BCA	Bicinchoninic acid
BiTE	Bispecific T cell engager
CAR	Chimeric-antigen receptor
CD	Cluster of differentiation
CDR	Complementarity-determining region
CEA	Carcinoembryonic antigen

ciu	Cell infectious unit
CTL	Cytotoxic T lymphocyte
CTLA-4	Cytotoxic T-lymphocyte-associated protein-4
DAMP	Damage-associated molecular pattern
DAPI	4',6-diamidino-2-phenylindole
DART	Dual-affinity re-targeting antibody
DC	Dendritic cell
DNA	Deoxyribonucleic acid
DRR	Durable response rate
EDTA	Ethylenediaminetetraacetic acid
eGFP	Enhanced green fluorescent protein
EGFR	Epidermal growth factor receptor
ELISA	Enzyme-linked immunosorbent assay
EpCAM	Epithelial cell adhesion molecule
EphA2	Ephrin type-A receptor 2
FDA	Food and Drug Administration
FITC	Fluorescein isothiocyanate
G	Gauge
GM-CSF	Granulocyte macrophage colony-stimulating factor
h	Hour
HA	Human influenza hemagglutinin

HEPES	2-[4-(2-hydroxyethyl)piperazin-1-yl]ethanesulfonic acid
His_6	Hexa histidine
HMGB1	High-mobility group box 1
HRP	Horseradish peroxidase
HSP	Heat-shock protein
HSV	Herpes simplex virus
ICD	Immunogenic cell death
ICI	Immune checkpoint inhibitor
IDO	Indoleamine 2,3-dioxygenase
IFN	Interferon
IgG	Immunoglobulin G
IL	Interleukin
i.t.	Intratumoral
i.v.	Intravenous
ld	Leader
LDH	Lactate dehydrogenase
mAb	Monoclonal antibody
MAGE-A3	Melanoma-associated antigen 3
MDSC	Myeloid-derived suppressor cell
MHC	Major histocompatibility complex
ml	Milliliter

mm	Millimeter
MOI	Multiplicity of infection
Moraten	More attenuated
mRNA	Messenger ribonucleic acid
MV	Measles virus
Nectin-4	Nectin cell adhesion molecule 4
NHL	Non-Hodgkin lymphoma
NK cell	Natural killer cell
NLR	Nucleotide-binding oligomerization domain-like receptor
NOD	Nucleotide-binding oligomerization domain
NSe	*Nar*I and *Spe*I elimination
oAd	Oncolytic adenovirus
ORF	Open reading frame
OS	Overall survival
OV	Oncolytic virus
PAMP	Pathogen-associated molecular pattern
PBL	Peripheral blood lymphocyte
PBMC	Peripheral blood mononuclear cell
PD-1	Programmed cell death-1
pDC	Plasmacytoid dendritic cell
PE	Phycoerythrin

PE-Cy7	Phycoerythrin-cyanine dye 7
PerCP-Cy5.5	Peridinin chlorophyll protein-cyanine dye 5.5
PRR	Pattern-recognition receptor
PSA	Prostate-specific antigen
PVDF	Polyvinylidene fluoride
RIG-1	Retinoic acid-inducible gene-1
RLR	Retinoic acid-inducible gene-1-like receptor
RNA	Ribonucleic acid
RNP	Ribonucleoprotein complex
RPV	Rinderpest virus
R/R	Relapsed or refractory
RT-PCR	Reverse transcription polymerase chain reaction
scFv	Single chain variable fragment
SDS-PAGE	Sodium dodecyl sulfate polyacrylamide gel electrophoresis
SLAMF1	Signaling lymphocytic activation molecule 1
SOC	Standard of care
TAA	Tumor-associated antigen
TandAb	Tandem diabody
TCR	T cell receptor
TGF-β	Transforming growth factor beta
TIL	Tumor-infiltrating lymphocyte

TLR	Toll-like receptor
TME	Tumor microenvironment
TNF	Tumor necrosis factor
TSA	Tumor-specific antigen
TSC	Tumor spheroid culture
T-VEC	Talimogene laherparepvec
VEGF	Vascular growth factor
vpBiTE	Virus-derived, purified bispecific T cell engager
VSV	Vesicular stomatitis virus
VV	Vaccinia virus
WHO	World Health Organization
XTT	2,3-Bis-(2-methoxy-4-nitro-5-sulfophenyl)-2H-tetrazolium-5-carboxyanilide

1. Introduction

1.1. Motivation

In 1971, President Richard Nixon signed the National Cancer Act and thereby declared “war on cancer”, which in those times represented a major cause of death worldwide. Back then, discovering the cure of cancer did not seem less utopian than President Kennedy’s pronouncement in 1961 to land a manned mission on the Moon. While first men set foot on the lunar surface in 1969, cancer still remains a leading cause of death with 8.7 million cancer-related deaths half a century later (*1*). Statistically, one in three men and one in four women will develop cancer during a lifetime (*1*). Still, the field of cancer research impressively developed in the past decades and we are by now able to precociously detect and better control some tumor diseases. But chances for cure appear to have no prospect of success in an advanced stage of disease or if standard therapy fails.

1.2. The Immune System and Cancer - a double-edged Sword

The immune system has the exceptional ability to recognize and clear neoplastic cells which eventually could give rise to cancer, a phenomenon known as “cancer immunosurveillance” (*2*). In doing so, cells of the immune system prevail with a remarkable specificity and efficiency, which outclasses all anticancer drugs known hitherto. Still, tumorigenesis takes place under the surveillance of a fully functional immune system. Perpetual immunological elimination of incipient cancer cells may facilitate the emergence of tumor cell variants, which acquired the ability to evade or even to counteract the immune system. This process corresponds to the broader concept of “cancer immunoediting” which elucidates the ambiguous role of the immune system in cancer prevention and progression (*3*). Cellular and molecular mechanisms of immune evasion are well described and immunoevasion was proposed to constitute an emerging hallmark of cancer (*4, 5*). The initiation of a sustained antitumor immune response is an iterative process described as the “cancer immunity cycle” (*6*). The patient’s individual cancer immune status may be impaired in one or more steps of this cycle of anticancer immunity. Specific manipulations of the immune system to enhance or reinitiate anticancer immunity is the main objective of cancer immunotherapy (*7, 8*).

1.3. Cancer Immunotherapy

1.3.1. A Historical Perspective

Ancient writings on papyrus report on Imhotep's – a deified Egyptian chancellor to the pharaoh, architect and physician (approximately 2,600 BC) – recommendation to treat swellings (tumors) with a poultice followed by incision of the tumor. This procedure causes an infection at the tumor site which may result in tumor regression (*9*). Various rudimentary approaches to stimulate the immune system in cancer therapy have been described over thousands of years. In the nineteenth century, Dr. William B. Coley, a 28-year-old surgeon in the first year of practice, was deeply affected by the death of his first sarcoma patient (*10*). Coley became interested in treatment of sarcomas and digged into historical medical literature. He found many physicians to report on spontaneous tumor regressions after coincidental bacterial infections (*11*). Inspired by the medical literature, Coley experimentally developed "Coley's toxin", a mixture of heat-killed *Streptococcus pyogenes* and *Serratia marcescens*. His first sarcoma patient treated with Coley's toxin went into a life-long complete remission and Coley became the "father of cancer immunotherapy" (*12*).

However, Coley's toxin and cancer immunotherapy in general were controversially discussed in medical science, due to low response rates and a lack of understanding the underlying mechanisms. Then, in the 1990s and 2000s some observations aroused attention to the field of cancer immunotherapy. Immunodeficient mice were more susceptible to carcinogen-induced tumors than wild-type mice (*13*). Furthermore, tumors were induced in immunodeficient mice and transplanted into naïve syngeneic immunocompetent mice. A significant number of mice (40 %) rejected tumor transplants derived from immunodeficient mice. In contrast, when tumors were induced in immunocompetent mice and transplanted into wild-type mice, no tumor rejection was observed (*14*). These findings directly proved the importance of immunity in cancer and revived the field of cancer immunotherapy.

1.3.2. The Principles of Cancer Immunotherapy

Cancer immunotherapy comprises various approaches in cancer treatment, which modify components of the immune system to enhance or reinitiate a sustained antitumor immune response. The initiation of an antitumor immune response is described by Chen and Mellman

as an iterative process which is effected in seven steps (*6*): Antigens from dying tumor cells are released (step 1). Tumor-specific and -associated antigens (TSAs/TAAs), e.g. derived from mutated genes, oncogenic viruses, oncofetal proteins or posttranslationally altered proteins (*15*), are ingested by immature migratory dendritic cells (DCs). Immunogenic cell death and proinflammatory cytokines mature DCs into activated immunogenic DCs which present tumor antigens on major histocompatibility complex (MHC) class I and II to T cells in lymphoid organs (step 2) (*16, 17*). Antigen-specific T cells are primed and activated by DCs and become cytotoxic T lymphocytes (CTLs) (step 3). Next, CTLs leave the lymphoid organs and traffic to the tumor site via the blood stream (step 4). At the tumor site, CTLs leave the blood stream and infiltrate the tumor, further referred to as tumor-infiltrating lymphocytes (TILs) (step 5). TILs recognize the specific tumor antigens on the tumor cells (step 6) and eliminate tumor cells (step 7). Elimination of tumor cells results in the release of more tumor antigens (step 1). The cancer immunity cycle continues which broadens and boosts the antitumor immune response (*6*).

However, single or multiple steps in the cycle of anticancer immunity are impaired in cancer patients, which hampers the immune system to establish or maintain a sustained antitumor immune response. Tumor cells might become unrecognizable for T cell-mediated elimination by impaired antigen processing or antigen presentation on MHC class I molecules (*18*). Immune checkpoint molecules e.g. cytotoxic T-lymphocyte-associated protein-4 (CTLA-4, cluster of differentiation (CD)152) and programmed cell death-1 (PD-1, CD279) inhibit T cell signaling. Tumor cells might express ligands for such immune checkpoint molecules to suppress immune function. A variety of immune inhibitory cytokines, e.g. transforming growth factor-β (TGF-β), vascular endothelial growth factor (VEGF) or indoleamine 2,3-dioxygenase (IDO) can be expressed by tumor cells or tumor-associated stromal cells (*19*). Also immunosuppressive leukocytes, such as regulatory T cells, myeloid-derived suppressor cells (MDSCs), plasmacytoid DCs (pDCs) and M2 macrophages produce inhibitory cytokines and support tumor development (*19*). Different immunotherapies have been developed to specifically target immune escape mechanisms, which might resolve immune blockade and lead to tumor remission. However, only few cancer patients seem to benefit from these therapies (*20*). The individual and heterogenic immunological landscape of tumors often requires additional immune regulating interventions. It remains a substantial challenge to understand the entirety of immune regulation and to identify biomarkers to select for cancer patients who will benefit from (most likely combined) cancer immunotherapies (*7*).

1.3.3. Classes of Cancer Immunotherapy

Modern cancer immunotherapies can generally be classified into “active” and “passive” approaches. On the one hand, active immunotherapies directly target the patient’s immune system to enhance or reinitiate a potent antitumor immune response. Examples for active immunotherapies are: (I) Cytokines: Interleukin (IL)-2, Interferon (IFN)-α2a and IFN-α2b non-specifically stimulate the patient’s immune system and are approved since the 1990s for treatment of multiple solid and hematological malignancies (*21*). (II) DC-based vaccines: Autologous DCs are loaded *ex vivo* with patient-specific TAAs and are reinfused into the patient to prime TAA-specific immune responses (*22*). Sipuleucel-T, the only licensed DC-based therapy, has been approved by the Food and Drug Administration (FDA) for treatment of metastatic, castration-resistant prostate cancer in 2010 (*23*). (III) Immune checkpoint inhibitors: Monoclonal antibodies (mAbs) target immunosuppressive receptors on T cells or the cognate ligands on antigen-presenting cells (APCs), tumor and stromal cells. Ipilimumab (anti-CTLA-4 mAb) was the first checkpoint inhibitor to be approved by the FDA for treatment of patients with unresectable or metastatic melanoma in 2011 (*24*).

On the other hand, passive immune therapeutics directly target tumor cells. Examples for passive immunotherapies are: (I) Tumor-targeting mAbs: Therapeutic mAbs are commonly applied as anticancer drugs and employ a variety of mechanisms to mediate cytotoxicity (*25*). mAbs can block signaling pathways which are important for tumor growth or survival. Other mAbs opsonize malignant cells to induce antibody-dependent cell-mediated cytotoxicity (ADCC). Antibody-drug conjugates (ADCs) deliver toxins or radionuclides to tumor cells. Rituximab, a CD20-targeting, opsonizing antibody, was the first-in-class tumor-targeting mAb to be approved by the FDA in 1997 for the treatment of patients with non-Hodgkin lymphoma (NHL) (*26*). (II) Oncolytic viruses (OVs): OVs derive from non-pathogenic virus strains, which preferentially infect and replicate in malignant cells. The direct cytopathic activity is mediated by excessive viral replication. OVs can be engineered to encode additional transgenes, such as therapeutic antibodies or immunostimulatory cytokines to enhance antitumor efficacy (*27*). The first-in-class oncolytic drug to be approved by the FDA in 2015 is talimogene laherparepvec (T-VEC) for the treatment of patients with recurrent, unresectable melanoma (*28*). (III) Adoptive T cell transfer: Autologous TILs or peripheral blood lymphocytes (PBLs) are selected based on their tumor-reactive capacities or modified to express genetically engineered T cell

receptors (TCRs) or chimeric-antigen receptors (CARs). T cells are expanded *ex vivo* and reinfused into the cancer patient (*29*). Recently, the first CAR T cell therapy (tisagenlecleucel) has been approved by the FDA for treatment of children and young adults with acute lymphoblastic leukemia (ALL) (*30*).

1.3.4. The Class of Bispecific T Cell Engagers (BiTEs)

BiTE antibodies are fusion proteins of two, flexibly linked single chain variable fragments (scFvs) (Figure 1.1). BiTEs simultaneously bind CD3ε, a component of the T cell co-receptor CD3, and any TAA expressed on the tumor cell surface. The short, five amino acids (AAs) linker connecting the two scFvs forces T cells into close proximity to tumor cells which in combination with T cell engagement via CD3 is sufficient to activate T cells (*31*). Activated T cells form cytolytic synapses which are identical to synapses formed upon regular T cell activation (*32*). $CD8^+$ cytotoxic T cells and $CD4^+$ helper and even regulatory T cells can be engaged which induces the expression of activation markers CD69 and CD25 and cytokines such as IL-2, IFN-γ, tumor necrosis factor (TNF), granzyme B and perforin (*33-38*). Thereby, BiTE antibodies can induce T cell proliferation and potent, serial tumor cell lysis at subpicomolar concentrations or low effector to target cell ratios (*36, 37, 39*). OKT3, an anti-CD3 mAb, is known to non-specifically activate T cells by TCR complex-clustering (*40*). However, monovalent CD3-binding by BiTEs is unable to induce T cell activation in the absence of tumor cells (*37*). BiTE-mediated T cell cytotoxicity is independent of proper antigen presentation by tumor cells, T cell co-stimulation and TCR specificity (*32, 36, 41*). Thus, BiTEs can engage polyclonal T cells to effectively eliminate tumor cells, which may have evolved immune escape mechanisms (*42*).

Blinatumomab, a CD19-targeting BiTE, is the first BiTE antibody which has been approved by the FDA for treatment of patients with relapsed or refractory (R/R) B cell precursor ALL (*43*). There is a high medical need for treatment options in R/R ALL patients (*44*). Blinatumomab was administered in short intravenous infusions in the initial phase I trials (*45*). Short terminal half-life of approximately 2 h were observed and peak serum levels caused severe toxicity which led to early termination of the trials. Step dosing and continuous intravenous infusion of blinatumomab reduced toxicities and stabilized blinatumomab plasma levels (*46*). A phase II clinical trial compared blinatumomab (n = 271) with standard of care (SOC) (n = 134).

Complete remission rates and median survival for blinatumomab were superior to SOC (46 *versus* 28 % and 7.8 *versus* 4.0 months, respectively) (*47*). Common grade 3 or higher adverse events (AEs) were infections, pyrexia and hematological toxicities (*48-51*). However, serious and even fatal AEs occurred which led to treatment discontinuation in 18 % of the patients, including neurotoxicity (*43*).

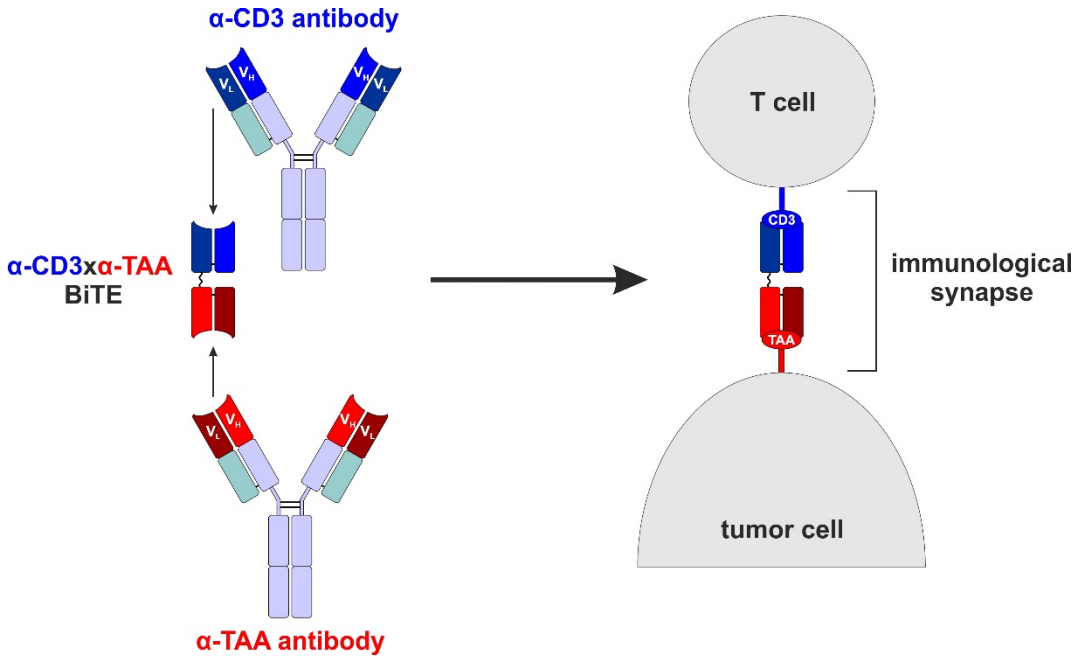

Figure 1.1: Representation of the bispecific T cell engager (BiTE) principle. (Left part) BiTEs consist of two single chain variable fragments (scFvs): One scFv is always directed against the T cell co-receptor CD3 (blue). The second scFv targets a tumor-associated antigen (TAA) expressed on the tumor cell surface (red). (Right part) Simultaneous binding of CD3 on the T cell and a TAA on the tumor cell activates the T cell and induces the formation of an immunological synapse, which results in tumor cell lysis. Adapted from (*52*).

Various BiTE antibodies for hematological and solid tumors are in preclinical and clinical development. Clinically most advanced BiTEs are AMG 110/MT 110 (anti-EpCAM, NCT00635596), AMG 211/MEDI-565 (anti-CEA, NCT02291614), AMG 212 (anti-PSMA, NCT01723475), BI 836909/AMG 420 (anti-BCMA, NCT02514239), and AMG 330 (anti-CD33, NCT02520427). All BiTE constructs demonstrate potent antitumor activity *in vitro*.

However, meaningful therapeutic effects with BiTEs targeting solid tumors have not been reported so far (*53-56*).

Several other T cell and also natural killer (NK) cell engaging antibody formats are currently under clinical investigation as anticancer drugs (*57, 58*). Examples: (I) Dual-affinity re-targeting (DART) antibodies are diabodies stabilized with an inter-chain disulfide bond (e.g. NCT02152956, NCT02248805) (*59*). (II) TrioMabs are immunoglobulin (Ig)G-like bispecific, trifunctional antibodies with a chimeric non-human Fc-region that additionally interacts with Fcγ receptor^{+} accessory cells (e.g. NCT00189345, NCT01569412, NCT01138579) (*60*). (III) Tetravalent, bispecific tandem diabodies (TandAb) were designed to target the NK cell activating receptor CD16 and simultaneously the lymphoma antigen CD30 (NCT02321592, NCT03192202) (*61*).

1.4. Oncolytic Viruses as Cancer Immunotherapeutics

Oncolytic viruses (OVs) are classified as passive immunotherapeutics based on their intrinsic antitumor activity (chapter 1.3.3.). On the contrary, OVs can induce potent and lasting tumor-directed immune responses which in some cases constitute the most detrimental antitumor effects (*62*). Hence, OVs can act as both, passive and active cancer immunotherapeutics.

According to Chen's and Mellman's concept of the cancer immunity cycle, the release of TAAs is the basis to induce an antitumor immune response (chapter 1.3.2.). Oncolytic cell death releases tumor antigens, which can be ingested by resident and infiltrating DCs. In addition, most viruses induce an immunogenic cell death (ICD) (*63*). The virus-induced ICD provides danger signals which recruit more DCs and mature them into potent antigen presenting cells (*64*). Danger signals are viral pathogen-associated molecular patterns (PAMPs; e.g. nucleic acids, viral proteins) and damage-associated molecular patterns (DAMPs; e.g. high-mobility group box 1 (HMGB1), heat-shock proteins (HSPs), ATP, uric acid). PAMPs and DAMPs are recognized by pattern-recognition receptors (PRRs), such as toll-like receptors (TLRs), retinoic acid-inducible gene-1 (RIG-1)-like receptors (RLRs) or nucleotide-binding oligomerization domain (NOD)-like receptors (NLRs) (*65*). PRR downstream signaling in the context of an acute inflammation induces the release of cytokines which recruit and activate further immune

cells in favor of an antitumor immune response (e.g. IL-6, IL-12, IFN-γ, TNF) (*62*). However, viral infections potentially induce antiviral cellular and humoral immune responses as well and rapid viral clearance will limit OV efficacy. Several strategies such as natural or engineered serotype switching, polymer coating of viral particles, cell carriers or transient host immunosuppression have been explored preclinically to protect OVs from premature clearance by the immune system (*66-73*).

OVs have been genetically modified to augment virus-mediated antitumor immunity by gene delivery of immune modulating transgenes (*74*). Examples: (I) Local expression of cytokines such as IL-2 (*75*), IL-12 (*76*), IFN-β (*77*) or granulocyte macrophage colony-stimulating factor (GM-CSF) (*78*) has demonstrated enhanced therapeutic antitumor efficacy. (II) TAA release and presentation by DCs after oncolysis can be considered an *in situ* vaccination. OVs encoding TAAs can boost the oncolytic vaccination effects and enhance antitumor immune responses (*79-84*). (III) Immune checkpoint inhibitory (ICI) antibodies have demonstrated significant clinical success in the treatment of several solid tumor entities (*85*). However, efficacy of ICI antibodies depends on an existing antitumor immune response and *vice versa* OV efficacy can be limited by immune checkpoints. Not unexpectedly, synergistic effects of ICI antibodies and OVs have been described and ICI antibody-encoding OVs have been developed (*86-94*).

1.4.1. Clinical Applications of Immune Modulator-Encoding OVs

The clinically most advanced OV encoding an immune modulator is T-VEC, an oncolytic herpes simplex virus (HSV) encoding GM-CSF. T-VEC has been approved by the FDA in 2015 for the treatment of patients with recurrent, unresectable melanoma (chapter 1.3.3.). A phase III trial compared treatment of melanoma patients with T-VEC (n = 295) to subcutaneous GM-CSF (n = 141). T-VEC was generally well tolerated and the durable response rate (DRR) and overall survival (OS) were significantly improved compared to the control arm (DRR: 16.3 % *versus* 2.1 %; OS: 23.3 *versus* 18.9 months) (*95*). Forty-seven % of injected lesions completely resolved. However, complete resolution of only 22 % of uninjected non-visceral lesions and 9 % of uninjected visceral lesions was achieved, suggesting that systemic antitumor immunity could be improved by combination with other systemically active immunotherapeutic drugs (*96*). Currently, T-VEC and different combinations with ICI antibodies or chemotherapeutics are under investigation for the treatment of melanoma (NCT01740297, NCT02263508,

NCT02366195) (*93*, *94*, *97*), breast cancer (NCT02658812, NCT02779855), head and neck cancer (NCT02626000), hepatocellular carcinoma and liver metastasis (NCT02509507), lymphoma (NCT02978625) and sarcoma (NCT02453191, NCT02923778). Other OVs encoding GM-CSF are currently under clinical development (JX-594, vaccinia virus (VV), NCT02630368, NCT02562755, NCT02977156; Oncos-102 and CG0070, oncolytic adenoviruses (oAd), NCT03003676, NCT02879669, NCT02963831, NCT02365818). Further OVs encoding immune modulators under clinical investigation are: VSV-IFNβ-NIS, a vesicular stomatitis virus encoding IFN-β and a sodium/iodide symporter (NIS) (NCT03017820, NCT02923466); PROSTVAC, a VV encoding the TAA prostate-specific antigen (PSA) and three immune costimulatory molecules (NCT02933255, NCT02326805, NCT02649439, NCT02772562, NCT02506114, NCT01145508, NCT02649855, NCT00450463, NCT02153918, NCT01867333, NCT01875250, NCT01322490); Ad5-yCD/mutTKSR39rep-hIL12, an oAd encoding IL-12 for treatment of patients with locally recurrent prostate cancer after radiotherapy (NCT02555397); MG1MA3, a heterologous virus prime-boost vaccination strategy with a non-replicating adenovirus encoding melanoma-associated antigen 3 (MAGE-A3) (AdMA3, prime) and an oncolytic maraba virus encoding the same TAA (MG1MA3, boost) (NCT02285816, NCT02879760).

1.4.2. Oncolytic Viruses encoding Bispecific T Cell Engagers (OV-BiTEs)

OVs have direct antitumor activity and the potential to reinitiate or enhance a preexisting antitumor immune response (chapter 1.3.3 and chapter 1.4.). However, physical and chemical barriers within the tumor microenvironment (TME), such as dense extracellular matrices, areas of necrosis, intratumoral stromal cells, hypoxic conditions, low extracellular pH or elevated interstitial pressure can limit viral infection, spread and oncolytic efficacy (*98*, *99*). Furthermore, tumor cells can evade an OV-mediated antitumor immune response by a variety of immune escape mechanisms (chapter 1.3.2.). On the contrary, BiTEs employ existing polyclonal T cells and mediate tumor-specific immune activation, even against tumor cells, which have evolved immune escape mechanisms (chapter 1.3.4.). However, serious and even fatal AEs can occur after continuous intravenous infusion, which is required to maintain therapeutic plasma levels. Furthermore, BiTEs have not yet proven to be effective against solid tumors. For solid tumors, a sufficient T cell density by preexisting or infiltrating T cells has to be given. After systemic application, BiTEs have to reach and penetrate the tumor, which is in

principle feasible as demonstrated in a mouse study with radionuclide-labeled anti-EpCAM BiTE (*100*). However, the implanted tumor cell lines homogeneously expressed EpCAM, while target antigen expression in cancer patients might be heterogeneous or negatively selected. These factors provide a strong rationale, that tumor-targeted BiTE expression by OV delivery can overcome some major limitations of either monotherapy alone. Interestingly, BiTEs could even engage antiviral CTLs to direct them against tumor cells, which might be valuable in preventing premature viral clearance by the immune system. The concept of OV-BiTE mode of action in the context of the cancer immunity cycle is illustrated in Figure 1.2.

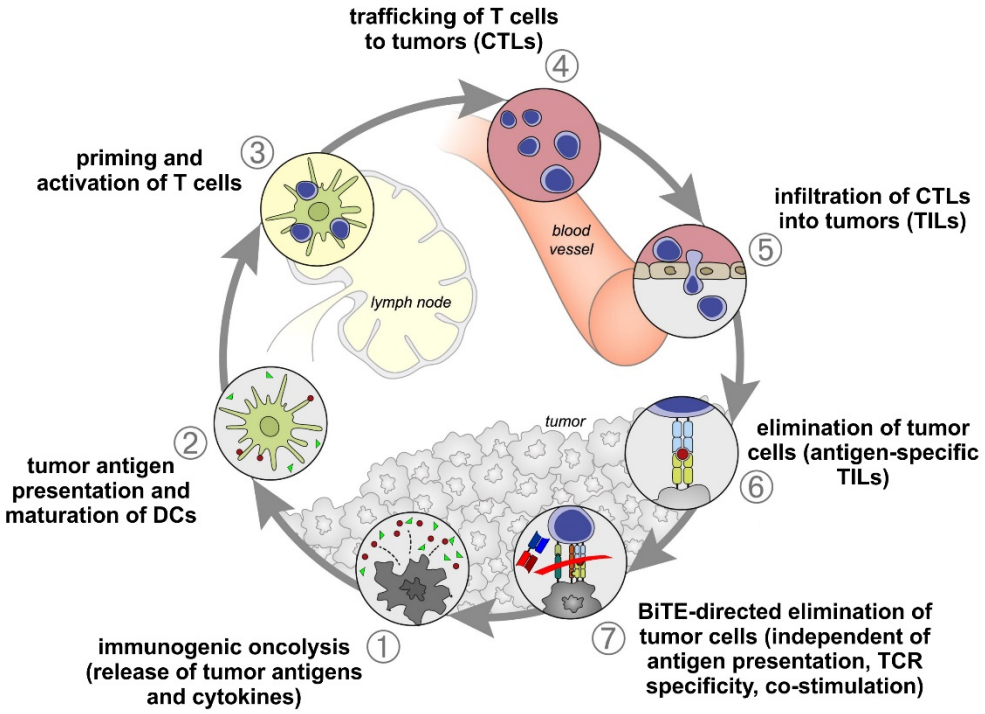

Figure 1.2: OV-BiTE in the cancer immunity cycle. Virus-induced immunogenic cell death releases tumor antigens (red dots) and pro-inflammatory cytokines (green triangles) (step 1). Tumor antigens, danger signals and cytokines are central for DC maturation. Mature DCs are potent antigen presenting cells, secrete further cytokines and activate T cells in tumor draining lymph nodes (steps 2+3). Cytotoxic T lymphocytes (CTLs) infiltrate into tumors (steps 4+5). Tumor infiltrating lymphocytes (TILs) recognize and eliminate tumor cells (step 6). Furthermore, BiTEs produced by OV-infected tumor cells engage polyclonal resident and infiltrating tumor antigen-specific T cells to eliminate tumor cells, independent of antigen presentation and co-stimulatory signals (step 7). Adapted from (*6*).

The potential of oncolytic viruses encoding bispecific T cell engagers (OV-BiTEs) has been investigated preclinically. The first report on OV-BiTEs was a vaccinia virus encoding an anti-EphA2 BiTE (VV-EphA2-BiTE) (*101*). VV-EphA2-BiTE induced T cell activation by means of IFN-γ and IL-2 production *in vitro* and *in vivo*. IL-2 production was not sufficient to induce T cell proliferation. However, T cell proliferation could be induced by additional supplementation of the culture medium with 100 U/ml human IL-2. Furthermore, VV-EphA2-BiTE was evaluated in preventing tumor growth in subcutaneous and lung colonization xenograft models by VV-EphA2-BiTE and peripheral blood mononuclear cell (PBMC) injections before tumor establishment.

More recently, Fajardo *et al.* reported on an oncolytic adenovirus encoding an EGFR-targeting BiTE (oAd-EGFR-BiTE) (*102*). oAd-EGFR-BiTE mediated T cell activation and induced T cell proliferation *in vitro*. Luciferase-expressing T cells were intravenously injected after oAd-EGFR-BiTE treatment of a subcutaneous xenograft model. Fajardo *et al.* observed significant T cell infiltration into the tumor by *in vivo* bioluminescence imaging, compared to mice treated with unmodified oAd. Both, intratumoral and intravenous injections of oAd-EGFR-BiTE demonstrated improved therapeutic efficacy in a subcutaneous xenograft model with the transfer of PBMCs.

A second BiTE-encoding oAd was recently reported by Freedman *et al.* (oAd-EpCAM-BiTE) (*103*). Peritoneal ascites and pleural effusions from chemotherapy-pretreated patients with different malignancies were inoculated with oAd-EpCAM-BiTE. Autologous T cells within the patient samples were activated and efficiently directed to primary human tumor cells *ex vivo*. Ascites or pleural fluids from some patients were immunosuppressive and significantly attenuated T cell activation and degranulation of PBMC-derived T cells by anti-CD3/CD28 bead activation. Interestingly, attenuated T cell functions were not observed in the presence of EpCAM-BiTE, demonstrating the potential of BiTEs to activate T cells in an immunosuppressive environment.

1.5. Measles Virus

1.5.1. Measles Virus Biology

Measles viruses (MVs) are single-stranded, negative sense RNA viruses of the *Morbillivirus* genus within the family of *Paramyxoviridae*. The enveloped, pleomorphic virion contains a non-segmented, ~16,000 nucleotides RNA genome which encodes for six structural (N, P, M, F, H and L) and two non-structural proteins (C and V). A schematic of the MV virion and MV genome structure is illustrated in Figure 1.3. The six transcription units are separated by non-transcribed intergenic sequences of three nucleotides and the genome is flanked by extracistronic regions at the 3′ (leader) and 5′ (trailer) ends. Leader and trailer sequences are essential for viral replication and mRNA transcription (*104*). The envelope is a host cell-derived lipid bilayer and contains the membrane-associated matrix (M) protein, lining the interior of the virion, and two transmembrane glycoproteins, fusion (F) and hemagglutinin (H) protein. The glycoprotein H forms dimers of homodimers (tetramers) and contains the receptor-binding domain, which determines cellular tropism. H protein tetramers form oligomeric complexes with trimeric F proteins. H protein receptor engagement induces H and F dissociation and a conformational change in F, which mediates MV-host cell membrane fusion (*105*). Basolateral expression of F and H facilitates cell-to-cell fusion and results in syncytia formation *in vitro* and *in vivo (106, 107)*. The M protein interacts with the cytoplasmic tails of the F and H glycoproteins and modulates their fusogenic capacity (*108, 109*). M protein also localizes to the host cell nucleus and Yu *et al*. recently demonstrated that M inhibits host cell transcription by binding to nuclear factors (*110*). Furthermore, M protein is in contact with the ribonucleoprotein complex (RNP) and thereby plays a crucial role in assembly of viral progeny (*111*). The helical RNP is a complex of the encapsidated RNA genome and the RNA polymerase. Each nucleocapsid (N) protein binds six nucleotides of the viral genome and the ribonucleocapsid is required as template for transcription and replication. Thus, it is necessary that the total number of nucleotides of the MV genome is a multiple of six, referred to as “the rule of six” (*112*). The ribonucleocapsid is associated with the viral RNA-dependent RNA polymerase, which consists of the phosphoprotein (P), a polymerase co-factor, and the large polymerase protein (L). The *P* open reading frame (ORF) additionally encodes two non-structural proteins, C and V. C protein is encoded by the *P* mRNA but translation is initiated 19 nucleotides downstream of the *P* translation initiator methionine. *V* has an altered reading frame by RNA editing, which produces

an alternative C-terminal domain. P, C and V modulate the cellular IFN response to suppress antiviral defense mechanisms and to enhance viral replication (*113*).

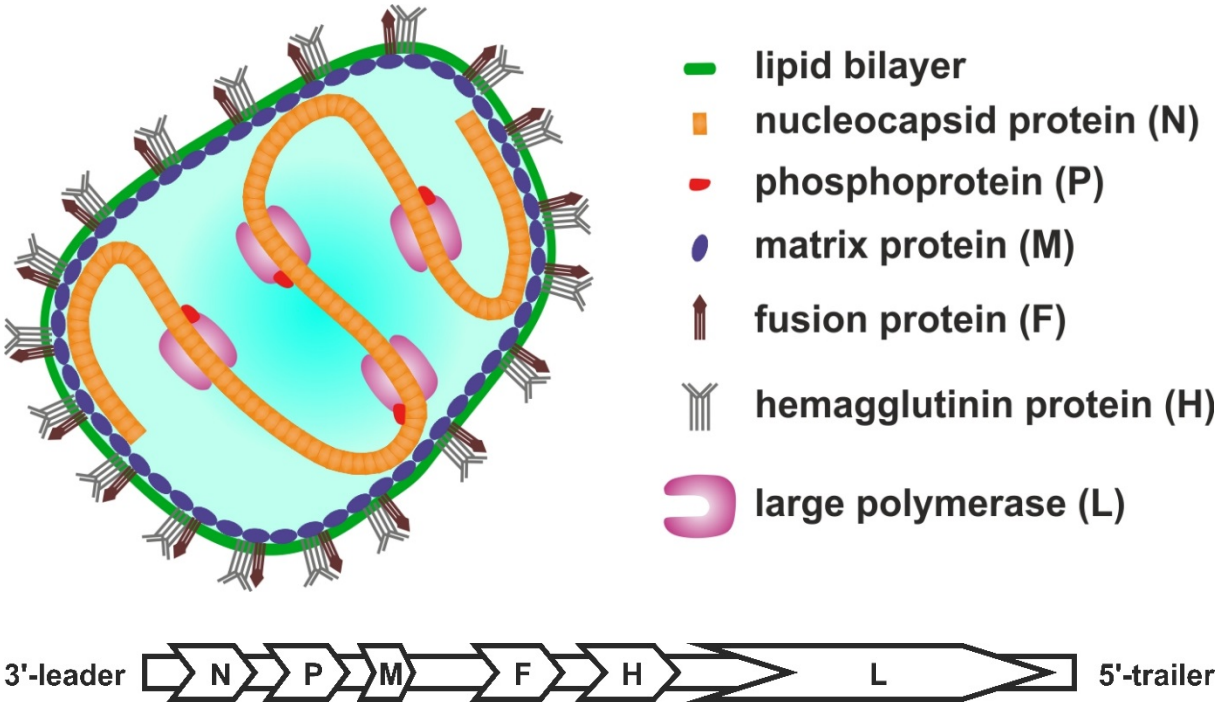

Figure 1.3: Schematic representation of the MV virion and MV genome. (Upper part) The measles virus particle is enveloped by a host cell-derived lipid bilayer (green). The matrix protein (blue) lines the interior of the virion and is in contact with the nucleocapsid (orange) and the luminal tails of the transmembrane glycoproteins, fusion (brown, trimeric) and hemagglutinin (grey, tetrameric). The polymerase (purple) and phosphoprotein (red) are associated with the nucleocapsid. The nucleocapsid consists of nucleocapsid proteins and encapsidates the viral RNA genome. (Lower part) Schematic of MV genome structure.

MV is directly transmitted by airborne spread, therefore extremely contagious and exclusively endemic to humans (*114*). However, MV is phylogenetically closest related to rinderpest virus (RPV), an eradicated pathogen of cattle (*115*). MV could be derived from RPV by adaptation to humans or MV and RPV have a common, zoonotic ancestor (*116*). Cellular receptors for H homodimers of MV include signaling lymphocytic activation molecule family member 1 (SLAMF1) (*117*), CD46 (*118, 119*) and nectin cell adhesion molecule 4 (nectin-4) (*120, 121*).

The route of infection occurs via the respiratory tract. MV H binds to CD209 on alveolar macrophages and DCs, which induces translocation of intracellular SLAMF1 to the cell surface and enables virus entry (*122, 123*). Infected DCs travel to draining lymphoid organs where T and B cells are infected by transmission. The virus amplifies and disseminates to secondary lymphoid organs, resulting in severe immunosuppression. During late infection, MV-infected lymphocytes in the respiratory tract transmit MV to epithelial cells via nectin-4 on the basolateral surface (*113*). MV progeny is released from the apical surface into the luminal side where it can exit the host's respiratory tract to infect other individuals (*124*). MV-induced immunosuppression is responsible for high rates of mortality through opportunistic infections such as pneumonia or diarrhea. Routine use of measles vaccination for infants prevented an estimated 20.3 million deaths during 2000-2015 (*125*). However, the World Health Organization (WHO) still estimated 134,200 measles-related deaths in 2015, mainly in unvaccinated communities or in regions with inadequate medical care (*125*).

1.5.2. Oncolytic Measles Viruses

MV was first isolated in 1954 in Ender's laboratory from a 13-year-old boy, David Edmonston (*126*). Most attenuated MV laboratory and vaccine strains including Zagreb, AIK-C, Schwarz, Moraten and Edmonston B are derived from the Edmonston isolate by propagation in human and avian culture systems (*127, 128*). The first live, attenuated MV vaccine (Edmonston B/Rubeovax) was licensed in 1963 in the USA. More attenuated, live vaccines were licensed in 1965 (Schwarz) and 1968 (Moraten), which remained protective in 50 years of clinical use (*114*). In 1971, natural MV infections of patients suffering from Burkitt's lymphoma, Hodgkin's disease and leukemia were reported to coincide with tumor regression and remission (*129-132*). However, interest in using MV vaccine strains as oncolytic therapeutics only increased in the 1990's and early 2000's, with a profound understanding of MV biology, MV genomic sequencing data (*133*), excellent MV vaccination safety records (*134*), the ability to genetically modify and rescue recombinant MVs (*135*), promising preclinical data (*136-139*), and a general increasing interest in the use of oncolytic viruses (*140*).

The H proteins of wild-type MV and MV vaccine strains have a high affinity to SLAMF1. However, predominantly MV vaccine strains also engage CD46 by one or more amino acid

exchanges in the H protein (*141-143*). CD46 is a complement regulator, which protects normal cells from damage by activated complement and is therefore ubiquitously expressed (*144*). In the context of cancer, CD46 is frequently overexpressed presumably to effectively protect tumor cells from complement-mediated lysis (*145*). Interestingly, surface density of CD46 positively correlates with MV entry and syncytia formation, which aids intercellular viral spread and enhances viral gene expression (*146*). Oncolytic MVs have been genetically engineered to modify MV tropism, monitor viral replication and kinetics *in vivo*, augment antitumor activity and to evade host antiviral immunity (*147*). Insertion of large transgenes (>6,000 nucleotides) in additional transcription units (ATUs) is feasible and transgenes are stably maintained *in vitro* and *in vivo (148, 149)*.

Encouraging results from clinical trials with cutaneous T cell lymphoma (*150*) and ovarian cancer (*151*, *152*) led to the recruitment of patients for further clinical studies, including multiple myeloma (NCT00450814, NCT02192775), ovarian cancer (NCT02068794), head and neck cancer (NCT01846091), glioblastoma multiforme (NCT00390299) and pleural mesothelioma (NCT01503177). No acquired drug resistance or dose limiting toxicities have been observed so far (*153*).

2. Aims and Objectives of the Study

The main purpose of this study is to provide proof of concept for therapeutic efficacy of oncolytic measles viruses encoding bispecific T cell engagers (MV-BiTE). Oncolytic MVs have been recognized as potent immunostimulatory anticancer agents. On the one hand, the immunogenic cell death of MV-infected tumor cells provides the release of tumor-associated antigens, which can be ingested by antigen-presenting cells (APCs) to prime an adaptive antitumor immune response. Besides tumor debulking, viral infection causes an inflammatory reaction with the release of cytokines and danger- and damage-associated molecular patterns, which further recruits and activates immune cells. On the other hand, BiTEs simultaneously bind T cells via CD3 and tumor cells via tumor-specific or tumor-associated antigens. Consequently, BiTEs activate T cells and selectively direct T cells to lyse tumor cells. Of advantage, BiTE-mediated T cell cytotoxicity is independent of T cell receptor specificity, antigen presentation by the tumor cells or T cell co-stimulation. Thus, BiTE therapy can circumvent some of the mechanisms evolved by tumor cells to escape an immune response. BiTEs lack the Fc-region and are small-format antibodies, which is advantageous in terms of tissue distribution. However, BiTEs have a short serum half-life and need to be administered continuously via infusion pumps. Moreover, systemic administration of BiTEs can cause severe side effects. In addition, BiTEs have failed to demonstrate meaningful therapeutic effects against solid tumors so far.

We hypothesize, that tumor-targeted expression of BiTEs by oncolytic MVs enhances therapeutic efficacy against solid tumors, as compared to either monotherapy alone. Furthermore, we hypothesize that tumor-restricted BiTE expression reduces systemic exposure to BiTEs and thus increases the safety profile of BiTE therapy. The concept of MV-BiTE therapy is illustrated in Figure 2.1.

The study objectives include:

1. To generate measles viruses encoding bispecific T cell engagers (MV-BiTE);
2. To characterize replication capacity and oncolytic activity of MV-BiTE;
3. To characterize BiTEs secreted by MV-BiTE-infected cells in terms of binding specificity and the ability to mediate T cell cytotoxicity;

4. To assess therapeutic efficacy in immunocompetent mice, to analyze tumor-infiltrating lymphocytes and to evaluate BiTE plasma levels after MV-BiTE treatment;
5. To assess therapeutic efficacy in xenografts of patient-derived colorectal cancer spheroids with the transfer of human PBMCs and to evaluate BiTE plasma levels after MV-BiTE treatment.

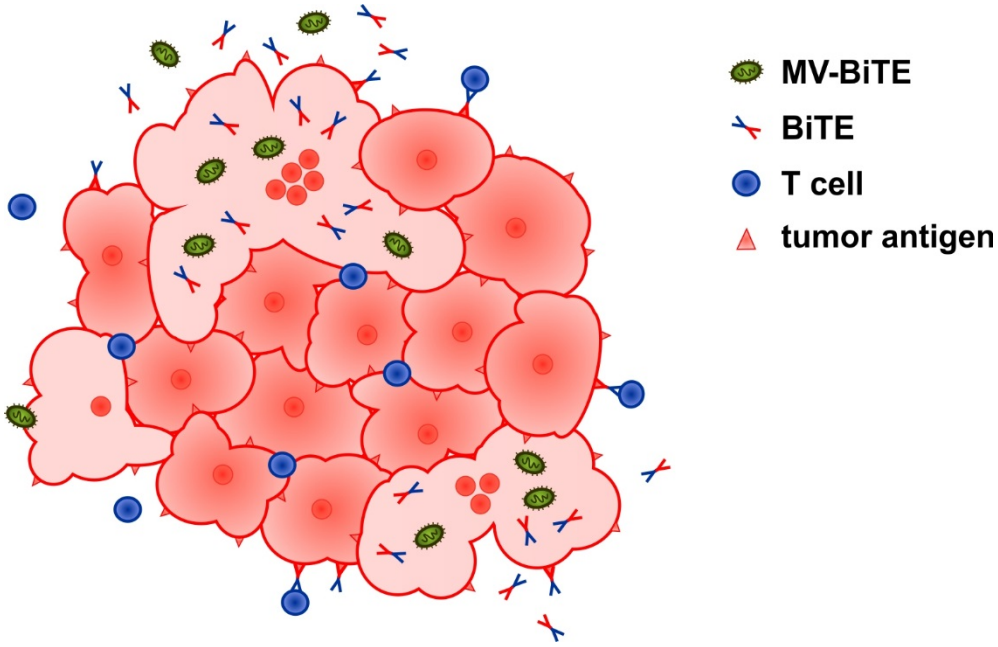

Figure 2.1: The concept of oncolytic measles viruses encoding bispecific T cell engagers (MV-BiTE). MV-BiTE preferentially infects and replicates in tumor cells. During viral replication, BiTEs are expressed and secreted by MV-BiTE-infected tumor cells. The oncolytic activity of MV infection is mediated by viral replication and the formation of large, multinucleated syncytia. As a bystander effect, secreted BiTEs simultaneously engage T cells and tumor cells and thus mediate tumor-specific T cell cytotoxicity.

3. Materials and Methods

3.1. Materials

3.1.1. Chemicals

Reagent	Company	Catalog
Antibiotic-antimycotic (ABAM) (100x)	Sigma-Aldrich	A5955
Agarose, molecular biology grade	Sigma-Aldrich	A9539
DAPI (4',6-diamidino-2-phenylindole)	Sigma-Aldrich	D8417
Dimethyl sulfoxide (DMSO)	Sigma-Aldrich	D2438
DNA gel loading dye (6x) (bromophenol blue, xylene cyanol FF and glycerin)	Thermo Fisher Scientific	R0611
Ethidium bromide, 0.07 %	1239-45-8	AppliChem
Ethylenediaminetetraacetic acid (EDTA) salt solution	Sigma-Aldrich	E7889-100ML
Glycerol	Sigma-Aldrich	G7757-1L
Imidazole, >99 %	Sigma-Aldrich	I5513-25G
Kanamycin	Sigma-Aldrich	K0129
Methanol, > 99.9 %	Carl-Roth	8388.1
Penicillin-Streptomycin,	Thermo Fisher Scientific	15070063
Skim milk powder, blotting grade	Carl-Roth	T145.2
Sodium chloride (NaCl), >99.5 %	Carl-Roth	3957.3
Hydrochloric acid (HCl), 37 %	Carl-Roth	4625.1
Sodium hydroxide (NaOH), 50 %	Carl-Roth	8655.1

3.1.2. Buffers

Buffer	Company	Catalog
Dulbecco's Phosphate-Buffered Saline (D-PBS) without calcium and magnesium	Thermo Fisher Scientific	14190250
Ammonium-Chloride-Potassium (ACK) lysing buffer	Thermo Fisher Scientific	A1049201
Laemmli buffer (4x)	Bio-Rad	61-0747
Novex Tris-Glycine transfer buffer (25x)	Thermo Fisher Scientific	LC3675
Rotiphorese SDS-PAGE running buffer (10x)	Carl-Roth	3060.1
Tris/Borate/EDTA (TBE)	Genaxxon bioscience	M3206.1000
Roti-Stock Tris-Buffered Saline-Tween (TBS-T) (10x)	Carl-Roth	1061.1
2-[4-(2-hydroxyethyl)piperazin-1-yl]ethanesulfonic acid (HEPES) (1 M)	Thermo Fisher Scientific	15630080
RIPA Lysis and Extraction Buffer	Thermo Fisher Scientific	89900

3.1.3. Growth Medium for Bacteria and Cell Culture

Medium	Company	Catalog
Dulbecco's Modifed Eagle Medium (DMEM)	Thermo Fisher Scientific	61965026
LB (Lysogeny Broth) medium	Carl-Roth	X964.1
Opti-MEM	Thermo Fisher Scientific	51985034
Roswell Park Memorial Institute medium 1640 (RPMI 1640)	Thermo Fisher Scientific	61870044
SOC outgrowth medium (Super Optimal broth with Catabolite repression)	New England Biolabs	B9020S

OptiPRO SFM (Serum-Free Medium)	Thermo Fisher Scientific	12309019

3.1.4. Oligonucleotides

Name	Sequence 5‘ → 3‘	T_A [°C]
Amp-1 forward	CCCCGAAGAACGTTTTC	53
Amp-2 reverse	TCGTCGTTTGGTATGGC	50
CMVP-94 forward	CAAAATGTCGTAACAACTCCGC	58
ColE-1 forward	CGGTAACTATCGTCTTGAGTCC	60
ColE-2 reverse	GTGCCTCACTGATTAAGCATTGG	61
eGFP-AscI reverse	TTTGGCGCGCCTTACTTGTACAGCT	55
hCD3 forward	CGTCAAGATGTCCTGCAAAG	55
His-tag_BiTE reverse	GTGGTGATGATGGTGGTGAG	56
Igκ-leader_BiTE forward	GGTACTGCTGCTCTGGGTTC	55
IRES-104 reverse	CCTCACATTGCCAAAAGACG	57
mCD3 forward	GTGCAACCAGGCAAATCTCT	55
MeV H-9018 forward	GTGTGCTTGCGGACTCAGAATC	62
MeV L-9249 reverse	CAGATAGCGAGTCCATAACGG	60
MluI-eGFP forward	TTACGCGTCGCCACCATG	55
pCG forward	TTGTGCTGTCTCATCATTTTG	56

pCG reverse	GTCCCCATAATTTTTGGCAG	56
pCG-MCSa_b forward	GGACGTGGTTTTCCTTTGAA	55
pJET 1.2 forward	CGACTCACTATAGGGAGAGCGGC	66
pJET 1.2 reverse	AAGAACATCGATTTTCCATGGCAG	59
pUC forward	GCCAGGGTTTTCCCAGTCACGA	64
pUC reverse	GAGCGGATAACAATTTCACACAGG	61
scFv_aCEA_*Sfo*I forward	CCCTTTGGCGCCCAGGTGAAACTGC	60
scFv_aCEA reverse	TGATGGTGATGGTGATGAGAACCTCTTGC	60
scFv_hCD20_*Sfo*I forward	TTTGGCGCCCAGGTTCAGCTGGTCCAGTCAGG	69
scFv_hCD20_*Sfo*I reverse	TGGTGATGGTGATGAGAACC	55
wPRE reverse	CATTAAAGCAGCGTATCCACATAGC	61

3.1.5. DNA Plasmids

Name	Description
pEX-A2-anti-mouse CD3-scFv	Cloning vector encoding a mouse CD3 targeting scFv with codon optimization (GENEius; Biolink Informationstechnologie, Martinsried) for expression in murine cells (Eurons MWG)
pUC29	Cloning vector, identical to pUC19 (*154*) except for expanded multiple cloning site
pJET 1.2	Cloning vector, GenBank: EF694056.1

pcDI dsRed	Eukaryotic expression vector for a variant of the *Discosoma* red fluorescent protein
pCG	Eukaryotic expression vector with a CMV promotor and a multiple cloning site (*155*)
pCG L	Eukaryotic expression vector encoding MV *L* (Edmonston B vaccine strain)
pCG N	Eukaryotic expression vector encoding MV *N* (Edmonston B vaccine strain)
pCG NSe H^{bl}-αCEA	Eukaryotic expression vector encoding MV *H* (Edmonston B vaccine strain), which is "blinded" for binding to CD46 and CD150 with Y481, R533A, S548L and F549S mutations and fused to a single chain antibody against human CEA with a hexa histidine tag at the C terminus
pCG P	Eukaryotic expression vector encoding MV *P* (Edmonston B vaccine strain)
pcpNSe H-ATU	MV (Edmonston B vaccine strain) antigenome with an additional transcription unit downstream of the *H* ORF; allows for rescue using the RNA polymerase II system
pcpNSe H-hCD3xCD20	MV (Edmonston B vaccine strain) antigenome encoding a BiTE antibody targeting human CD3 and human CD20 downstream of the *H* ORF; allows for rescue using the RNA polymerase II system
pcpNSe H-hCD3xCEA	MV (Edmonston B vaccine strain) antigenome encoding a BiTE antibody targeting human CD3 and human CEA downstream of the *H* ORF; allows for rescue using the RNA polymerase II system
pcpNSe H-mCD3xCD20	MV (Edmonston B vaccine strain) antigenome encoding a BiTE antibody targeting murine CD3 and human CD20 downstream of the *H* ORF; allows for rescue using the RNA polymerase II system
pcpNSe H-mCD3xCEA	MV (Edmonston B vaccine strain) antigenome encoding a BiTE antibody targeting murine CD3 and human CEA downstream of the *H* ORF; allows for rescue using the RNA polymerase II system

pcpNSe leader-eGFP H-ATU	MV (Edmonston B vaccine strain) antigenome with the *eGFP* ORF upstream of the *N* ORF and an additional transcription unit downstream of the *H* ORF; allows for rescue using the RNA polymerase II system
pcpNSe leader-eGFP H-hCD3xCD20	MV (Edmonston B vaccine strain) antigenome with the *eGFP* ORF upstream of the *N* ORF and encoding a BiTE antibody targeting human CD3 and human CD20 downstream of the *H* ORF; allows for rescue using the RNA polymerase II system
pcpNSe leader-eGFP H-hCD3xCEA	MV (Edmonston B vaccine strain) antigenome with the *eGFP* ORF upstream of the *N* ORF and encoding a BiTE antibody targeting human CD3 and human CEA downstream of the *H* ORF; allows for rescue using the RNA polymerase II system
pcpNSe leader-eGFP H-mCD3xCD20	MV (Edmonston B vaccine strain) antigenome with the *eGFP* ORF upstream of the *N* ORF and encoding a BiTE antibody targeting murine CD3 and human CD20 downstream of the *H* ORF; allows for rescue using the RNA polymerase II system
pcpNSe leader-eGFP H-mCD3xCEA	MV (Edmonston B vaccine strain) antigenome with the *eGFP* ORF upstream of the *N* ORF and encoding a BiTE antibody targeting murine CD3 and human CEA downstream of the *H* ORF; allows for rescue using the RNA polymerase II system

3.1.6. Restriction Enzymes

Enzyme	Conditions	Company	Catalog
***Asc*I**	CutSmart	New England Biolabs	R0558
***BamH*I**	Roche B	Roche	10798975001
***BstZ*I**	*Eco52*I-buffer	Thermo Fisher Scientific	ER0331
***EcoR*I**	Roche H	Roche	10703737001
***Hind*III**	NEB2.1	New England Biolabs	R0104
***MauB*I**	Tango	Thermo Fisher Scientific	ER2081
***Mlu*I**	NEB3.1	New England Biolabs	R0198

***Nde*I**	CutSmart	New England Biolabs	R0111
***Nhe*I-HF**	CutSmart	New England Biolabs	R3131
***Not*I-HF**	CutSmart	New England Biolabs	R3189
***Pac*I**	CutSmart	New England Biolabs	R0547
***Pvu*II**	CutSmart	New England Biolabs	R0151
***Sal*I-HF**	CutSmart	New England Biolabs	R3138
***Sbf*I**	CutSmart	New England Biolabs	R0642
***Sca*I-HF**	CutSmart	New England Biolabs	R3122
***Sfo*I**	CutSmart	New England Biolabs	R0606
***Spe*I**	CutSmart	New England Biolabs	R0133
***Xba*I**	CutSmart	New England Biolabs	R0145

3.1.7. Antibodies

Antibody	Description	Company	Catalog
α-β-actin-Peroxidase	murine IgG1, 1:20,000 clone AC-15	Sigma-Aldrich	A3854
α-HA	mouse IgG1, κ, 1:10,000, clone HA-7	Sigma-Aldrich	H9658
α-HA-biotin	rat IgG1, κ, 1:500, clone 3F10	Sigma-Aldrich	12158167001
α-HA-PE	mouse IgG1κ, 1:11, clone GG8-1F3.3.1	Miltenyi Biotec	130-092-257
α-His-FITC	mouse IgG1, κ, 1:10, clone 13/45/31-2	Dianova	DIA 920

α-human CD46-PE	mouse IgG1, κ, 1:100, clone TRA-2-10	BioLegend	352401
α-human CEA-PE	mouse IgG1, κ, 1:11, clone CB30	abcam	ab42796
α-mouse CD3-PerCP-Cy5.5	rat IgG2b, κ, 1:100, clone 17A2	BD Biosciences	560527
α-mouse CD4-APC-Cy7	rat IgG2b, κ, 1:100, clone GK1.5	BD Biosciences	561830
α-mouse CD8a-APC	rat IgG2a, κ, 1:100, clone 53-6.7	BD Biosciences	561093
α-mouse CD25-PE-Cy7	rat IgG1, κ, 1:100, clone PC61	BD Biosciences	561780
α-mouse CD69-PE	Armenian hamster IgG, 1:100, clone H1.2F3	BioLegend	104507
α-mouse CD16/CD32 (Fc block)	rat IgG2b, κ, 1: 100, clone 2.4G2	BD Biosciences	553141
α-mouse IgG-HRP	rabbit polyclonal, 1:2,000	Bethyl	A90-217P
Armenian hamster IgG-PE	isotype control, 1:100, clone HTK888	BioLegend	400907
mouse IgG1, κ-PE	isotype control, 1:11, clone MOPC-21	BD Biosciences	555749
mouse IgG1, κ-FITC	isotype control, 1:10, clone X40	BD Biosciences	345815
rat IgG2a, κ-APC	isotype control, 1:100, clone R35-95	BD Biosciences	553932
rat IgG2b, κ-APC-Cy7	isotype control, 1:100, clone A95-1	BD Biosciences	552773
rat IgG2b, κ-PerCP-Cy5.5	isotype control, 1:100, clone A95-1	BD Biosciences	550764

3.1.8. Cell cultures

Cell culture	Description	Medium	Source
B16	Murine melanoma cell line derived from a spontaneous tumor of a C57BL/6 mouse	RPMI + 10 % FCS	D. M. Nettelbeck, Heidelberg, Germany
B16-CD20	B16 cells transduced with a lentiviral vector for stable expression of human CD20	RPMI + 10 % FCS	C. E. Engeland, Heidelberg, Germany
B16-CD20-CD46	B16 cells transduced with a lentiviral vector for stable expression of human CD20 and human 46	RPMI + 10 % FCS	B. Hoyler, Heidelberg, Germany
MC38	Murine colon adenocarcinoma cell line derived from a chemically induced tumor in a C57BL/6 mouse	DMEM + 10 % FCS	R. Cattaneo, Rochester, MN
MC38-CEA	MC38 cells transduced with a lentiviral vector for stable expression of human CEA variant	DMEM + 10 % FCS	R. Cattaneo, Rochester, MN
MC38-CEA-CD46	MC38 cells transduced with a lentiviral vector for stable expression of human CEA variant and human 46	DMEM + 10 % FCS	B. Hoyler, Heidelberg, Germany
TSC8	Primary human colorectal cancer tissue or derived metastases	Advanced DMEM/F-12 + 0.6 % glucose, 1 % penicillin/streptomycin, 2 mM L-glutamine, 4 µg/ml heparin, 5 mM HEPES, 4 mg/ml BSA, 10 ng/ml FGF basic, 20 ng/ml EGF	University Hospital Heidelberg

TSC17	Primary human colorectal cancer tissue or derived metastases	Advanced DMEM/F-12 + 0.6 % glucose, 1 % penicillin/streptomycin, 2 mM L-glutamine, 4 µg/ml heparin, 5 mM HEPES, 4 mg/ml BSA, 10 ng/ml FGF basic, 20 ng/ml EGF	University Hospital Heidelberg
TSC23	Primary human colorectal cancer tissue or derived metastases	Advanced DMEM/F-12 + 0.6 % glucose, 1 % penicillin/streptomycin, 2 mM L-glutamine, 4 µg/ml heparin, 5 mM HEPES, 4 mg/ml BSA, 10 ng/ml FGF basic, 20 ng/ml EGF	University Hospital Heidelberg
Vero	African green monkey *Cercopithecus aethiops* kidney epithelial cell line	DMEM + 10 % FCS	ATCC, Manassas, VA

3.1.9. Recombinant Viruses

Virus	Description
MV	MV derived from the Edmonston B vaccine strain
MV-eGFP-hCD3xCD20	MV derived from the Edmonston B vaccine strain encoding eGFP downstream of the *N* ORF and a BiTE antibody against human CD3 and human CD20 downstream of the *H* ORF
MV-eGFP-hCD3xCEA	MV derived from the Edmonston B vaccine strain encoding eGFP downstream of the *N* ORF and a BiTE antibody against human CD3 and human CEA downstream of the *H* ORF
MV-eGFP-mCD3xCD20	MV derived from the Edmonston B vaccine strain encoding eGFP downstream of the *N* ORF and a BiTE antibody against murine CD3 and human CD20 downstream of the *H* ORF

MV-eGFP-mCD3xCEA	MV derived from the Edmonston B vaccine strain encoding eGFP downstream of the *N* ORF and a BiTE antibody against murine CD3 and human CEA downstream of the *H* ORF
MV-hCD3xCD20	MV derived from the Edmonston B vaccine strain encoding a BiTE antibody against human CD3 and human CD20 downstream of the *H* ORF
MV-hCD3xCEA	MV derived from the Edmonston B vaccine strain encoding a BiTE antibody against human CD3 and human CEA downstream of the *H* ORF
MV-mCD3xCD20	MV derived from the Edmonston B vaccine strain encoding a BiTE antibody against murine CD3 and human CD20 downstream of the *H* ORF
MV-mCD3xCEA	MV derived from the Edmonston B vaccine strain encoding a BiTE antibody against murine CD3 and human CEA downstream of the *H* ORF

3.2. Methods

3.2.1. DNA and RNA Molecular Biology Methods

Polymerase Chain Reaction

DNA fragments were amplified for cloning or detection of particular DNA sequences by polymerase chain reactions (PCRs). For detection purposes, DNA fragments were amplified using 0.6 U One*Taq* DNA polymerase (NEB, M0480L), 1x One*Taq* standard reaction buffer (NEB, M0480), 200 µM deoxynucleotide triphosphate (dNTP) mix (Thermo Fisher Scientific, R0192), 500 nM of the respective forward and reverse primers (chapter 3.1.4) and up to 1 µg template DNA. The final volume was adjusted to 25 µl with nuclease-free water. For cloning, DNA fragments were amplified using 0.4 U Phusion High-Fidelity DNA Polymerase (NEB, M0530), 1x Phusion HF buffer (NEB, M0530), 200 µM dNTP mix, 500 nM of the respective forward and reverse primers and up to 250 ng template DNA. The final volume was adjusted to 20 µl with nuclease-free water. For GC-rich template DNA sequences, 3 % DMSO was added to the reaction. All reaction components were gently mixed and assembled on ice. The PCR

reactions were quickly transferred into a T1 PCR cycler (Biometra, Göttingen). Thermocycling conditions are listed in table 3.1.

Table 3.1: Thermocycling conditions with different polymerases. The thermocycling conditions for PCRs using One*Taq* or Phusion polymerases are shown. Annealing temperatures for used primers are described in chapter 3.1.4. The lower annealing temperature was chosen for primer pairs with different annealing temperatures. Extension times were adapted to the fragment size of the expected PCR product.

	One*Taq* polymerase		**Phusion polymerase**		
Step	**T [°C]**	**Time [s]**	**T [°C]**	**Time [s]**	**Cycles**
Initial denaturation	96	120	98	120	1
Denaturation	96	30	98	20	25-35
Annealing	50-68	30	50-72	30	
Extension	68	60/kb	72	30/kb	
Final extension	68	300	72	300	1
Hold	4	∞	4	∞	1

Agarose Gel Electrophoresis

For analysis of PCR products or DNA digestions, DNA fragments were subjected to agarose gel electrophoresis (AGE). Agarose gels were casted with TBE buffer and ethidium bromide at a final concentration of 0.5 µg/ml. DNA samples were pre-mixed with DNA gel loading dye (Thermo Fisher Scientific, R0611) and loaded onto 0.7 % agarose gels for DNA fragments of 0.8 – 10 kb or 1.2 % agarose gels for DNA fragments of 0.4 – 5 kb. DNA fragments were separated in TBE buffer at 120 V for 45 min and subsequently visualized under an UV transilluminator at 265 nm wavelength. Pre-stained DNA ladders with DNA fragments of a defined size were separated in parallel to estimate the DNA fragment sizes in the samples (Thermo Fisher Scientific, SM0321 or SM0311).

Cloning of DNA Fragments

DNA sequences were modified and assembled in cloning vectors. Therefore, DNA was cleaved with suitable restriction enzymes (chapter 3.1.6) and vector backbones were dephosphorylated using the Rapid DNA Dephos and Ligation kit (Sigma Aldrich, 04 898 117 001). DNA fragments were separated by agarose gel electrophoresis and DNA fragments of interest were excised from the agarose gel by using a clean scalpel. The DNA from excised gel fragments was extracted using the Qiaquick Gel Extraction kit (Qiagen, 28704). DNA fragments generated by PCR were purified using the Qiaquick PCR purifcation kit (Qiagen, 28104). The dephosphorylated vector backbones and inserts were ligated at a molecular ratio of 1:3 using the Rapid DNA Dephos and Ligation kit. Chemically competent *Escherichia coli* were transformed with 2 µl ligation reaction as described further.

DNA Plasmid Preparations

DNA plasmids were propagated using bacteria. Therefore, chemically competent *Escherichia coli* (*E. coli*) were thawed on ice and 2 µl ligation reaction or 1 ng DNA was added. NEB 10-β *E. coli* were used for large DNA plasmids encoding the MV antigenome (NEB, C3019H) and One Shot TOP10 *E. coli* were used for smaller DNA plasmids of up to 8 kb (Thermo Fisher Scientific, C404006). After 30 min on ice, bacteria were transformed by heat shock for exactly 40 s at 42 °C and immediately placed back on ice. After 5 min on ice, 450 µl SOC medium was added and bacteria were incubated at 37 °C for 1 h. Subsequently, 40 – 200 µl of the bacterial culture were plated onto agar plates (10 cm dishes) containing 100 µg/ml ampicillin. Plates were incubated at 37 °C overnight. Single colonies were picked with a sterile toothpick. Aliquots of 12.5 µl sterile water were inoculated with the picked colonies and single colony PCRs were performed to identify colonies harboring the correct ligation product. In addition, aliquots of 4 ml LB medium with 100 µg/ml ampicillin were inoculated with the picked colonies and incubated at 37 °C and 800 rpm overnight (mini cultures). On the next day, DNA plasmids from the mini cultures were isolated and purified using the QIAprep Spin Miniprep kit (Qiagen, 27106). For maxi cultures, 200 ml LB medium with 100 µg/ml ampicillin in baffled Erlenmayer flasks were inoculated with 100 µl mini culture and incubated at 37 °C and 125 rpm. After 12 h at 37 °C, DNA plasmids from the maxi cultures were isolated and purified using the QIAfilter Plasmid Purification kit (Qiagen, 12263). The obtained DNA concentrations were determined

using a Nano-Drop ND-1000 spectrophotometer (Thermo Fisher Scientific) by measuring absorbance at 260 nm wavelength. The correct DNA sequences were validated by cleavage of the DNA plasmids using the restriction enzyme *Hind*III (chapter 3.1.6) and Sanger sequencing (GATC Biotech, Konstanz).

RNA Isolation and cDNA Synthesis

RNA molecules were isolated from cells to validate transgene expression using the RNeasy Mini kit (Qiagen, 74104). Contaminating DNA in the RNA solution was removed by treatment with DNase according to the manufacturer's instructions. The obtained RNA was reverse transcribed into complementary DNA (cDNA) using the Maxima H Minus First Strand cDNA Synthesis kit (Thermo Fisher Scientific, K1681). Primers specific for the gene of interest were used to amplify the respective DNA fragments from the cDNA by PCR. PCR products were analyzed by agarose gel electrophoresis as described above.

3.2.2. Cell Culture Methods

Cultivation of Cell Lines

Cells lines were cultivated in cell culture-treated Nunc EasYFlasks with filter caps (Thermo Fisher Scientific, 156499 (75 cm^2), 159910 (175 cm^2)). For subcultivation, cells at approximately 80 % confluency were washed with D-PBS and dissociated using 0.05 % trypsin-EDTA (Thermo Fisher Scientific, 25300054). After cells have dissociated, complete growth medium (chapter 3.1.8) was added and cells were subcultivated at a ratio of 1:20. All cell lines were maintained at 37 °C in a humidified atmosphere with 5 % CO_2. For seeding, dissociated cells were stained with 0.4 % trypan blue solution (Sigma-Aldrich, T8154) and counted using a Neubauer-improved hemocytometer (Marienfeld, 0640010). All cell lines were routinely tested for *Mycoplasma* contamination using the PCR-based VenorGeM *Mycoplasma* Detection kit (Sigma-Aldrich, MP0025). Cell culture medium was supplemented with fetal calf serum (FCS) (Biosera). Beforehand, FCS was heat-inactivated at 56 °C for 30 min and filtrated through a 0.22 µm pore-size EMD Millipore Stericup Sterile Vacuum Filter Unit (Thermo Fisher Scientific, SCGPU05RE).

Cryopreservation of Cell Lines

Cell lines were cryopreserved for long-term storage in liquid nitrogen. Therefore, cells were washed with D-PBS and cell numbers were determined as describes above. Cell pellets were gently resuspended in freezing medium (culture medium supplemented with 60 % (v/v) FCS and 10 % (v/v) DMSO) at a concentration of $1x10^6$ cells/ml. One ml aliquots were gently transferred into cryogenic tubes (Thermo Fisher Scientific, 375418). Tubes were placed into precooled (at +4 °C) freezing containers (Thermo Fisher Scientific, 5100-0001) and immediately stored at -80 °C. After 24 hours, cells were stored in liquid nitrogen tanks for long-term storage.

Cultivation of Primary Human Colorectal Cancer Spheroids

Tumor spheroid cultures (TSCs) were derived from primary human colorectal cancer tissues or colorectal cancer derived metastases. Tumor fragments were obtained from the University Hospital Heidelberg in accordance with the Declaration of Helsinki. Informed consent was given by each patient as approved by the Heidelberg University Ethics Review Board. Single-cell suspensions from tumor fragments were prepared by mechanical dissociation and treatment with Dispase (BD Biosciences, 354235). Single-cell suspensions were cultured under non-adhesive conditions in serum-free medium supplemented with growth factors (chapter 3.1.8). After a few days, cultured cells formed multicellular spheroids. Primary TSCs were tested for authenticity and contamination by Multiplex Cell Line Authentication (MCA) and Cell Contamination Test Analyses (McCT) (Multiplexion, Heidelberg).

Isolation of Human PBMCs

Peripheral blood mononuclear cells (PBMCs) were isolated from blood samples obtained from healthy donors. Informed consent was given by each donor as approved by the Heidelberg University Ethics Review Board. For isolation of PBMCs, sterile Leucosep tubes (Greiner Bio One, 227 290) were filled with 15 ml separation medium (Ficoll Paque Plus, GE Healthcare, 17-1440-02). Whole blood samples were diluted 2 to 3-fold in D-PBS supplemented with 2 mM EDTA. Diluted blood samples were poured into the prepared Leucosep tubes (35 ml per tube). Tubes were centrifuged at 400 x *g*, room temperature for 30 min without brakes. The

PBMC-containing layers were extracted and pooled. PBMCs were washed with D-PBS supplemented with 2 mM EDTA and centrifuged once at 300 x *g*, room temperature for 10 min and subsequently twice at 200 x *g*, room temperature for 10 min. Cell numbers were determined as described above.

Isolation of Splenocytes

Spleens were explanted from C57BL/6J mice and stored on ice in D-PBS until further processing. Within 2 hours, spleens were meshed through 100 µm cell strainers (Neolab, 352360) into 10 ml D-PBS. Splenocytes were centrifuged at 300 x *g* for 5 min and pellets were resuspended in 1 ml ACK lysing buffer (Thermo Fisher Scientific, A1049201). After 10 min incubation at room temperature, ACK lysing solution was diluted with 9 ml D-PBS and cells were centrifuged at 300 x *g* for 5 min, resuspended in 1 ml D-PBS, counted and stored on ice until further use.

Isolation of Murine T cells from Splenocytes

Murine T cells were isolated from splenocytes using the Pan T Cell Isolation kit II (Miltenyi Biotec, 130-095-130) according to the manufacturer's instruction. In brief, T cells were isolated from splenocytes by negative selection using magnetically activated cell sorting (MACS). Non-T cells were labeled with biotinylated antibodies and anti-biotin magnetic beads. Splenocytes were loaded onto MS columns (Miltenyi Biotec, 130-042-201) and the columns were placed into a magnetic stand. Labeled non-T cells were retained and unlabeled T cells were washed out. T cells were collected, counted and stored on ice until further use.

3.2.3. Recombinant Measles Viruses

Rescue of Viral Particles

Recombinant measles virus particles were rescued from DNA plasmids using the RNA polymerase II-dependent expression system described by Martin *et al*. (*156*). In brief, 5 µg DNA plasmids encoding the MV antigenome, 500 ng pCG N, 100 ng pCG P, 500 ng pCG L and 100 ng pcDI dsRed were mixed with the transfection reagent FuGENE HD (Promega, E2311). The DNA and the transfection reagent were mixed in 200 µl DMEM without

supplements at a final concentration of 3 µl FuGENE HD per µg DNA. Vero cells in 6-well plates at 70 % confluency were washed twice and 1.8 ml DMEM supplemented with 2 % FCS and 50 µg/ml kanamycin was added. The transfection mixture was added dropwise and cells were incubated at 37 °C and 5 % CO_2. Twenty-four hours post transfection, the transfection medium was replaced by DMEM supplemented with 10 % FCS and 50 µg/ml kanamycin. The formation of syncytia was monitored daily. When syncytia had formed, medium was removed and cells were scraped in 1 ml OptiMEM using a cell lifter (Sigma-Aldrich, CLS3008). Scraped cell suspensions were vortexed briefly and used to propagate the rescued virus.

Measles Virus Propagation

For the first propagation after the rescue of viral particles, Vero cells were seeded in a 10 cm dish. At 90 % confluency, culture medium was replaced by 4 ml OptiMEM and cells were inoculated with 0.5 ml of the cell suspension from the rescue of viral particles. Cells were incubated at 32 °C in a humidified atmosphere with 5 % CO_2. Twelve hours after the inoculation, 6 ml DMEM supplemented with 10 % FCS was added to each 10 cm dish. Cells were incubated at 32 °C until syncytia have spread throughout the entire dish (approximately 55 to 65 h after inoculation). Then, medium was replaced by 1 ml OptiMEM and cells were scraped. The resulting cell suspension was briefly vortexed, frozen in liquid nitrogen and stored at -80 °C. Frozen cell suspensions were thawed at 37 °C, briefly vortexed and centrifuged for 5 min at 5,000 x *g* and 4 °C. The supernatant was split in 100 µl (for titration assay) and 900 µl (for further propagation) and aliquots were frozen in liquid nitrogen and stored at -80 °C. Virus titers were determined in titration assays as described further. For further propagations, Vero cells were seeded in 15 cm dishes (up to 40 dishes per virus for animal studies). At 90 % confluency, culture medium was replaced by 8 ml OptiMEM and cells were inoculated with the recombinant measles virus at a multiplicity of infection (MOI) of 0.03. In general, the MOI describes the ratio of an agents (here: infectious viral particles) to infection targets (here: Vero cells). An MOI of 0.03 means that a certain number of cells X is inoculated with X*0.03 infectious viral particles. Inoculated cells were incubated at 32 °C in a humidified atmosphere with 5 % CO_2. Twelve hours after the inoculation, 8 ml DMEM supplemented with 10 % FCS was added to each 15 cm dish. Cells were incubated at 32 °C and viral particles were harvested as described above.

Titration Assay

The concentration of cell infectious particles in virus suspensions was determined by titration assays. Therefore, virus suspensions were titrated in 10-fold dilution steps in DMEM supplemented with 10 % FCS on 96-well plates. Titrations were performed in octuplicates to determine titers after virus propagations or quadruplicates for one-step growth curves. Vero cells were added at a concentration of $1.5x10^5$ cells/ml and plates were incubated at 37 °C in a humidified atmosphere with 5 % CO_2. After 48 h, syncytia were counted and virus titers in cell infectious units per ml (ciu/ml) were calculated as following: mean number of syncytia per well x dilution factor.

Infection Assays to Monitor Cytopathic Effects

Susceptibility of target cells to MV infection was monitored in infection assays in terms of syncytia formation and eGFP expression. Therefore, infection target cell were inoculated with the respective MV at an MOI of 0.03 (Vero cells) or at an MOI of 1 (Vero cells, murine target cells, TSCs). Cells were monitored for syncytia formation and eGFP expression using a Axiovert 200 fluorescence microscope (Carl Zeiss) and Axiovision 4.7 software (Carl Zeiss). Representative images were acquired 24 to 48 h post infection at a 50-fold magnification.

Virus Growth Kinetics

Virus growth kinetics on different target cells were assessed by generating one-step growth curves. Cells were seeded at 80 % confluency in 12-well plates ($1x10^5$ Vero cells and murine cells per well, respectively) or 24-well plates ($5x10^4$ TSC cells per well). Cells were inoculated in duplicates per time point with the respective MV at an MOI of 1 in 300 µl OptiMEM and 150 µl OptiMEM, respectively. Plates were incubated at 37 °C in a humidified atmosphere with 5 % CO_2. After 12 hours, the inoculum was replaced by 1 ml culture medium (RPMI supplemented with 10 % FCS for TSCs). Cells were scraped and harvested in the culture medium at 12, 24, 36, 48, 72, and 96 hours post infection. Progeny viral particles were determined in titration assays as described above to generate growth curves.

Cell Viability Assay

Viability of cells after inoculation with MV was analyzed to assess virus-mediated cytotoxicity using the Colorimetric Cell Viability kit III (PromoCell, PK-CA20-300-1000) according to the manufacturer's instruction. In brief, cells were seeded at 80 % confluency in 12-well plates ($1x10^5$ cells per well). Cells were inoculated in triplicates per time point with the respective MV at an MOI of 1 in 300 µl OptiMEM. Plates were incubated at 37 °C in a humidified atmosphere with 5 % CO_2. After 12 hours, the inoculum was replaced by 1 ml culture medium and cell viability was determined at 12, 24, 36, 48, 72, and 96 hours post infection. Thereby, the metabolic activity of mitochondrial enzymes in living cells was determined. The tetrazolium salt XTT (2,3-Bis-(2-methoxy-4-nitro-5-sulfophenyl)-2H-tetrazolium-5-carboxanilide) is reduced into a colored formazan compound, which was measured using a spectrophotometer (Tecan Infinite M200) at a wavelength of 450 nm. Background absorbance at a wavelength of 630 nm was subtracted from signal absorbance. Percentage of viable cells was calculated in relation to metabolic activity of mock-infected cells.

BiTE Production

Vero cells were seeded at 95 % confluency in 15 cm dishes ($1.2x10^7$ cells per dish) and allowed to adhere for 5 h. Subsequently, culture medium was removed and cells were inoculated with the respective MV at an MOI of 0.03 in 10 ml serum-free OptiPRO SFM. Dishes were incubated at 37 °C in a humidified atmosphere with 5 % CO_2. After 12 h, the inoculum was replaced by 12 ml fresh OptiPRO SFM and dishes were transferred to 32 °C. Supernatants were harvested when syncytia had spread throughout the entire dish (approximately 60 to 65 h after inoculation). Subsequently, supernatants were centrifuged at 4,000 x *g* for 10 min at 4 °C and passed through a 0.22 µm pore-size syringe filter unit (Merck, SLGP033RB). BiTEs were purified from the filtered supernatants as described below.

BiTE Purification

BiTEs were purified by affinity chromatography using Ni-NTA spin columns (Qiagen, 31014) according to the manufacturer's instruction. In brief, 600 µl sterile-filtered supernatant was applied to the spin columns and centrifuged at 200 x *g* for 5 min at 4 °C. This step was repeated up to 10 times per column (6 ml per column). Then, columns were washed once with 10 mM imidazole

solution and twice with 20 mM imidazole solution. BiTEs were eluted from the columns with 500 mM imidazole solution. Each imidazole solution was prepared with PBS, supplemented with 200 mM NaCl and set to pH 7.0 to 8.0 with HCl. Eluted BiTEs were washed with PBS and concentrated using 15 ml centrifugal filter units with a vertical membrane that retains proteins larger than 10 kDa (Merck, UFC901024). Filter units were centrifuged at 4,000 x *g* for 20 min at 4 °C. The retained BiTE-containing fraction was diluted with 15 ml PBS and concentrated twice to reduce imidazole concentrations below 0.1 mM. BiTE concentrations were measured using Novagen BCA Protein Assay kit (Merck, 712853) according to the manufacturer's instructions.

3.2.4. Measles Virus Encoded Transgene Expression

SDS-PAGE

BiTE expression by MV-infected cells was analyzed by Western blot, Coomassie Blue staining and magnetic pull-down of labeled cells. Therefore, proteins were separated by sodium dodecyl sulfate-polyacrylamide gel electrophoresis (SDS-PAGE). Cell lysates were prepared using RIPA buffer (Thermo Fisher Scientific, 89900). To investigate BiTE secretion into the cell culture medium by MV-infected cells, supernatants were concentrated 20-fold using 15 ml centrifugal filter units (Merck, UFC901024) or BiTEs were purified beforehand. Samples were supplemented with Laemmli buffer (Bio-Rad, 61-0747) and incubated at 95 °C for 5 min. Subsequently, samples were cooled on ice and briefly spun down. Samples were loaded onto a 12 % polyacrylamide gel (Bio-Rad, 4561041) in running buffer (Carl-Roth, 3060.1). A prestained protein ladder (Thermo Fisher Scientific, 26616) served as molecular weight standard. Proteins were separated at 200 V for 40 min at room temperature.

Western Blot

After SDS-PAGE, separated proteins were transferred onto a methanol activated polyvinylidene fluoride (PVDF) membrane (Merck, IPVH07850). The protein transfer was performed in a wet-chamber with Tris-Glycine transfer buffer (Thermo Fisher Scientific, LC3675) at 100 V and 4 °C for 1 h. Subsequently, membranes were blocked in 5 % powdered milk (Carl-Roth, T145.2) in TBS-T (Carl-Roth, 1061.1) at 4 °C overnight. BiTEs were detected using mouse anti-HA antibody (clone HA-7, diluted 1:10,000 in 5 % powdered milk in TBS-

T) for 1 h at room temperature. Blots were washed three times for 10 min with TBS-T to remove unbound anti-HA antibody. BiTE-bound anti-HA antibody was detected using HRP-coupled rabbit anti-mouse IgG antibody (diluted 1:2,000 in 5 % powdered milk in TBS-T) for 1 h at room temperature. Blots were washed three times for 10 min with TBS-T. Blots were covered with 1 ml chemiluminescent substrate (Thermo Fisher Scientific, 10177533) and incubated for 3 min in the dark. HRP-specific signals were recorded using a ChemiDOC XRS Imaging System (Bio-Rad).

Coomassie Blue Staining

After SDS-PAGE, separated proteins were stained with Imperial Protein Stain (Thermo Fisher Scientific, 24615) according to manufacturer's instruction. In brief, gels were washed three times for 5 min with water. Subsequently, gels were covered with 25 ml of the staining reagent and incubated on a shaker. After 2 h, the staining reagent was removed and gels were washed with 200 ml water overnight. Images of the stained gels were acquired using a ChemiDOC XRS Imaging System (Bio-Rad).

Enzyme-Linked Immunosorbent Assay (ELISA)

BiTE expression, BiTE binding and BiTE plasma levels were analyzed by ELISA. Therefore, ninety-six-well plates (Thermo Fisher Scientific, 44-2404-21) were coated with recombinant human CEA (5 µg/ml, Bio-Rad, PHP282), human CD20 (1 µg/ml, Abnova, H00000931-P01), human CD3 (5 µg/ml, biorbyt, orb138433), mouse CD3 (5 µg/ml, biorbyt, orb138426), mouse PD-L1 (5 µg/ml, Thermo Fisher Scientific, 50010M08H25) or mouse CTLA-4 (5 µg/ml, Thermo Fisher Scientific, 50503M08H25) in 100 µl PBS per well. After incubation at 4 °C overnight, wells were blocked with blocking buffer (D-PBS supplemented with 5 % FCS) for 2 h at room temperature. Blocked wells were washed three times with 200 µl D-PBS. Samples were prepared in 100 µl D-PBS, added to the plate and incubated for 2 h at room temperature. Subsequently, plates were washed three times with 200 µl washing buffer (D-PBS supplemented with 0.05% Tween20 (Biotium, 22002)). Next, plates were incubated with 100 µl anti-HA-biotin antibody per well (1:500 in blocking buffer, clone 3F10, Sigma-Aldrich, 12158167001). After 1 h at room temperature, plates were washed five times with 200 µl

washing buffer. Subsequently, plates were incubated with 100 µl horseradish peroxidase-streptavidin per well (1 mg/ml, Dianova, 016-030-084) for 15 min at room temperature. Afterwards, plates were washed seven times with 200 µl washing buffer and BiTEs were detected with 100 µl 1-Step Ultra TMB-ELISA substrate solution per well (Thermo Fisher Scientific, 34028). After 5-30 min, the enzymatic reaction was stopped by adding 100 µl Stop Solution (Takara, MK021). Absorbance was measured using a spectrophotometer (Tecan Infinite M200) at a wavelength of 450 nm. Background absorbance at a wavelength of 570 nm was subtracted from signal absorbance.

Magnetic Pull-Down of BiTE-Labeled Cells

An assay with the magnetic pull-down of BiTE-labeled cells was established to validate BiTE binding to target cells. Therefore, $2.5x10^6$ target cells were incubated in 200 µl D-PBS with 2 µg/ml BiTE for 30 min on ice. Cells were washed with D-PBS and resuspended in 200 µl D-PBS with anti-HA-biotin antibody (1:50, clone 3F10, Sigma-Aldrich, 12158167001). After 30 min on ice, cells were washed twice with D-PBS. Cells were resuspended in 80 µl D-PBS and 20 µl anti-biotin magnetic beads were added (Miltenyi Biotec, 130-090-485). After 15 min on ice, cells were washed with MACS buffer (D-PBS supplemented with 1 % FCS and 2 mM EDTA). Cells were applied to MS columns (Miltenyi Biotec, 130-042-201) and columns were placed into a magnetic stand. Columns were washed three times with 500 µl MACS buffer and flow through fractions were collected. Magnetically labeled (BiTE-bound cells) were retained in the columns and unlabeled cells were washed out. Columns were removed from the magnetic stand. One ml MACS buffer was applied to the columns and labeled cells were flushed out by using the plunger supplied with the columns. Cells from the elution and flow through fractions were centrifuged at 300 x *g* for 5 min at 4 °C. Cell pellets were lysed in 75 µl RIPA buffer. Lysis solutions were centrifuged at 16,000 x *g* for 20 min at 4 °C. Proteins in two µl supernatant were separated by SDS-PAGE as described above. Presence of cells in the elution and flow through fraction was investigated by Western blot analysis using anti-β-actin-Peroxidase (1:20,000, Sigma-Aldrich, A3854).

3.2.5. Flow Cytometry

BiTE binding and antigen expression levels were analyzed by flow cytometry. For analysis of BiTE binding, $1x10^6$ target cells were washed with D-PBS and incubated with 1 µg/ml BiTE in 100 µl FACS buffer (D-PBS supplemented with 1 % FCS). After 30 min on ice, cells were washed with FACS buffer. For analysis of BiTE binding and antigen expression levels, $1x10^6$ target cells were stained in 50 µl FACS buffer with specific antibodies and isotype controls according to the descriptions listed in chapter 3.1.7. Each experiment was designed to include unstained and single-color stained samples. For multicolor analysis, fluorescence minus one (FMO) controls were included as well. Cells were stained for 30 min in the dark and on ice. If mouse cells were analyzed, 1 µl α-mouse CD16/CD32 (Fc block) was added to each sample 5 min before cells were stained with the specific antibodies. After the staining, cells were washed with 1 ml FACS buffer. Cell pellets were resuspended in 500 µl FACS buffer or 500 µl DAPI solution (1 µg/ml DAPI in FACS buffer) to discriminate live from dead cells. Subsequently, cells were washed with 1 ml FACS buffer. Samples were analyzed using an LSRII flow cytometer (BD Biosciences) with FACS Diva software version 8.0.1 (BD Biosciences). For each sample, 10,000 events were recorded and analyzed using FlowJo V10 software (Tree Star Inc.).

3.2.6. Cytotoxicity Assay

BiTE-mediated T cell cytotoxicity was evaluated in lactate dehydrogenase (LDH) release assays by using the CytoTox 96 Non-Radioactive Cytotoxicity Assay kit (Promega, G1780). Tumor cells were co-cultured with murine T cells or human PBMCs. BiTEs were added and percentage of specific tumor cell lysis was determined after 24 to 48 hours incubation at 37 °C in a humidified atmosphere with 5 % CO_2. The optimal tumor cell number depends on the intracellular LDH content and was determined for each cell line beforehand. Therefore, $2x10^4$ tumor cells were titrated in 2-fold dilution steps in 100 µl PBMC medium (RPMI 1640 supplemented with 10 % FCS, 10 mM HEPES and 1 % ABAM) on 96-well plates (Sigma-Aldrich, Z707899-162EA). A medium only control was included to assess the unspecific LDH content in the medium. Cells were lysed and the amount of released LDH was measured according to the manufacturer's instruction. In brief, 10 µl lysis solution was added to each well and the plates were incubated for 45 min at 37 °C. Plates were centrifuged at 250 x *g* for 4 min

at room temperature. Fifty µl of each supernatant was transferred to new 96-well plates. Fifty µl substrate was added per well and incubated in the dark for 30 min at room temperature. Subsequently, 50 µl stop solution was added per well and signal absorbance was measured at a wavelength of 490 nm using a spectrophotometer (Tecan Infinite M200). For the optimal tumor cell number, the signal absorbance values were at least 2-fold higher compared to the background absorbance in the medium only controls.

For the cytotoxicity assays, murine T cells were isolated from splenocytes as described above. $5x10^3$ MC38-CEA cells were incubated for 48 hours with murine T cells at a ratio of 12:1 and 1 µg/ml mCD3xCEA BiTE was titrated in 10-fold dilution steps. Murine cytotoxic T lymphocytes (mCTLs) were incubated for 24 hours with $5x10^3$ MC38-CEA cells and 1 µg/ml mCD3xCEA BiTE. mCTLs were titrated in 2-fold dilution steps starting with a ratio of 25:1. Human PBMCs were isolated from healthy donor blood as described above. $5x10^3$ MC38-CEA cells were incubated for 24 hours with PBMCs at a ratio of 50:1. Ten µg/ml hCD3xCEA BiTE was titrated in 10-fold dilution steps. $2.5x10^3$ TSC8, $5x10^3$ TSC17 or $1x10^4$ TSC23 were incubated for 24 hours with PBMCs at a ratio of 50:1. One µg/ml hCD3xCEA BiTE was titrated in 10-fold dilution steps. Each experiment was designed to include medium only control and spontaneous and maximum LDH release of tumor and immune cells, respectively. Cytotoxicity assays were developed as described above. Background absorbance was subtracted from each signal absorbance value. Percentage specific lysis of tumor cells was calculated as following:

$$100\ x\ \frac{experimental - effector\ spontaneous - tumor\ spontaneous}{tumor\ maximum - tumor\ spontaneous}$$

3.2.7. Cytometric Bead Array (CBA)

Cytometric bead arrays (CBA) were performed to analyze BiTE-mediated cytokine secretion by T cells. Mouse and human Th1/Th2/Th17 Cytokine kits were used according to the manufacturers's instruction, respectively (BD Biosciences, 560485/560484). In brief, murine T cells isolated from splenocytes or human donor-derived PBMCs were co-cultured with $5x10^3$ tumor cells at a ratio of 50:1 in 200 µl PBMC medium (RPMI 1640 supplemented with 10 % FCS, 10 mM HEPES and 1 % ABAM). BiTEs were added to a final concentration of 1 µg/ml. After 24 h at 37 °C in a humidified atmosphere with 5 % CO_2, cells were centrifuged at 2,000

x *g* for 10 min at 4 °C and supernatants were transferred to new reaction tubes, twice. Supernatants were stored at -80 °C until analysis. Samples with non-target tumor cells or BiTEs targeting non-relevant tumor antigens were used as internal controls.

3.2.8. *In Vivo* Experiments

All experimental procedures, which involved the use of animals, were approved by the responsible Animal Protection Officer at the German Cancer Research Center (DKFZ, Heidelberg) and by the regional authority according to the German Animal Protection Law. C57BL/6J mice were obtained from Harlan Laboratories (Rossdorf) or the Central Animal Laboratory of the DKFZ. NOD.Cg-*Prkdc*^{scid} *Il2rg*^{tm1Wjl}/SzJ (NSG) mice were obtained from Charles River (Sulzbach). Animals were housed in pathogen-free, individually ventilated cages (IVCs) at the Animal Laboratory Services Core Facility at the DKFZ. Six to eight weeks old, female mice were used for all experiments.

Tumor Cell Implantation

Low-passage tumor cells were expanded under cell type-specific conditions as described above. At the day of implantation, cells were dissociated and washed twice with D-PBS. Cell numbers were determined as described above and cells were resuspended at a final concentration of 1x10^7 cells/ml in D-PBS. TSCs were resuspended in 100 µl matrigel (BD Biosciences, 354248). Cells were stored on ice and implanted within 2 hours. 1x10^6 tumor cells (100 µl) were injected subcutaneously into the shaved, right flank region of each mouse using 1 ml syringes (VWR, 720-2561) and 26 G needles (B. Braun, 1023-0100).

Monitoring and Treatment

After tumor cell implantation, mice were monitored daily. When developing tumors were visible, tumors were measured daily using a digital caliper. Tumor volumes were estimated by using following formula: $largest\ diameter\ x\ smallest\ diameter^2 x\ 0.5$. Treatment was initiated when tumors reached a mean volume of 50 mm^3 (for murine tumor cells) and 100 mm^3

(for TSCs), respectively. MC38-CEA-bearing mice were treated with intratumoral injections of 100 µl of $1x10^6$ ciu of MV-BiTE or carrier fluid (OptiMEM) on four consecutive days. B16-CD20-CD46-bearing mice received the same treatment for five consecutive days. TSC-bearing mice were treated with intratumoral injections of 50 µl of $1x10^6$ ciu of MV-BiTE or carrier fluid (OptiMEM) on four consecutive days. On the first day of treatment, TSC-bearing mice additionally received 50 µl of $1x10^7$ healthy donor-derived PBMCs or carrier fluid (PBS) intratumorally. For all intratumoral injections, 1 ml syringes and 26 G needles were used. Tumors were measured every third day. Endpoints were defined as tumor volumes of >1,000 mm^3, tumor diameter > 15 mm, tumor ulceration, tumor bleeding or severe signs of illness. Severe signs of illness include one or more of the following symptoms: ruffled fur, squinted eyes, inactivity or non-responsiveness, hunched posture, labored breathing or body weight loss >20 %. Mice fulfilling one or more of the predefined endpoints were sacrificed.

3.2.9. Analysis of Primary Mouse Material

Analysis of Tumor-Infiltrating Lymphocytes (TILs)

TILs were analyzed by flow cytometry. Therefore, explanted tumors were cut into small pieces using a clean scalpel. Tumor pieces were incubated in 5 ml digestion buffer (RPMI 1640 supplemented with 5 % FCS and 200 U/ml collagenase type I (Thermo Fisher Scientific, 17100017)) for 30 min at 37 °C. Digested tumor cells were meshed through a 100 µm cell strainer (Neolab, 352360) into 10 ml D-PBS. Cell numbers were determined as described above and centrifuged at 300 x *g* for 5 min at 4 °C. Cell pellets were resuspended at a final concentration of $2x10^6$ cells per 50 µl in FACS buffer (D-PBS supplemented with 1 % FCS). Cells were stained with specific antibodies and analyzed as described above.

Analysis of Intratumoral Cytokines

Intratumoral concentrations of specific cytokines were analyzed using the Cytometric Bead Array (CBA) mouse Th1/Th2/Th17 Cytokine kit (BD Biosciences, 560485) according to the manufacturer's instruction. Explanted tumor pieces were frozen in liquid nitrogen and stored at -80 °C until further processing. Frozen tumor pieces were thawed on ice and cut into small

pieces using a clean scalpel. Tumor pieces were homogenized in lysis buffer (one protease inhibitor cocktail Tablet (Sigma-Aldrich, 05892791001) dissolved in 10 mM Tris-HCl (pH 8.0), 150 mM NaCl, 10 % Glycerol, 5 mM EDTA and 1 % NP-40) using a pestle. Homogenized tumor samples were incubated for 1 h at 4 °C under constant rotation. Subsequently, samples were sonicated in automated 30 seconds on/off cycles for 7 min at high intensity using a sonication system with a cooling water pump (Bioruptor Standard, Diagenode, UCD-200). Cell debris was removed by centrifugation at 13,000 x *g* for 15 min at 4 °C. Supernatants were stored at -80 °C until analysis.

Analysis of BiTE Plasma Levels

Systemic exposure of BiTEs after MV-BiTE treatment was analyzed by ELISA as described above (chapter 3.2.4). Peripheral blood was collected from the saphenous vein. Therefore, mice were placed in a restraining tube and the left shank and thigh were shaved. The saphenous vein was punctured with a 26 G needle and 100 µl blood was collected using a heparin collection tube with capillary action (Sarstedt, 16.443). Bleeding was stopped by applying pressure on the punctured area using a sterile cotton swab. Plasma was prepared from blood by centrifugation for 10 min at 2,000 x *g* at room temperature and stored at -80 °C until analysis.

3.2.10. Statistical Analysis

Statistical analyses were performed using GraphPad Prism software (v6.04, GraphPad Software). Data show mean with standard deviation (SD). Statistical analyses of column data with one independent variable were performed by one-way ANOVA and p values were adjusted for multiple comparisons by Tukey's test. For competitive ELISAs, the mean of each column was compared to the mean of one control column and p values were adjusted for multiple comparisons by Dunnett's test. Statistical analyses of grouped data with two independent variables were performed by two-way ANOVA and p values were adjusted for multiple comparisons by Sidak's test. Curve comparison of two groups for survival analyses were performed by log-rank (Mantle-Cox) test and p values were adjusted for multiple comparison by Bonferroni's correction.

4. Results

The study concept is based on the hypothesis that tumor-targeted expression of bispecific T cell engagers (BiTEs) by oncolytic measles viruses (MVs) increases therapeutic antitumor efficacy of measles virotherapy. Furthermore, local BiTE expression increases therapeutic BiTE concentrations at the tumor site, as compared to systemic BiTE applications. At the same time, potential BiTE-related systemic adverse events (AEs) are alleviated. MVs encoding BiTEs (MV-BiTE) were generated and characterized *in vitro* in terms of virus replication, oncolytic activity and transgene expression. BiTEs from MV-BiTE-infected cells were purified and analyzed for binding specificity and cytotoxicity in co-culture assays *in vitro*. Therapeutic efficacy of MV-BiTE was assessed in immunocompetent mouse models of colon adenocarcinoma and melanoma[*], as well as in xenografts with patient-derived colorectal cancer spheroids in immunodeficient mice.

4.1. Generation of BiTE-encoding Measles Viruses

4.1.1. Cloning of BiTE Antibody Constructs

BiTE antibodies generally comprise two single chain variable fragments (scFvs), which are translated in tandem from a single gene (Figure 4.1). Therefore, the variable chain domains were connected by non-immunogenic, flexible peptide linkers. One scFv contains the entire complementarity-determining region (CDR) and consists of a variable heavy and light chain domain (V_H and V_L). The V_H and V_L domains were connected by three repeats of the amino acid (AA) sequence glycine-glycine-glycine-glycine-serine ($(Gly_4Ser)_3$). The $(Gly_4Ser)_3$-sequence is a standard linker that improves stability of the scFvs. The 15 AAs span a distance of approximately 35 Å, which is a sufficient length to ensure monomeric formation of scFvs (*157*). The two scFvs were connected by a short middle linker of five AAs (Gly_4Ser) to ensure close proximity of the simultaneously engaged T cell and tumor cell. A human influenza hemagglutinin (HA)-tag and a hexa histidine (His_6)-tag were fused to the N- and C-terminus, respectively. The N-terminal Kozak consensus sequence is meant to enhance translation of

[*]Johannes Heidbüchel joined the BiTE project as a Master student under the supervision of Tobias Speck. He continued working with the CD20-targeting MV-BiTEs as a PhD student. All results concerning the B16-CD20-CD46 melanoma model are shown in the Appendix. His contribution is always indicated.

BiTE mRNA transcripts and the immunoglobulin kappa light chain signal sequence (Igκ leader) to promote protein secretion after translation. Different BiTE antibody constructs were generated to target human CD3 (OKT3) or murine CD3 (145-2C11) and human carcinoembryonic antigen (CEA) (MFE-23) or human CD20 (B9E9), respectively (Figure 4.1).

4.1.2. Cloning of Recombinant MV-BiTE

Measles viruses (MVs) derived from the Edmonston B vaccine strain (chapter 1.5.2) were genetically modified to express secretable BiTEs (MV-BiTE). The utilized Edmonston B derivative has additional unique restriction sites by *Nar*I and *Spe*I elimination (NSe). pcpNSe plasmids encode the antigenomic MV-NSe cDNA and can be modified to carry additional transcription units (ATUs) that enable transgene expression in infected cells. MV-NSe containing an ATU downstream of the *H* open reading frame (ORF) and enhanced green fluorescent protein (eGFP) in leader position (upstream of *N* ORF) have been generated previously (pcpNSe ld-eGFP H-ATU; pcpNSe H-ATU) (*92*). Each BiTE-encoding sequence was inserted into an ATU downstream of the *H* ORF (Figure 4.1).

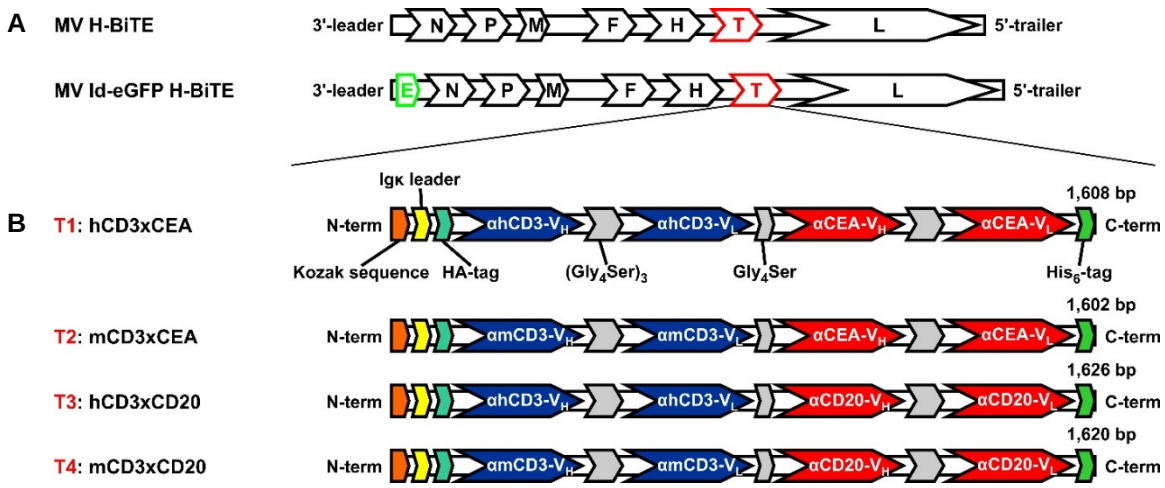

Figure 4.1: Schematic representation of the recombinant MV genomes and transgenes. (**A**) The BiTE-encoding transgene T was inserted downstream of the *H* gene open reading frame (ORF). MV-BiTE, which additionally encode the eGFP sequence E upstream of the *N* gene ORF were generated as well. (**B**) Four different BiTE-encoding transgenes T1 – T4 were generated. T1 and T3 encode for human CD3-targeting BiTEs, which are directed against the tumor associated antigens human CEA and human CD20, respectively. T2 and T4 encode for murine CD3-targeting BiTEs, which are as well directed against human CEA and human CD20, respectively. The transgene sequence lengths range from 1,602 to 1,626 base pairs (bp).

4.2. Characterization of Recombinant Measles Viruses

4.2.1. Susceptibility of Target Cells to MV-BiTE Infection

The capability of eGFP-encoding MV-BiTE to infect target cells was investigated. The expression of eGFP and syncytia formation served as indicators for productivity of infection and viral spread.

Vero cells are the MV producer cell line and highly susceptible to MV infection (Figure 4.2 A). Images of Vero cells are included in the analysis as an internal positive control. Expectedly, strong eGFP signals and the formation of large syncytia were observed after MV-infection of Vero cells.

Furthermore, we inoculated murine cell lines with MV-BiTE, which were used for the *in vivo* efficacy studies. B16 and MC38 are murine melanoma and colon adenocarcinoma cell lines, respectively, and are syngeneic and tumorigenic to C57BL/6 mice. Murine cells lack the expression of MV entry receptors and are therefore not susceptible to MV infection. Expectedly, inoculation of MC38-CEA cells with recombinant MV resulted in low levels of eGFP expression and no syncytia formation. MC38-CEA-CD46 cells express human CD46, an entry receptor for MV vaccine strains (chapter 1.5.2). However, murine cells are generally less permissive for MV infection as compared with human or non-human primate cells. Expectedly, inoculation of MC38-CEA-CD46 cells with recombinant MV resulted in moderate levels of eGFP expression and the formation of small syncytia (Figure 4.2 B). Similar levels of eGFP and syncytia formation were observed for MV-infected B16-CD20-CD46 (Figure A.1).[*]

Tumor spheroid cultures (TSCs) from patients with colon cancer were used to study therapeutic efficacy of MV-BiTE in xenografts. Three different TSCs with varying levels of endogenous CEA expression were inoculated with MV-BiTE (Figure 4.10 D). Strong eGFP expression and the formation of large syncytia were observed (Figure 4.2 C).

[*] Results generated by Tobias Speck

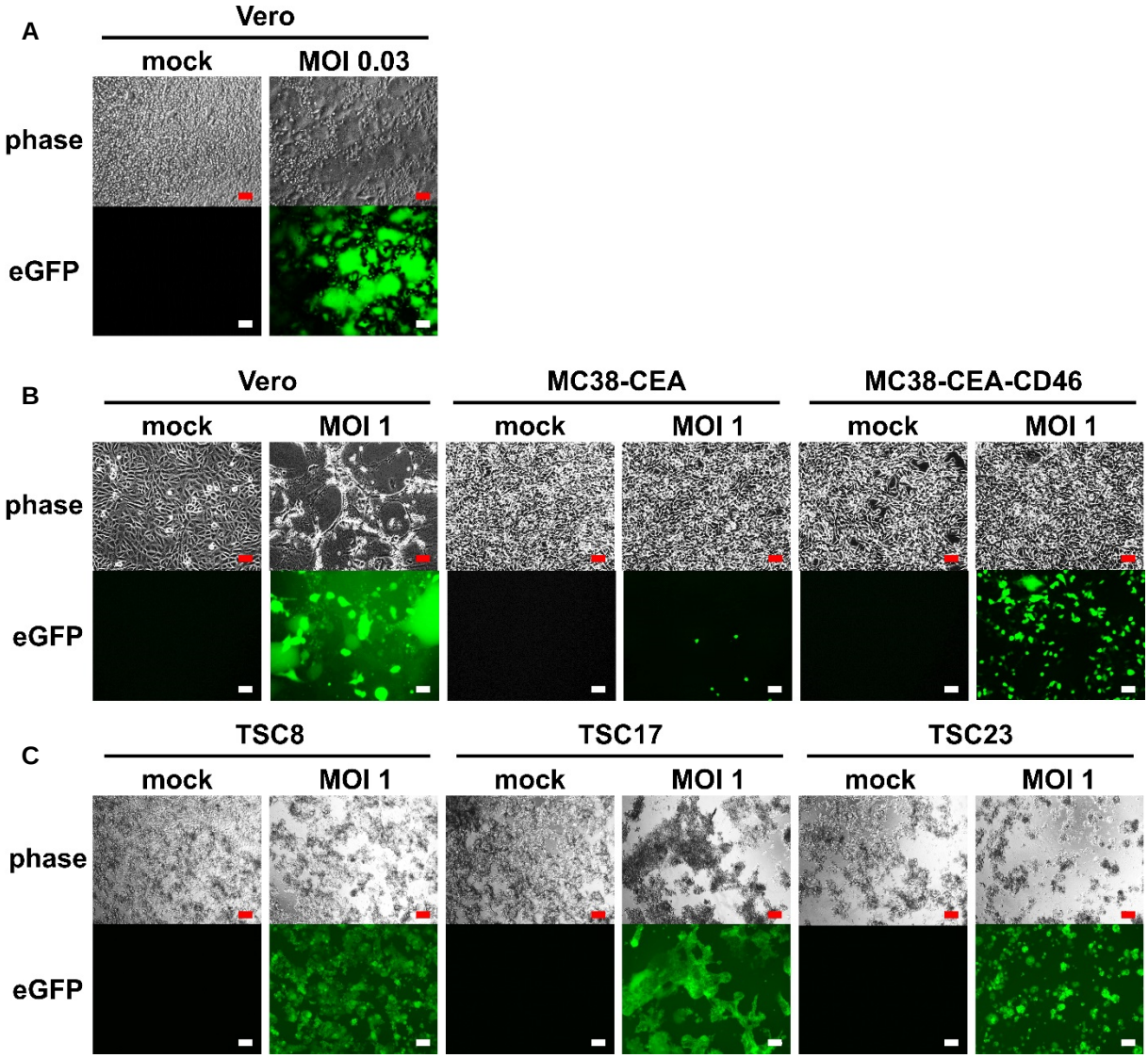

Figure 4.2: Susceptibility of target cells to MV-BiTE. (**A**) Vero cells were inoculated with MV-eGFP-mCD3xCEA at a multiplicity of infection (MOI) of 0.03. Images were acquired 48 h post inoculation. (**B**) The susceptibility for MV infection of MC38-CEA and MC38-CEA-CD46 was compared to Vero cells. Cells were inoculated with MV-eGFP-mCD3xCEA at an MOI of 1. Images were acquired 48 h post inoculation. (**C**) Low-passage tumor spheroid cultures TSC8, TSC17 and TSC23 were inoculated with MV-eGFP-hCD3xCEA at an MOI of 1. Images were acquired 24 h post inoculation. (**A-C**) Scale bars: 200 µm.

4.2.2. Growth Kinetics of Recombinant MV-BiTE

MV-mediated cytopathic effects and transgene expression correlate with the capacity of the viruses to replicate. Therefore, we generated one-step growth curves to characterize replication kinetics of the recombinant viruses as compared with the unmodified MV.

Replication kinetics of all non-eGFP-encoding MV-BiTE were assessed on Vero cells, which are the relevant constructs for the *in vivo* efficacy studies. All tested recombinant viruses had similar replication kinetics, which were comparable to replication of the unmodified MV (Figure 4.3). Production of virus progeny peaked at 36 h post infection with 2.25 – 7.75x10^5 cell infectious units (ciu)/ml. Next, MV-BiTE replication kinetics were assessed on murine cell lines. Consistent with the infection tests, the least virus progeny were generated on MC38-CEA with maximum titers in the range of 4x10^2 – 5.25x10^3 ciu/ml 12-24 h post infection. Higher virus titers were generated on MC38-CEA-CD46, as compared to MC38-CEA. Maximum titers of up to 1.25x10^4 ciu/ml were reached 36-48 h post infection. Highest virus titers on murine cells were reached on B16-CD20-CD46 with 1.75 – 5.75x10^5 ciu/ml 36-48 h post infection, a similar range as compared to virus progeny generated on Vero cells (Figure A.2 A).[*] However in comparison to Vero cells, virus replication was delayed on B16-CD20-CD46 and dropped close to or below detection limit (= 25 ciu/ml) at 96 h post infection. Virus replication was moderate on TSCs with highest titers in the range of 6x10^2 – 1.9x10^3 ciu/ml (TSC8), 6x10^3 – 1.1x10^4 ciu/ml (TSC17) and 1.55x10^3 - 4.5x10^3 ciu/ml (TSC23). However, virus replication on all TSCs was stable and continued beyond 96 h. Conclusively, replication of the recombinant MVs was not compromised by insertion of BiTE-encoding sequences in an ATU downstream of the *H* ORF.

4.2.3. Direct Cytotoxic Capacity of Recombinant MV-BiTE

All tested MV-BiTE had similar replication kinetics in one-step growth curves. However, virus replication largely differed among the various tumor cells. We performed metabolic cell viability assays (XTT) to assess MV-mediated cytopathic effects on the tested tumor cells.

[*] Results generated by Tobias Speck and Johannes Heidbüchel

MV-BiTE and unmodified MV similarly reduced cell viability of Vero cells at 48 h post infection by 90 % as compared to mock-treated Vero cells (Figure 4.4). Consistent with replication kinetics, MV cytopathic effects on murine cells were delayed. Viability of MC38-CEA-CD46 cells was reduced by 90 % at 96 h post infection. In contrast, MC38-CEA cell viability was reduced by 40 – 60 % at most at 96 h post infection. Viability of B16-CD20-CD46 cells was reduced by 56 – 72 % at 48 h post infection and relative viability increased to 70 – 80 % at 96 h post infection (Figure A.2 B).*

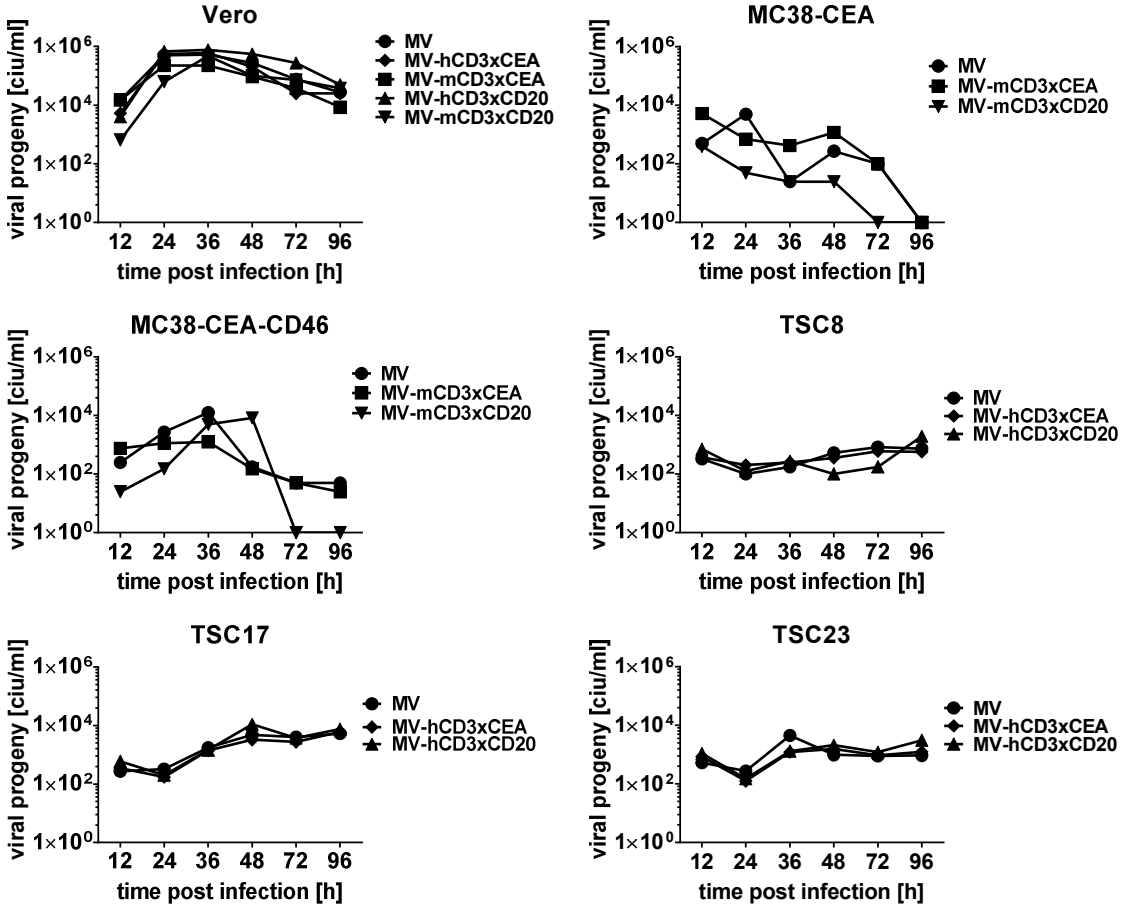

Figure 4.3: Replication kinetics of MV-BiTE. Indicated cells were inoculated with MV-BiTE and unmodified MV at a multiplicity of infection (MOI) of 1. Viral progeny were determined by titration assays 12, 24, 36, 48, 72 and 96 hours post infection. Titration assays were performed in quadruplicates, which results in a detection limit of 25 cell infectious units (ciu)/ml. One-step growth curves were generated to compare MV replication kinetics in terms of viral progeny in ciu/ml.

* Results generated by Tobias Speck and Johannes Heidbüchel

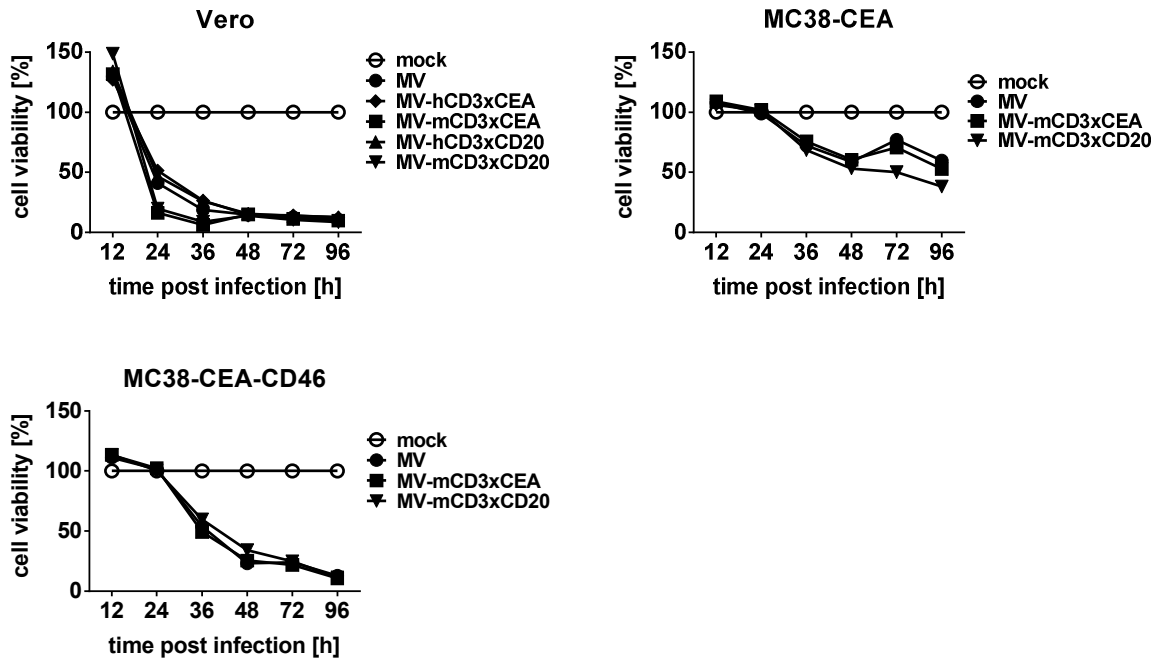

Figure 4.4: Cytotoxic capacity of MV-BiTE. Indicated cells were inoculated with medium only (mock), MV-BiTE or unmodified MV at a multiplicity of infection (MOI) of 1. Cell viability was determined in triplicates 12, 24, 36, 48, 72 and 96 hours post infection. Cell viability in % was normalized to cell viability of non-infected cells (mock), as described in chapter 3.2.3.

4.2.4. Transgene Expression of Recombinant MV-BiTE

BiTE expression from MV-BiTE-infected cells was analyzed by RT-PCR and Western blot. For RT-PCR, Vero cells were infected with the respective MV-BiTE at an MOI of 0.03. *BiTE* mRNA was detected in cell lysates 95 h post infection (Figure 4.5 A). For Western blot analysis, Vero (MOI 0.03) or MC38-CEA-CD46 cells (MOI 1) were infected with MV-mCD3xCEA. BiTE expression was analyzed in cell lysates by anti-HA antibody staining 12 – 96 h post infection (Figure 4.5 B). BiTE expression in Vero cells was first detectable at 36 h post infection and continually increased until 96 h post infection. Similarly, in MC38-CEA-CD46 cells, BiTE expression was first detectable at 36 h post infection. However, expression peaked at 48 h post infection and then gradually decreased until 96 h post infection.

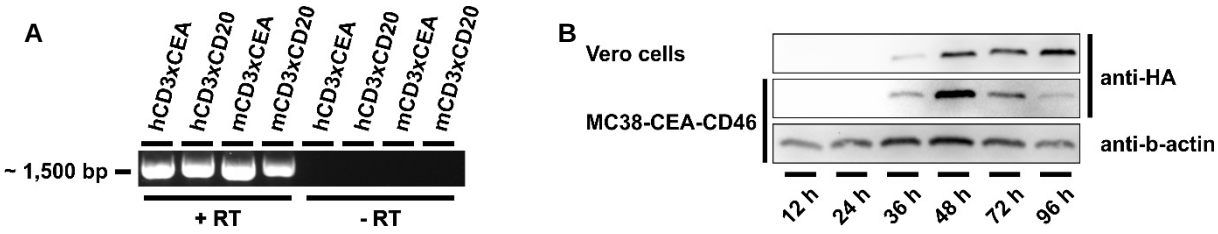

Figure 4.5: BiTE expression by MV-BiTE-infected cells. (**A**) RT-PCR: Vero cells were infected with MV-BiTE at a multiplicity of infection (MOI) of 0.03. Cells were lysed at 95 h post infection and RNA was isolated. BiTE-specific sequences from the transcribed cDNA were amplified by PCR and subjected to gel electrophoresis. Fragments of the expected size of approximately 1,500 base pairs (bp) were detected. Minus reverse transcriptase (-RT) samples served as negative controls for DNA contaminations in the RNA samples. (**B**) Western blot analysis: Cells were infected at MOI 0.03 (Vero) or MOI 1 (MC38-CEA-CD46). Cells were lysed at indicated time points and proteins were separated by SDS-PAGE. Proteins were blotted onto PVDF membranes and stained with anti-HA (BiTE) or anti-β-actin antibodies (loading control).

BiTE secretion from MV-BiTE-infected cells into culture supernatant was investigated by protein staining of SDS-PAGE and ELISA. For SDS-PAGE analysis, cell-free supernatants from MV-BiTE-infected Vero cells were harvested and concentrated 20-fold using centrifugal filter units. Proteins were separated on an SDS-PAGE gel and subsequently stained with a coomassie dye. Proteins with the expected molecular weight of BiTEs of approximately 58 kilodalton (kDa) were detected in culture supernatants of MV-BiTE-infected cells (Figure 4.6 A). In the supernatant of non-infected cells, no protein of the corresponding molecular weight was detectable. For ELISA, cells were infected with MV-BiTE at cell type-specific MOIs. Cell-free supernatants were harvested at 24 – 96 h post infection and analyzed by ELISA with recombinant human protein. Consistent with Western blot analysis of cell lysates, BiTE secretion by MV-BiTE-infected Vero cells was detectable after 24 h post infection and BiTE concentration continually increased over time until 96 h post infection (Figure 4.6 B). BiTE concentrations in culture supernatants from MV-BiTE-infected MC38-CEA-CD46 cells peaked at 48 – 72 h post infection and decreased until 96 h post infection. However, maximum BiTE concentrations were three times lower as compared with BiTE concentrations in the supernatant of Vero cells. Low levels of BiTE were secreted by MV-BiTE-infected MC38-CEA cells. Consistent with replication kinetics, maximum BiTE concentrations were reached at 24 h post

infection and declined over time until 96 h post infection. Furthermore, supernatants from MV-BiTE-infected TSCs were analyzed by ELISA and compared to supernatants from TSCs infected with unmodified MV (Figure 4.6 C). TSCs were infected at MOI 1. Moderate but continuous BiTE expression over 96 hours was observed for TSC8 and TSC23. Continually increasing BiTE levels were observed in culture supernatants of TSC17. Highest BiTE levels were detected in supernatant of TSC17 96 hours post infection. Absorbance values in remained at background level.

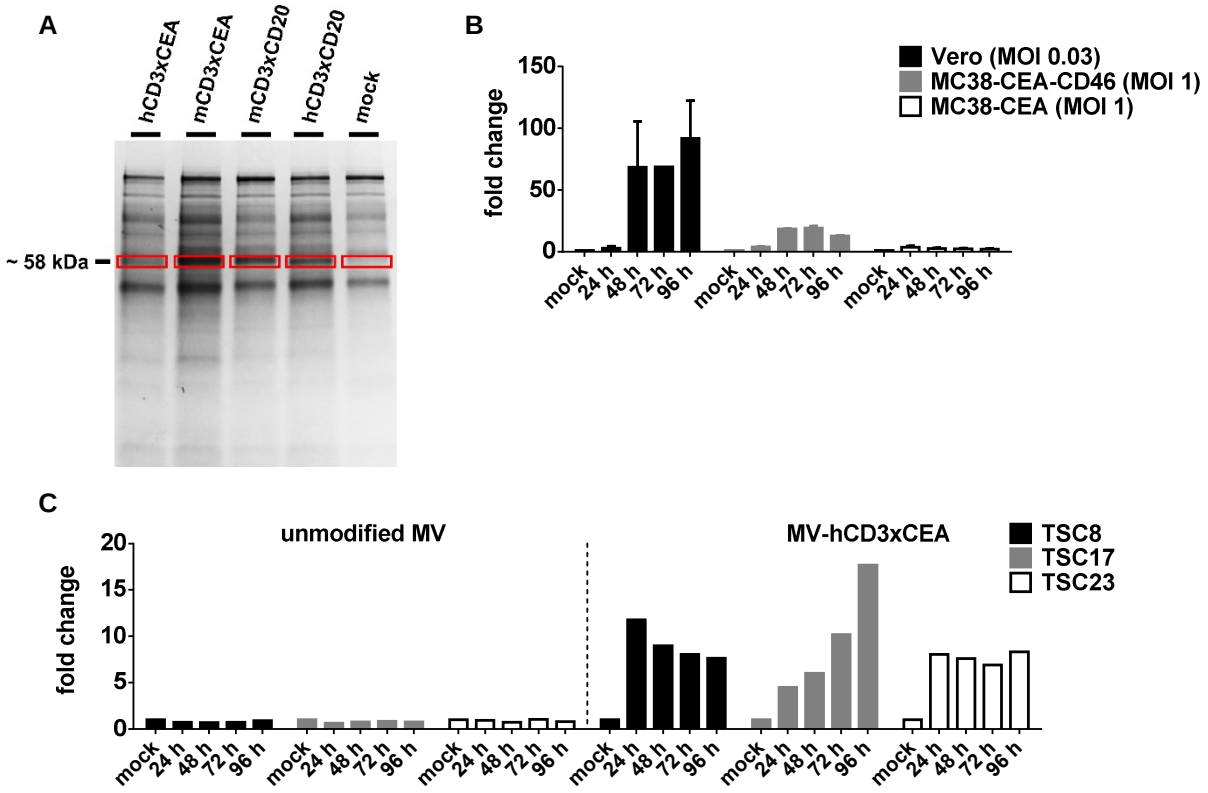

Figure 4.6: BiTE secretion by MV-BiTE-infected cells. (**A**) SDS-PAGE: Vero cells were inoculated with serum-free medium (mock) or MV-BiTE at a multiplicity of infection (MOI) of 0.03. Cells culture supernatants were collected 63 h post infection and concentrated 20-fold. Proteins were separated by SDS-PAGE and stained with a coomassie R-250 dye-based reagent. The expected molecular weight for BiTE antibodies is approximately 55 – 58 kilodalton (kDa) (red boxes). (**B**) ELISA: Cells were infected with MV-mCD3xCEA at MOI 0.03 (Vero) or MOI 1 (MC38 cells). (**C**) TSCs were infected with unmodified MV or MV-hCD3xCEA at MOI 1. Error bars represent standard deviation. (**B, C**) Cell culture supernatants were collected 24, 48, 72 and 96 hours post infection and relative BiTE concentrations were determined by ELISA with recombinant human CEA. Absorbance values of BiTE-containing supernatants were normalized to medium only (mock) and are shown as fold change over mock.

4.3. Functional Characterization of MV-encoded BiTEs

4.3.1. Purification of BiTEs Expressed by MV-infected Cells

BiTEs were purified from culture supernatants of MV-BiTE-infected cells (vpBiTEs) to characterize BiTE functionality *in vitro*. Culture supernatants were sterile-filtered and BiTEs were purified by affinity chromatography using immobilized nickel-ion (Ni^{2+}) spin columns. BiTEs were eluted from the Ni-columns by addition of imidazole. Imidazole in the eluate was washed out with PBS using centrifugal filter units with a vertical membrane that retains proteins with a molecular weight larger than 10 kDa. Different steps of the purification procedure were analyzed by Western blot using an anti-HA-tag antibody (Figure 4.7 A). BiTEs were not detectable in the flow through or washing fractions after the columns were loaded with BiTE-containing supernatant. Both elution fractions with different concentrations of imidazole contained BiTE antibodies. vpBiTEs were subjected to SDS-PAGE gel electrophoresis and subsequently stained with a coomassie dys. Clear bands of the expected band size were detected (Figure 4.7 B).

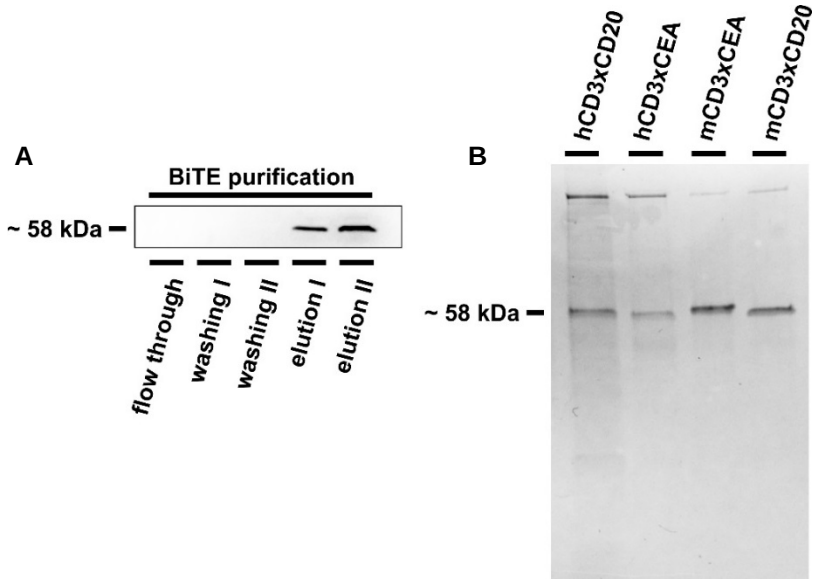

Figure 4.7: Purification of BiTEs secreted by MV-BiTE-infected cells. (**A**) Vero cells were inoculated with MV-mCD3xCEA at a multiplicity of infection (MOI) of 0.03 in serum-free medium. Cell culture supernatant was collected 62 h post infection and purified by affinity chromatography. Different fractions of the purification procedure were analyzed by Western blot and BiTE was detected by anti-HA antibody. (**B**) Purified BiTEs were subjected to SDS-PAGE gel electrophoresis and quality of purification was analyzed by coomassie staining.

4.3.2. Binding Specificity of Purified BiTEs

Binding specificity of MV-expressed vpBiTEs was evaluated using sandwich and competitive ELISAs, magnetic pull-down of BiTE-labeled cells and flow cytometry. First, specific binding of vpBiTEs to recombinant human CEA (rhCEA) and two control peptides (murine PD-L1 and CTLA-4) was assessed with sandwich ELISAs (Figure 4.8 A). Expectedly, the anti-CEA BiTEs bound to rhCEA, while there was no significant binding-specific signal detected using CD20-targeting BiTEs. Concurrently, anti-CEA BiTEs did not bind to the two control peptides. For the competitive ELISAs, vpBiTEs were incubated with target cells and subsequently target cells were pelleted. Unbound BiTE remained in the supernatant, which was transferred on ELISA plates coated with the competing, cell-type specific recombinant protein (MC38-CEA: rhCEA, PBMCs: rhCD3). The more target antigen-expressing cells were incubated with BiTE, the less BiTE was detected in the supernatant (Figure 4.8 B). Binding specificity to target cells was compared to non-target cells (rhCEA: MC38) or mock controls (rhCD3: PBS).

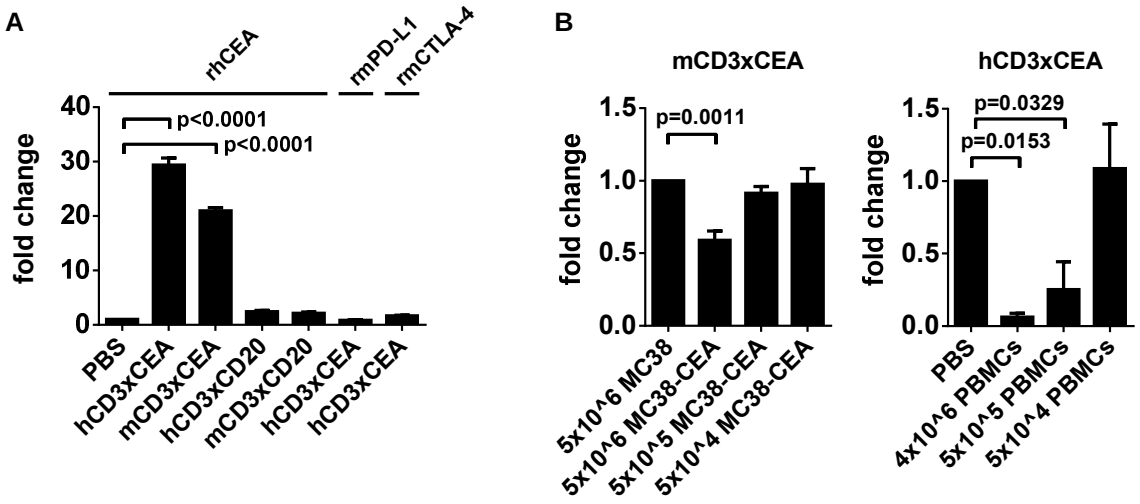

Figure 4.8: Evaluation of BiTE binding specificity by ELISAs. (**A**) Sandwich ELISA: Binding of CEA-targeting purified BiTEs to recombinant human CEA was analyzed. CD20-targeting BiTEs and non-relevant protein (recombinant murine PD-L1 and CTLA-4) served as specificity controls. PBS was included as negative control. (**B**) Competitive ELISAs: Binding of purified BiTEs to cell-expressed target antigen was evaluated (MC38-CEA: human CEA, PBMCs: human CD3). Non-target cells or PBS served as internal controls. (**A, B**) Absorbance values were normalized to PBS or non-target cells and are shown as fold change over controls. Mean of triplicate samples with standard deviation is shown. Statistical analysis was performed by one-way ANOVA and p values were adjusted for multiple comparisons by Dunnett's test.

Furthermore, we investigated BiTE binding to cell-expressed target antigen by magnetic pull-down of BiTE-bound target cells. vpBiTEs were incubated with target cells and free BiTE was removed. Remaining, cell-bound BiTEs were labeled with anti-HA-biotin antibodies and subsequently with anti-biotin magnetic beads. Labeled cells were separated from unlabeled cells by magnetic-activated cell sorting (MACS). Cells in the flow through (unlabeled cells) and eluted from the MACS columns (labeled cells) were lysed and analyzed by Western blot using anti-β-actin antibody (Figure 4.9). MC38-CEA cells were detected in the BiTE-labeled fractions, while there were no cells detectable in the corresponding fraction with MC38 cells. In all flow through fractions unlabeled cells were detectable.

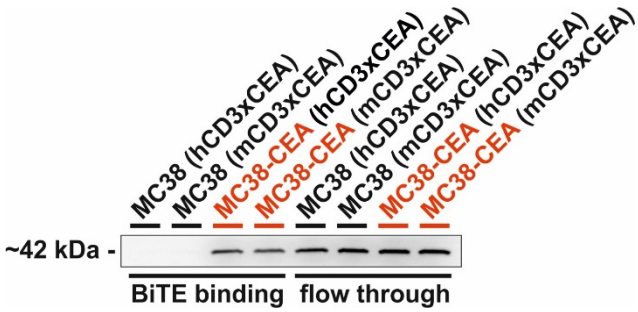

Figure 4.9: Magnetic pull-down of BiTE-labeled target cells. Binding of CEA-targeting BiTEs to MC38-CEA target cells was evaluated. Target cells were incubated with CEA-targeting purified BiTEs. MC38 cells were included as specificity controls. BiTE-bound cells were magnetically labeled (via the BiTE N-terminal HA-tag) and separated from unlabeled cells on a MACS separator. Flow through and magnetically retained fractions were collected separately and lysed. Lysates were analyzed by Western blot using anti-β-actin antibody. Left panel: BiTE binding to cells in the magnetically retained fraction. Right panel: Unlabeled cells in the flow through fraction. Red print indicates the CEA-expressing target cells.

The final BiTE binding test to cell-expressed target antigen was evaluated by flow cytometry (Figure 4.10). Human CD3-targeting BiTEs bound to CD3+ T cells within human peripheral blood mononuclear cells (PBMCs). *Vice versa*, murine CD3-targeting BiTEs bound to CD3+ T cells within murine splenocytes. Likewise, mCD3xCEA BiTE bound to MC38-CEA cells, but not to MC38 cells. Similarly, hCD3xCEA BiTE bound to CEA-expressing TSCs. The level of BiTE binding to TSCs correlated with the CEA-expression level, as determined by flow cytometric analysis using anti-CEA-PE antibody (Figure 4.10 D).

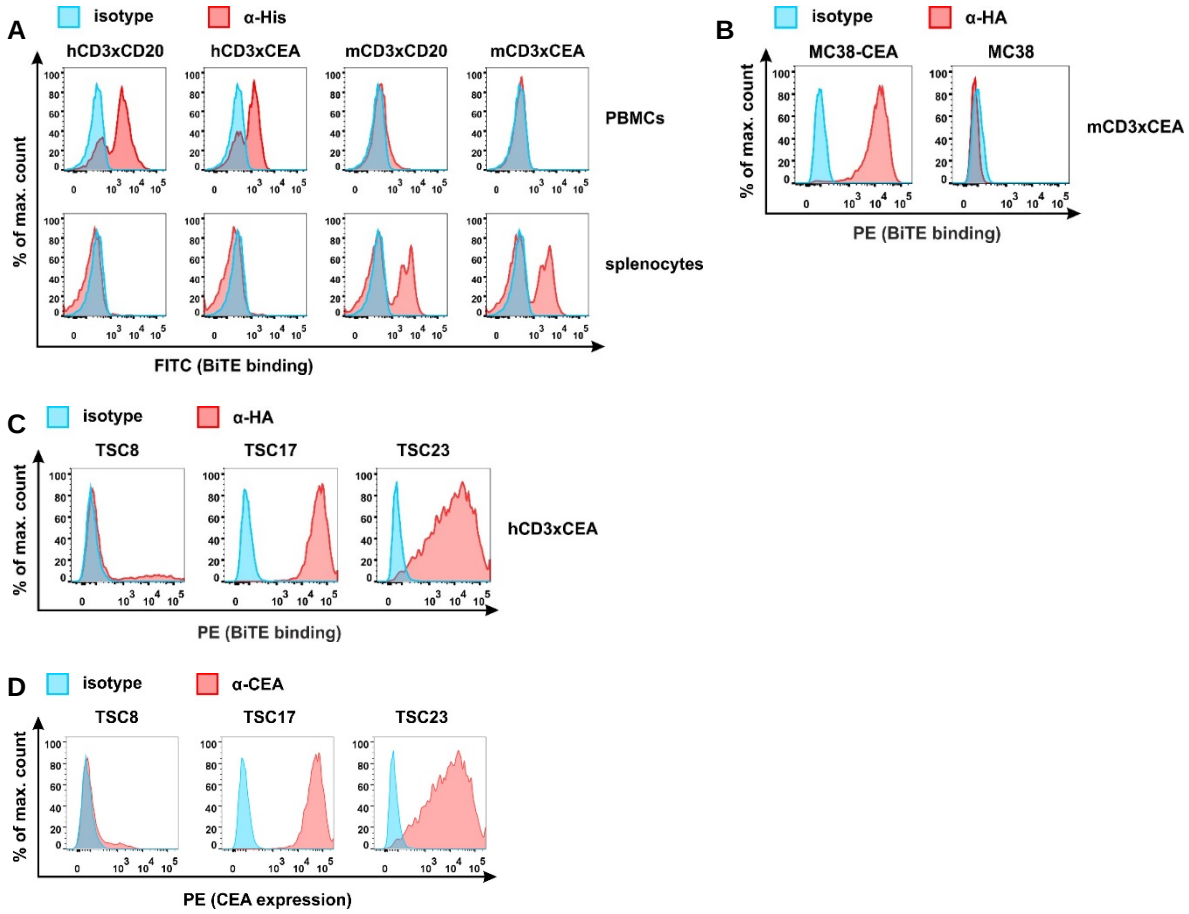

Figure 4.10: Flow cytometric analysis of BiTE binding. (**A**) Purified BiTEs were incubated with human PBMCs and murine splenocytes, respectively. BiTE binding to T cells was detected by anti-His-FITC antibody. (**B**) MC38-CEA cells were incubated with purified mCD3xCEA BiTE. MC38 cells served as specificity control. (**C**) Purified hCD3xCEA BiTEs were incubated with single-cell suspensions of TSC8, TSC17 or TSC23. (**B, C**) BiTE binding to tumor cells was detected by anti-HA-PE antibody. (**D**) Endogenous CEA-expression levels of TSCs were investigated using an anti-CEA-PE antibody. (**A-D**) Overlay histograms of detection and isotype antibodies are shown. Each peak is normalized to its mode.

4.3.3. BiTE-mediated T Cell Cytotoxicity

The potential of vpBiTEs to mediate T cell cytotoxicity was evaluated using lactate dehydrogenase (LDH) release assays. Therefore, vpBiTEs were added to co-cultures of tumor cells and T cells. BiTE-mediated T cell cytotoxicity was assessed by LDH release of lysed tumor cells and non-target tumor cells or control BiTEs were used as specificity controls.

hCD3xCEA vpBiTE directed cytolytic activity of T cells within human PBMCs against MC38-CEA cells in a concentration-dependent manner (Figure 4.11 A). Concurrently, hCD3xCD20 BiTE-engaged T cells did not lyse MC38-CEA cells. Highest specific lysis of 52 – 59 % was observed at hCD3xCEA BiTE concentrations >100 ng/ml.

T cells were isolated from murine splenocytes by negative selection (mTCs). mCD3xCEA vpBiTE mediated mTC cytotoxicity against MC38-CEA cells in a concentration-dependent manner, comparable to hCD3xCEA BiTE and human PBMCs (Figure 4.11 B). Highest specific lysis of 24 - 25 % was observed at mCD3xCEA BiTE concentrations >100 ng/ml. mCD3xCEA BiTE-engaged mTCs did not lyse non-target cells of the parental cell line MC38. Furthermore, Trp-2-specific murine cytotoxic T lymphocytes (mCTLs) were re-directed by mCD3xCEA vpBiTE to lyse Trp-2 negative MC38-CEA cells (Figure 4.11 C). Activated mCTLs demonstrated high specific lysis of 46 – 58 % over the entire range of tested effector to target cell (E:T) ratios, while MC38 cells were not lysed.

hCD3xCEA vpBiTE also directed PBMC-derived human T cells against CEA-expressing TSCs (Figure 4.11 D). Specific lysis occurred in a concentration-dependent manner. Highest specific lysis was observed at 1 µg/ml hCD3xCEA (37 % TSC8, 40 % TSC17, 35 % TSC23). Notably, increased baseline levels of LDH release from TSCs in the presence of hCD3xCD20 vpBiTE were observed. However, these levels remained significantly lower compared to hCD3xCEA containing samples at BiTE concentrations >100 ng/ml.

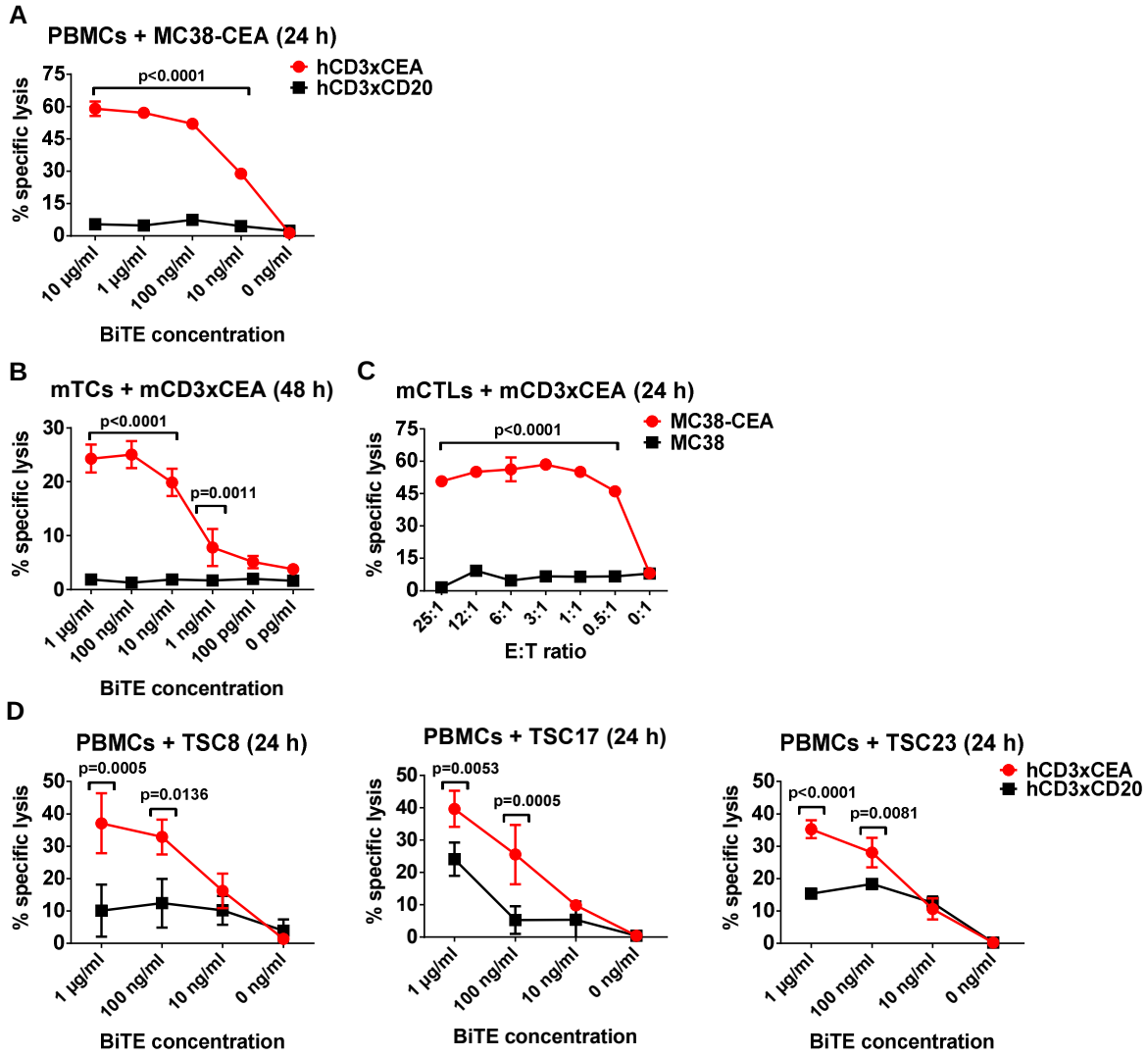

Figure 4.11: BiTE-mediated T cell cytotoxicity *in vitro*. Purified BiTEs were added to co-cultures of tumor cells and T cells. BiTE-mediated cytotoxicity was assessed by lactate dehydrogenase (LDH) release assays. (**A**) Human PBMCs were co-cultured with MC38-CEA cells at a ratio of 50:1. BiTEs were added at indicated concentrations. hCD3xCD20 BiTE served as specificity control. (**B**) Murine T cells (mTCs) isolated from splenocytes were co-cultured with MC38-CEA cells at a ratio of 12:1. mCD3xCEA BiTE was added at indicated concentrations. (**C**) Murine cytotoxic T lymphocytes (mCTLs) were co-cultured with MC38-CEA cells at indicated ratios. mCD3xCEA BiTE was added at a concentration of 1 µg/ml. (**B, C**) MC38 cells were included as specificity controls. (**D**) Human PBMCs were co-cultured with TSCs at a ratio of 50:1. hCD3xCEA BiTE was added at indicated concentrations. hCD3xCD20 BiTE served as specificity controls. (**A-D**) Mean of triplicate samples with standard deviation is shown. Statistical analysis was performed by two-way ANOVA and p values were adjusted for multiple comparisons by Sidak's test.

Cytokines are a hallmark of T cell activation and cytotoxicity. Thus, we analyzed cytokines secreted by BiTE-engaged T cells in the supernatant of co-cultures with tumor cells. Cytokine concentrations were quantified using a cytokine bead array (CBA). Low cytokine levels (shown are IFN-γ, TNF and IL-2) were secreted by T cells isolated from murine splenocytes in the presence of MC38-CEA cells and mCD3xCEA vpBiTE (Figure 4.12 A). TNF levels in the supernatant were significantly increased, compared to supernatants from co-cultures with MC38 cells. Levels of IFN-γ and IL-2 were not significantly increased. T cells within human PBMCs secreted high levels of cytokines in co-cultures with TSCs and hCD3xCEA vpBiTE (Figure 4.12 B). Significantly increased levels of IFN-γ, TNF and IL-2 were detected, compared to co-cultures with hCD3xC20 vpBiTE. Highest cytokine levels were observed in co-cultures with TSC8.

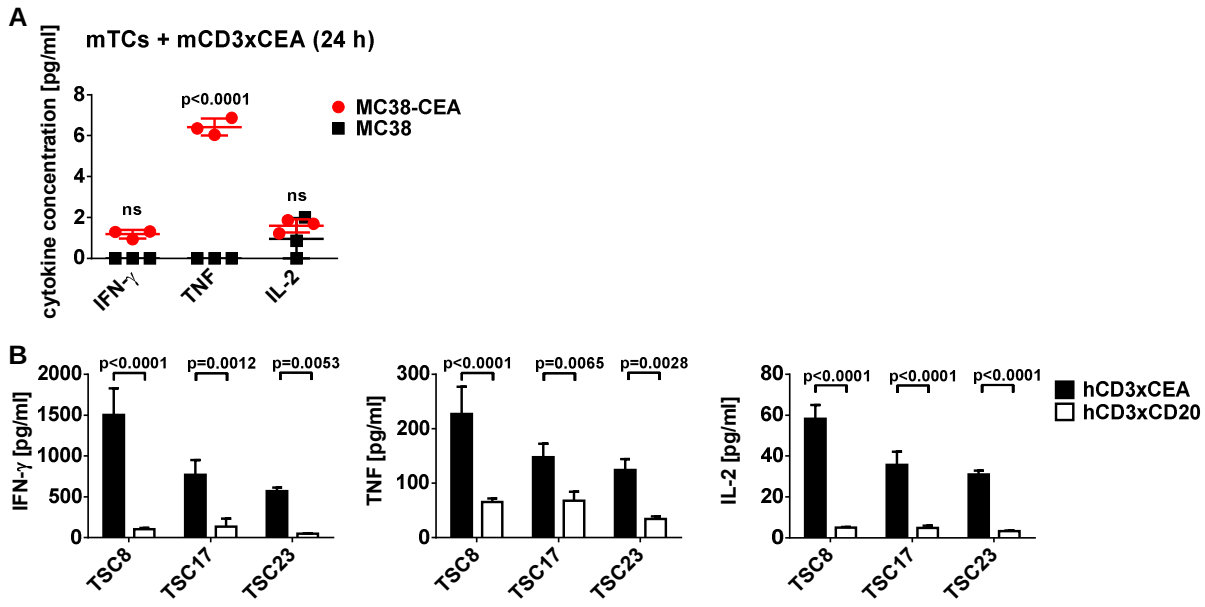

Figure 4.12: BiTE-mediated cytokine secretion by T cells *in vitro*. Purified BiTEs were added to co-cultures of tumor cells and T cells. Secreted cytokines were quantified by cytokine bead arrays. (**A**) Murine T cells isolated from splenocytes were co-cultured with MC38-CEA cells at a ratio of 50:1. mCD3xCEA BiTE was added at a concentration of 1 µg/ml. MC38-CEA cells served as specificity control. (**B**) Human PBMCs were co-cultured with indicated TSCs at a ratio of 50:1. hCD3xCEA BiTE was added at a concentration of 1 µg/ml. hCD3xCD20 BiTE served as specificity control. (**A, B**) Concentrations of IFN-γ, TNF and IL-2 in co-culture supernatants after 24 hours are shown. Mean of triplicate samples with standard deviation is shown. Statistical analysis was performed by two-way ANOVA and p values were adjusted for multiple comparisons by Sidak's test.

4.4. Therapeutic Efficacy of MV-BiTE in Immunocompetent Mice

The therapeutic potential of MVs encoding BiTEs was evaluated in the syngeneic tumor models of MC38-CEA and B16-CD20-CD46. Tumor cells were implanted subcutaneously into the right flanks of immunocompetent C57BL/6 mice. When tumors reached a mean volume of 40-50 mm^3, mice were treated with intratumoral injections of $1x10^6$ ciu of MV-BiTE or carrier fluid (OptiMEM) on four or five consecutive days (n = 20 per group). Tumor progression and survival of mice was followed for 10 mice per group. Endpoints were defined as tumor volumes of >1,000 mm^3, tumor diameter > 15 mm, tumor ulceration, tumor bleeding or severe signs of illness. Mice fulfilling one or more of the predefined endpoints were sacrificed. Furthermore, 10 mice per group were sacrificed 24 hours after the last treatment to analyze treatment-related immunostimulatory effects.

In the MC38-CEA model, efficacy of MV encoding the CEA-targeting BiTE was compared to MV-mCD3xCD20 and mock treatment (carrier fluid) (Figure 4.13). Both MV-BiTE treatments prolonged survival as compared with survival of mock-treated mice. On day 10 after tumor implantation, the first mouse (mock treatment group) was sacrificed because of tumor ulceration with a tumor volume of 227 mm^3. The mean tumor volume of mock-treated mice on day 10 was 105 mm^3. Tumor growth of mice treated with MV-BiTE was delayed and reached volumes of 60 mm^3 (MV-mCD3xCEA) and 44 mm^3 (MV-mCD3xCD20) on day 10 post implantation (Figure 4.13 A). Median survival (5/10 mice alive) of mock-treated mice was 15 days, compared to 41 days for mice treated with MV-mCD3xCD20. Median survival for mice treated with MV-mCD3xCEA was not reached. 7/10 mice treated with MV-mCD3xCEA experienced durable remissions, compared to 4/10 mice treated with MV-mCD3xCD20 and 0/10 mock-treated mice. Frequencies of reached endpoints were 16 % tumor volume and 84 % tumor ulceration. MV-BiTE treatments led to significantly prolonged survival with $p < 0.001$ for MV-mCD3xCEA and $p < 0.01$ for MV-mCD3xCD20, as compared to mock treatment. However, survival of MV-mCD3xCEA-treated mice was not significantly prolonged compared to MV-mCD3xCD20-treated mice.

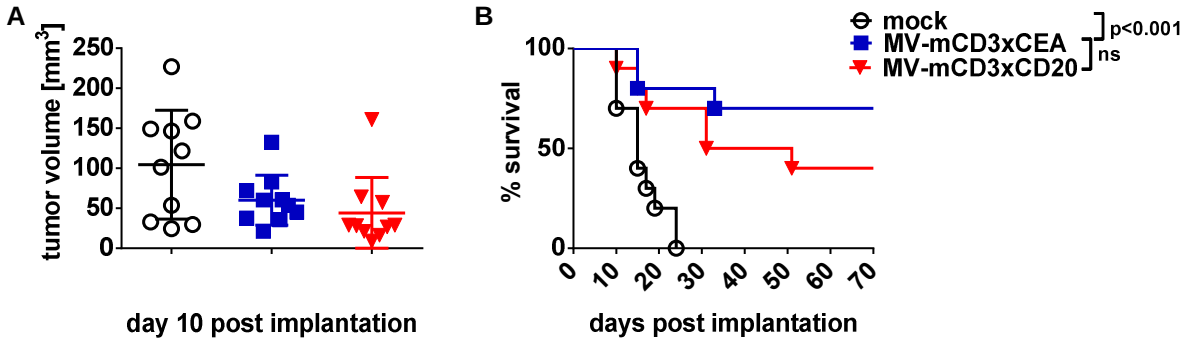

Figure 4.13: Therapeutic efficacy of MV-BiTE against murine MC38-CEA. $1x10^6$ MC38-CEA cells were subcutaneously implanted into the flank of C57BL/6 mice. Mice were treated with intratumoral injections of carrier fluid (mock) or $1x10^6$ cell infectious units of indicated MV-BiTE on days 4, 5, 6, and 7 post implantation (n = 10 mice/group). (**A**) Tumor volumes of individual mice 10 days post implantation. Mean values with standard deviations are indicated. (**B**) Kaplan-Meier survival analysis. Log-rank (Mantel-Cox) test was performed for statistical comparison of survival curves and p values were corrected for multiple comparisons by the Bonferroni method.

In the B16-CD20-CD46 model, efficacy of MV-mCD3xCD20 was compared to MV-mCD3xCEA, unmodified MV and mock (carrier fluid) (Figure A.3).* Treatment with MV-mCD3xCEA and unmodified MV similarly prolonged survival, as compared with mock treatment. Median survival of mock-treated mice was 16.5 days, compared to 23.5 days for mice treated with MV-mCD3xCEA and 25 days for mice treated with unmodified MV. In this model, treatment with MV-mCD3xCD20 significantly prolonged survival, compared to treatment with MV-mCD3xCEA ($p < 0.05$, median survival: 30 days). Interestingly, treatment with purified BiTE only did not result in prolonged survival, compared to mock treatment (median survival: 18 days *vs*. 15 days). However, treatment with UV-inactivated MV-mCD3xCD20 showed similar therapeutic effects as treatment with non-irradiated MV-mCD3xCD20 ($p < 0.001$ compared to purified BiTE treatment, respectively) (Figure A.4).† Furthermore, MV-mCD3xCD20 treatment conferred protective antitumor immunity against the parental cell line B16 (Figure A.5).‡

* Results generated by Johannes Heidbüchel
† Results generated by Johannes Heidbüchel
‡ Results generated by Tobias Speck

Plasma levels of BiTE in peripheral blood of MC38-CEA-bearing mice treated with MV-BiTE were analyzed to assess systemic exposure of injected or *de novo* synthesized BiTE. Blood was drawn 2 hours and 24 hours after the fourth treatment. Blood plasma was analyzed by ELISA with recombinant human CEA. BiTE plasma levels in MV-BiTE-treated mice were not elevated, as compared to mock-treated mice (Figure 4.14).

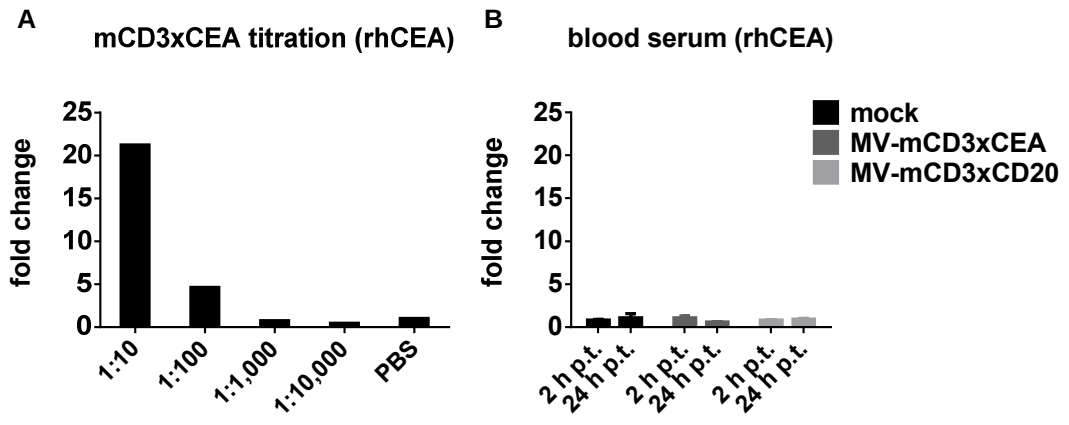

Figure 4.14: BiTE plasma levels after MV-BiTE treatment of MC38-CEA-bearing mice. MC38-CEA cells were subcutaneously implanted into the flank of C57BL/6 mice. Mice were treated with intratumoral injections of carrier fluid (mock) or indicated MV-BiTE on four consecutive days. (**A**) Purified mCD3xCEA BiTE was titrated and analyzed by ELISA with recombinant human (rh)CEA. (**B**) Blood was drawn from MC38-CEA-bearing mice 2 and 24 hours after the fourth treatment. Blood plasma was analyzed by ELISA with rhCEA of the indicated treatment groups (n = 3-5 mice/group). (**A, B**) Absorbance values were normalized to PBS and are shown as fold change over PBS. Mean of three to five samples with standard deviation is shown.

4.4.1. Analysis of MV-BiTE Mediated Immunostimulatory Effects

Tumor-infiltrating lymphocytes (TILs) and intratumoral cytokine concentrations were analyzed to investigate the immunostimulatory effects mediated by MV-BiTE treatment. Tumors from 10 mice per group were explanted 24 hours after the last day of treatment (as described in chapter 4.4). Explanted tumors were processed to single-cell suspensions and prepared for analysis of TIL differentiation and activation by flow cytometry (Figure 4.15 A). The gating strategy is shown in Figure A.6. Notably, high percentage of lymphocytes were found in MC38-

CEA tumors of all treatment groups, including mock treatment. Increased percentage of lymphocytes were found in MV-BiTE-treated tumors (MV-mCD3xCEA: 33 % of live cells, MV-mCD3xCD20: 35 % of live cells), as compared with mock-treated tumors (28 % of live cells). However, only MV-mCD3xCD20 treatment significantly increased percentage of infiltrating lymphocytes ($p = 0.0113$). The ratio of CD8+ to CD4+ T cells was approximately 2-fold higher for both MV-BiTE treatment groups, as compared with mock treatment. At the same time, the expression of the activation marker CD69 on CD8+ T cells was increased after MV-BiTE treatment, compared to mock treatment (60-61 % *vs.* 54 %) and the differentiation marker CD25 on CD4+ T cells was decreased (32-38 % *vs.* 48 %). Notably, most changes in TIL populations, activation or differentiation remained statistically not significant.

In contrast, less lymphocytes than 1 % of live cells were detected in mock-treated B16-CD20-CD46 tumors (Figure A.7).[*] Subtle elevated percentage of lymphocytes were found in MV-mCD3xCEA-treated tumors (4 %, 0.7 to 9 % of live cells) and significantly increased numbers after MV-mCD3xCD20 treatment (16 %, 2.5 to 46 % of live cells, $p = 0.0003$), as compared with mock treatment. The CD8+ to CD4+ T cell ratio of 1.2 in mock-treated tumors was similar to the ratio found in mock-treated MC38-CEA tumors. The ratio was increased for MV-mCD3xCEA-treated B16-CD20-CD46 tumors (ratio of 2.9) and significantly increased after MV-mCD3xCD20 treatment (ratio of 8.8).

Intratumoral concentrations of specific cytokines were analyzed by CBA assays. Protein levels of IL-2, IL-4, IL-6, IL-10, TNF, IFN-γ, and IL-17A were simultaneously quantified in tumor samples to investigate the expression of Th1, Th2, or Th17 cytokines. In the MC38-CEA model, increased levels of IFN-γ were obtained in MV-BiTE-treated tumors (Figure 4.15 B). However, significantly increased levels of IFN-γ were obtained only in MV-mCD3xCD30-treated tumors. Levels of IL-2, IL-4, IL-6, IL-10, TNF, and IL-17A in MV-BiTE-treated tumors were elevated as well, however were not significantly increased, as compared with mock-treated tumors. In general, highest cytokine levels were detected in MV-mCD3xCD20-treated tumors. Except for IL-10 concentrations, which was highest for MV-mCD3xCEA-treated tumors.

[*] Results generated by Johannes Heidbüchel

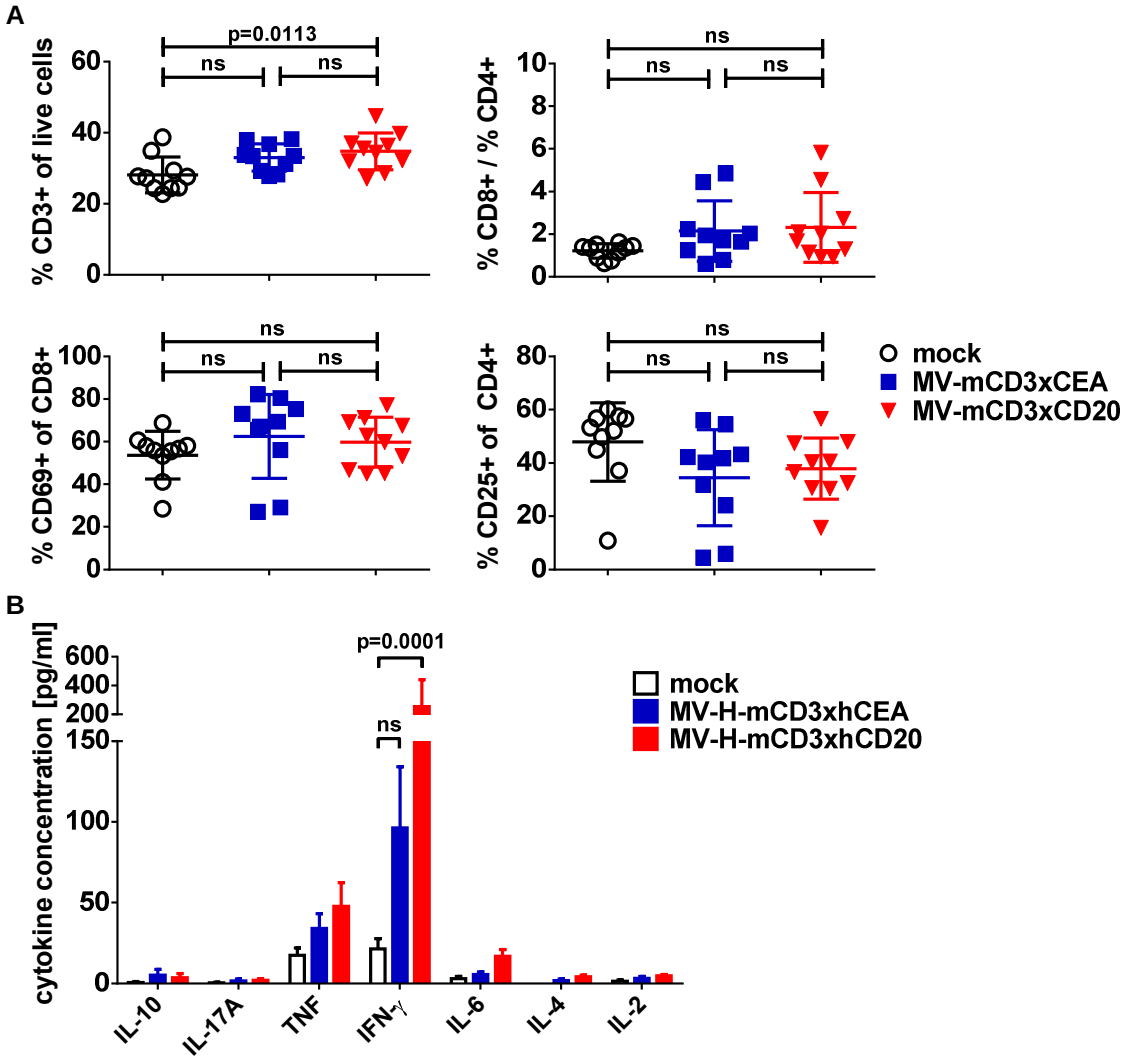

Figure 4.15: Immunostimulatory effects of MV-BiTE treatment in MC38-CEA bearing mice. MC38-CEA cells were subcutaneously implanted into the flank of C57BL/6 mice. Mice were treated with intratumoral injections of carrier fluid (mock) or the indicated MV-BiTE on four consecutive days. Tumors were explanted one day after the last treatment. (**A**) Analysis of tumor-infiltrating lymphocytes (TILs). Single-cell suspensions were prepared for flow cytometric analysis of TIL subpopulations (*n* = 10 mice/group). Mean values with standard deviation are shown. Statistical analysis was performed by one-way ANOVA and p values were adjusted for multiple comparisons by Tukey's test. (**B**) Cytokine profiles of MV-BiTE-treated mice. Intratumoral cytokines were quantified by cytokine bead arrays. Mean values with standard deviation are shown. Statistical analysis was performed by two-way ANOVA and p values were adjusted for multiple comparisons by Dunnett's test.

In the B16-CD20-CD46 model, intratumoral cytokine concentrations after mock, MV-mCD3xCD20 and MV-mCD3xCEA treatment were assessed (Figure A.8).* Both MV-BiTE treatments significantly increased levels of IFN-γ, as compared with mock treatment ($p < 0.0001$). In addition, TNF concentrations in MV-mCD3xCD20-treated tumors were significantly increased, compared to mock-treated tumors ($p = 0.0015$). In general, elevated cytokine concentrations were found in MV-BiTE-treated tumors, as compared with mock-treated tumors, except for IL-6 concentrations.

4.5. Therapeutic Efficacy of MV-BiTE in TSC Xenografts

The therapeutic efficacy of MV-BiTE against CEA-expressing human colon cancer xenografts was evaluated. Single-cell suspensions of $1x10^6$ TSC8, TSC17 and TSC23 were implanted subcutaneously into the right flanks of immunocompromised NSG mice. Efficacy of MV-hCD3xCEA with the transfer of PBMCs was compared to mock, PBMCs only and MV-hCD3xCEA only treatments. Beforehand, healthy donor-derived PBMCs were tested for alloreactive T cell responses against the TSCs *in vitro* and non-reactive donors were selected. When tumors reached a mean volume of 100 mm^3, mice received intratumoral injections of $1x10^6$ ciu MV-hCD3xCEA on four consecutive days. On the first day of treatment, mice additionally received $1x10^7$ healthy donor-derived PBMCs or carrier fluid (PBS) intratumorally. Notably, TSC17-bearing mice received only $3.3x10^6$ PBMCs due to an unexpectedly low-yield in PBMC isolation. Tumor progression and survival were followed for 10 mice per group. Predefined endpoints were tumor volumes of >1,000 mm^3, tumor diameter of > 15 mm, tumor ulceration, tumor bleeding or severe signs of illness.

Treatment with MV-hCD3xCEA only significantly prolonged survival of TSC8-bearing NSG mice, as compared to treatments with mock or PBMCs only ($p < 0.001$) (Figure 4.16 A, B). Treatment with MV-hCD3xCEA and the transfer of PBMCs significantly prolonged survival, as compared to treatment with MV-hCD3xCEA only ($p < 0.01$). The first mouse (treatment with PBMCs only) was sacrificed on day 17 after TSC8 implantation with a tumor volume of 1,023 mm^3. On day 17, the mean tumor volume of mice treated with PBMCs only was largest

* Results generated by Tobias Speck

with 596 mm^3, compared to 345 mm^3 (mock), 237 mm^3 (MV-hCD3xCEA only) and 144 mm^3 (MV-hCD3xCEA + PBMCs) (Figure 4.16 A). Median survival of mock-treated mice was 22 days, compared to 20 days (PBMCs only), 36 days (MV-hCD3xCEA only) and 64 days (MV-hCD3xCEA + PBMCs) (Figure 4.16 B). Individual tumor growth curves are shown in Figure 4.17 A. Reached endpoints were tumor volume (90 %) and tumor diameter (10 %).

For the TSC17 xenograft model, treatment with MV-hCD3xCEA only did not prolong survival and transfer of PBMCs only even significantly shortened survival as compared to mock treatment ($p < 0.05$). However, treatment with MV-hCD3xCEA and the transfer of PBMCs prolonged survival, compared to mock treatment (statistically not significant) (Figure 4.16 D). First mice reached the tumor diameter endpoint on day 33 after TSC17 implantation (mock treatment and PBMCs only). Mean tumor volumes on day 33 were 402 mm^3 (mock), 617 mm^3 (PBMCs only), 313 mm^3 (MV-hCD3xCEA only) and 293 mm^3 (MV-hCD3xCEA + PBMCs) (Figure 4.16 C). Median survival of mock-treated mice was 48 days, compared to 39.5 days (PBMCs only), 52.5 days (MV-hCD3xCEA only) and 66.5 days (MV-hCD3xCEA + PBMCs). Individual tumor growth curves are shown in Figure 4.17 B. The frequencies of reached endpoints were 67 % tumor volume and 33 % tumor diameter.

In the TSC23 model, treatment with MV-hCD3xCEA only significantly prolonged survival, as compared with mock treatment ($p < 0.01$) (Figure 4.16 E, F). Treatment with PBMCs only did neither significantly prolong nor shorten survival, compared to mock treatment and MV-hCD3xCEA only. Notably, 50 % of TSC23-bearing mice treated with PBMCs only developed graft-versus-host disease (GvHD). Mice suffering from GvHD showed severe signs of illness, which coincided with tumor shrinkage. However, treatment with MV-hCD3xCEA with the transfer of PBMCs significantly prolonged survival, as compared to treatment with MV-hCD3xCEA only ($p < 0.001$). Interestingly, no mice treated with MV-hCD3xCEA with the transfer of PBMCs developed GvHD. On day 19 after TSC23 implantation, the first mouse from the mock treatment group reached the tumor volume endpoint with 1,082 mm^3. The mean tumor volume of mock-treated mice on day 19 was 514 mm^3. Again, the mean tumor volume of mice treated with PBMCs only was largest with 533 mm^3, as compared to mock-treated mice, MV-hCD3xCEA only (309 mm^3) and MV-hCD3xCEA with the transfer of PBMCs (166 mm^3) (Figure 4.16 E). Median survival after mock treatment was 28 days, compared to 36 days (PBMCs only), 41 days (MV-hCD3xCEA only) and 65.5 days (MV-hCD3xCEA + PBMCs)

(Figure 4.16 F). Individual tumor growth curves are shown in Figure 4.17 C. The frequencies of reached endpoints were 57 % tumor volume, 27 % tumor diameter and 17 % severe signs of illness.

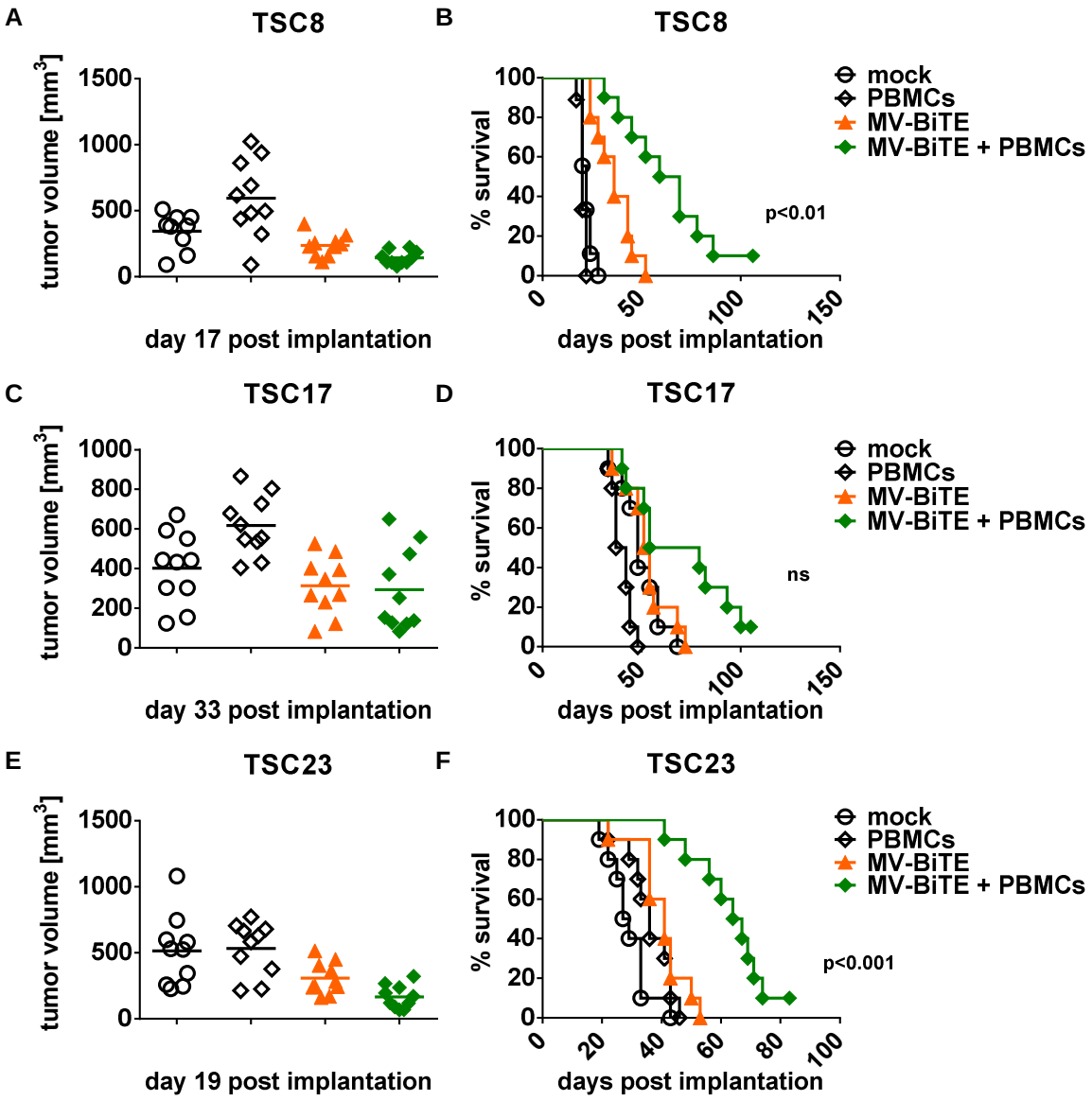

Figure 4.16: Therapeutic efficacy of MV-BiTE against human colon cancer xenografts. $1x10^6$ tumor spheroid cultures (TSCs) were subcutaneously implanted into the flank of NSG mice. Mice were treated with intratumoral injections of carrier fluid (mock) or $1x10^6$ cell infectious units of MV-hCD3xCEA on four consecutive days (n = 9-10 mice/group). On the first day of treatment, TSC8- and TSC23-bearing mice additionally received an intratumoral transfer of $1x10^7$ human PBMCs. TSC17-bearing mice received a transfer of $3.3x10^6$ PBMCs. (**A, C, E**) Tumor volumes of individual mice. On day 17 (TSC8), day 33 (TSC17) or day 19

(TSC23) post implantation first tumors reached one of the predefined endpoints and the respective mice were sacrificed. Mean values are indicated. (**B, D, F**) Kaplan-Meier survival analyses. Statistical comparison between MV-BiTE with the transfer of PBMCs and MV-BiTE only treatment groups is indicated in the graphs. Log-rank (Mantel-Cox) test was performed for statistical comparison of survival curves and p values were corrected for multiple comparisons by the Bonferroni method.

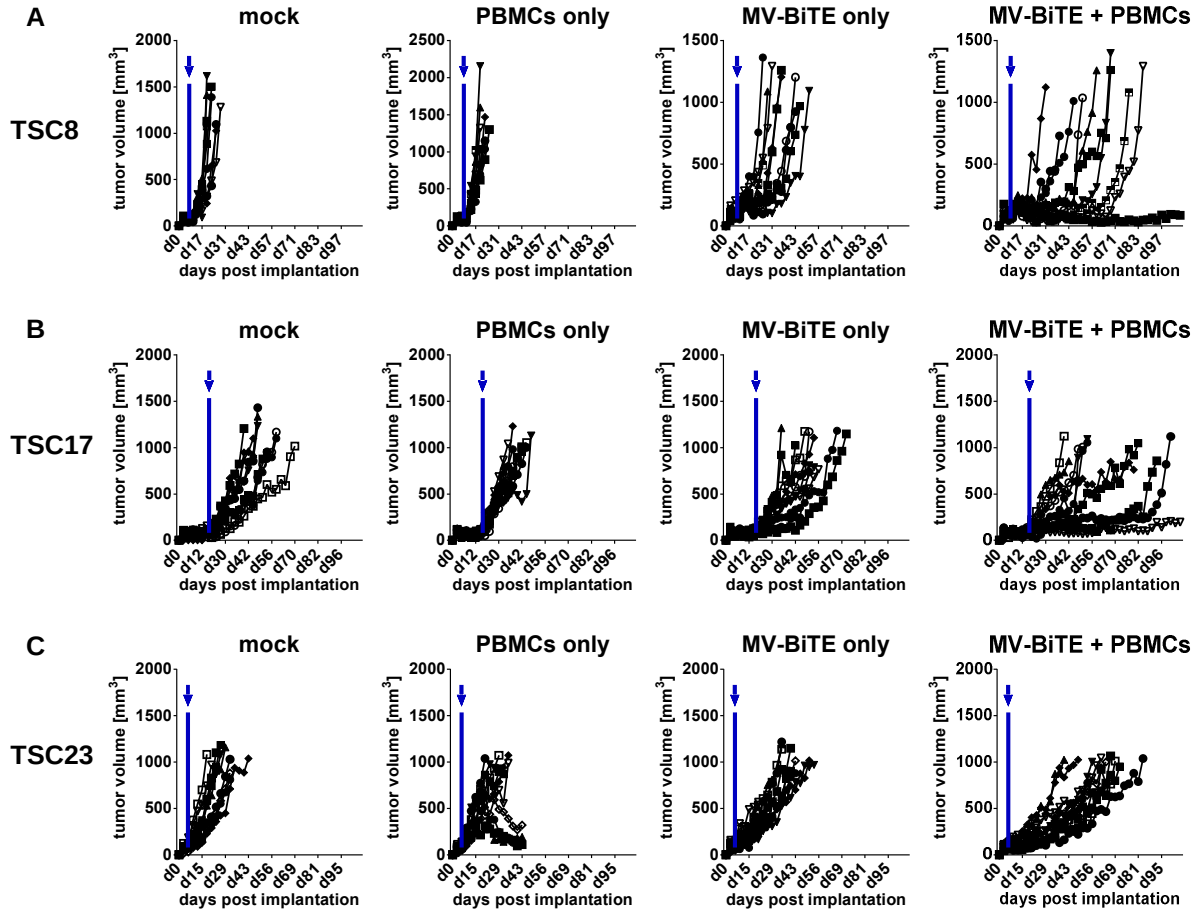

Figure 4.17: Individual tumor growth of MV-BiTE-treated human colon cancer xenografts. Tumor spheroid cultures (TSCs) were implanted subcutaneously into the flank of NSG mice. When tumors reached a mean volume of 100 mm^3, mice were treated with intratumoral injections of carrier fluid (mock) or MV-hCD3xCEA on four consecutive days (*n* = 9-10 mice/group). On the first day of treatment, TSC8- and TSC23-bearing mice additionally received an intratumoral transfer of $1x10^7$ human PBMCs. TSC17-bearing mice received a transfer of $3.3x10^6$ PBMCs. (**A-C**) Individual tumor growth curves of (**A**) TSC8-bearing mice, (**B**) TSC17-bearing mice and (**C**) TSC23-bearing mice. Initiation of treatment is indicated by blue arrows and lines.

In general, no signs of BiTE-related toxicities were observed. BiTE plasma levels in peripheral blood of mice treated with MV-BiTE were evaluated 24 hours after the fourth treatment and compared to PBMCs only-treated mice and the BiTE content of one dose MV-hCD3xCEA. BiTE plasma levels of MV-BiTE-treated mice remained below detection limit (Figure 4.18).

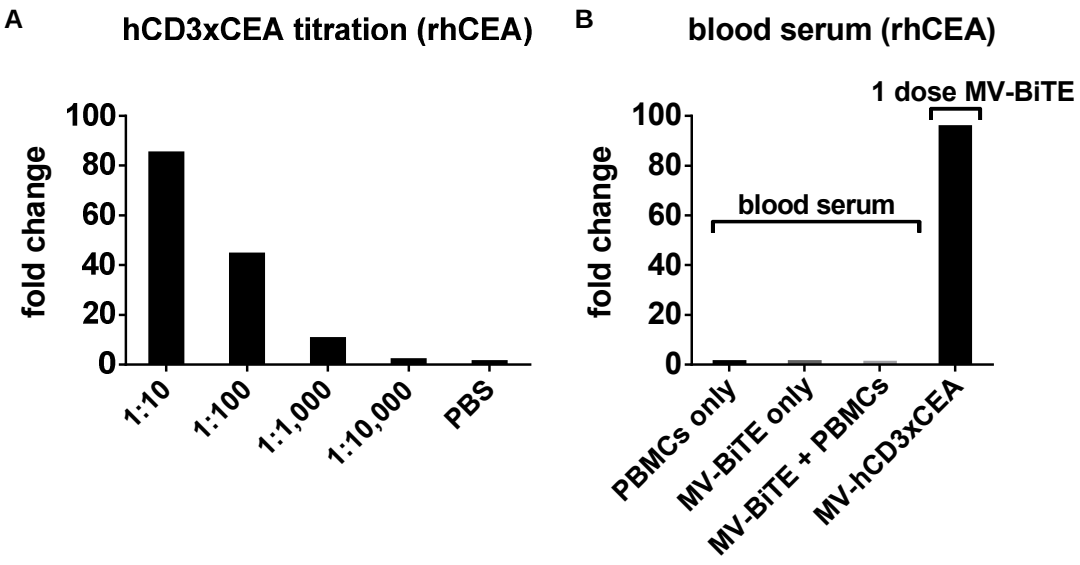

Figure 4.18: BiTE plasma levels after treatment of TSC23-bearing mice with MV-BiTE. TSC23 cells were implanted subcutaneously into the flank of NSG mice. Mice were treated with intratumoral injections of carrier fluid (mock) or MV-hCD3xCEA on four consecutive days. On the first day of treatment, mice additionally received an intratumoral transfer of $1x10^7$ human PBMCs. (**A**) Purified hCD3xCEA BiTE was titrated and analyzed by ELISA with recombinant human (rh)CEA. (**B**) Blood was drawn from TSC23-bearing mice 24 hours after the fourth treatment. Blood plasma was analyzed by ELISA with rhCEA for the indicated treatment groups (n = 5 mice/group). (**A, B**) Absorbance values were normalized to PBS and are shown as fold change over PBS.

5. Discussion

5.1. The Promise of Cancer Immunovirotherapy

The primary choice of treatment for many patients with localized tumor diseases remains surgery (*158*). For non-localized tumor diseases, systemic cancer therapies are required such as cytotoxic chemotherapy, hormonal agents or targeted therapy (*159*). However, long-term treatment success is limited to a minority of patients or to a few tumor diseases with particular mutations. In recent years, immunotherapy has become a major field of research in modern oncology. Immune checkpoint inhibitory antibodies, adoptive T cell therapies and vaccines have provided proof for the therapeutic potential of our body's immune system to fight cancers (*160*).

Oncolytic viruses (OVs) selectively infect and lyse tumor cells, which can result in massive tumor debulking (*132, 152, 153, 161-165*). Besides direct oncolysis, OVs have been recognized as potent immunostimulatory agents in the past decade (*166*). The immunostimulatory effects of the viral infection and oncolytic "*in situ* vaccination" may even induce systemic antitumor immunity (*166*). This promise of natural and genetically engineered OVs is currently being explored in clinical studies worldwide (*96, 167-180*). Noteworthy, most genetic modifications aim to support the immunostimulatory activity of OVs by expression of transgenes, which encode for cytokines such as GM-CSF, IFN-β, IL-12 or tumor-associated antigens (chapter 1.4.1 and references therein).

This study reports on oncolytic measles viruses, which were engineered to encode bispecific T cell engaging antibodies (MV-BiTE). On the one hand, oncolytic MVs have been described to induce an immunogenic cell death (ICD) (*181-183*). On the other hand, BiTEs simultaneously engage local T cells and tumor cells and thereby activate the engaged T cells. Besides bystander tumor lysis, BiTE-engaged T cells have been described to secrete cytokines, which support the establishment of an antitumor immune response (chapter 1.3.4 and references therein). Thus, tumor-restricted expression of BiTEs may synergize with the oncolytic viral vector. This study demonstrates that therapeutic efficacy of oncolytic MVs can be enhanced by encoding BiTEs within the viral genome. To this end, immunocompetent mouse models and patient-derived

xenografts with the transfer of human PBMCs were employed to study MV-BiTE efficacy, mode of action and safety aspects.

5.2. Recombinant BiTE-Encoding Measles Viruses

A recombinant MV clone generated from cDNA of the Edmonston B vaccine strain was used in this study to investigate the therapeutic efficacy of MV-BiTE. Compared to other MV vaccine strains, such as Schwarz/Moraten or Zagreb, the original Edmonston B vaccine strain is less attenuated (*184*). However, the recombinant MVs derived from the Edmonston B vaccine strain have been reported to be less immunogenic in immunocompetent mice expressing human CD46, as compared with recombinant MVs derived from Schwarz strain (*185*). Reduced immunogenicity is probably a result of acquired genetic alterations. Sequence comparisons of different MV genomes revealed that viruses derived from the recombinant Edmonston B cDNA genetically diverged from the original Edmonston B vaccine strain (*185*). Several amino acid substitutions have occurred in the P/V/C proteins, which might influence viral interferon defense mechanisms and thereby affect viral replication. However, a reduced immunogenicity of the vector might delay viral clearance by the immune system and thus increase expression of the delivered transgene. Whether one particular recombinant MV vaccine strain is superior over the other strains in terms of therapeutic efficacy has not been analyzed systematically to date. Presumably, it cannot be generalized due to inter-individual differences in the patient's immune system and the tumor interferon status (*186*). On the on hand, recombinant MVs derived from the Edmonston B vaccine strain might be beneficial in tumors with highly attenuated antiviral defense mechanisms, if the encoded transgene requires higher local concentrations. On the other hand, recombinant MVs derived from the Schwarz vaccine strain might be beneficial in tumors with less attenuated antiviral defense mechanisms in order to effectively replicate. However, the more immunogenic Schwarz strain-derived MVs might be cleared by the immune system prematurely, which limits transgene expression.

The BiTE-encoding sequence lengths are approximately 1,600 base pairs. A previous study by Engeland *et al.* investigated the therapeutic efficacy of MVs encoding anti-CTLA-4 and anti-PD-L1 dimeric antibodies with a similar sequence length (*92*). Rescue of viral particles was not successful if the anti-CTLA-4 antibody sequence was inserted upstream of the *N* open reading

frame (ORF) and downstream of the *P* ORF, respectively. These insertion sites would result in strong transgene expression (*187*) and have been used to study MVs encoding smaller transgenes, such as cytokines and prodrug convertases (*76, 78, 188-190*). However, insertion of the antibody sequence downstream of the *H* ORF finally resulted in the formation of viral particles. Thus, BiTE-encoding sequences were as well inserted into an additional transcription unit (ATU) downstream of the *H* ORF. Rescue of viral particles was successful for all BiTE-encoding constructs (BiTEs: hCD3xCEA, mCD3xCEA, hCD3xCD20, mCD3xCD20).

Oncolytic efficacy depends on the dose of virus administration, which is limited for some oncolytic viruses by manufacturing issues, including MVs (*191*). Propagation of MV-BiTE resulted in titers of approximately $5x10^7$ (+/- $3x10^7$) cell infectious units (ciu)/ml and typically 20 – 25 ml of virus suspension were obtained from the third passage. The total amount of approximately $1x10^9$ ciu of MV-BiTE concentrated in 20 – 25 ml virus suspension was sufficient to conduct *in vivo* experiments. Transgene expression and oncolytic activity depend on viral replication. Therefore, virus growth kinetics of the individual MV-BiTE constructs were assessed and compared to unmodified MV. Importantly, replication of MV-BiTE was not impaired by encoding the additional transgene. Thus, similar cytopathic effects of MV-BiTE were expected and demonstrated in cell viability assays (XTTs).

5.3. Mouse Models to Study Therapeutic Efficacy of MV-BiTE

In general, murine cells are not susceptible to MV infection because they lack expression of MV entry receptors. There is no known murine homologue of human CD46 and the MV H protein is unable to bind to mouse SLAMF1 (*143*). Non-human primate cells expressing mouse nectin-4 are susceptible to MV infection, however infection is much less efficient in terms of infection rates, viral spread and the production of viral progeny, as compared to the respective cells expressing the human homologue (*121*). MV particles are able to enter murine MC38-CEA cells at a very low rate (Figure 4.2 B MC38-CEA), probably by receptor-independent mechanisms such as macropinocytosis (*192*). To generate more susceptible murine cell lines, MC38-CEA and B16-CD20 cells were stably transduced to express human CD46 using lentiviruses. B16-CD20-CD46 and MC38-CEA-CD46 were susceptible to MV infection and produced higher virus titers than compared with the respective parental cell lines. Still, murine

cells expressing human CD46 are less permissive for MV infection, as compared to Vero cells, probably, because MV has been adapted to efficiently replicate in human cells (*193, 194*). Furthermore, the MV accessory proteins C and V might be less efficient in antagonizing mouse IFN activity (*195*). Unfortunately, implanted MC38-CEA-CD46 cells were rejected by immunocompetent C57BL/6J mice. Interestingly, B16-CD20-CD46 tumor growth in C57BL/6J mice was unimpaired. MC38 is a chemically induced murine tumor model, which acquired many immunogenic mutations (*196*). The B16 tumor model spontaneously arose in a C57BL/6 mouse under the surveillance of an intact immune system (*197*). Thus, the MC38 tumor model *per se* is much more immunogenic than the B16 tumor model (*198*). The immunogenic nature of MC38 cells in combination with the expression of human CEA and human CD46 results in frequent tumor rejection while B16-CD20-CD46 tumor growth is immunologically tolerated.

As discussed above, there are major limitations to the MC38-CEA model in terms of MV infection, replication and thus transgene expression. However, it is essential to use immunocompetent models in order to study the effects mediated by an immunomodulatory drug. MV-BiTE demonstrated oncolytic activity against MC38-CEA *in vitro* (Figure 4.4). Supported by these results and because of a lack of an alternative syngeneic CEA-expressing mouse model, we decided to use MC38-CEA to investigate the therapeutic potential of MV-BiTE *in vivo*. In addition, we established patient-derived, CEA-expressing xenografts of tumor spheroid cultures (TSCs) with the transfer of unstimulated human PBMCs. On the one hand, this model neglects the complex interplay between the immune system, MV-BiTE and the immune contexture of the tumor microenvironment (TME) (type, function, density and organization of immune cells (*199*)). On the other hand, the humanized model more adequately reflects the MV-BiTE pharmacodynamics and –kinetics in terms of oncolytic activity, viral capability to replicate and spread, and *de novo* synthesis of the MV-encoded transgene.

5.4. Characterization of MV-Encoded BiTEs

Transgene expression and secretion by MV-BiTE-infected cells was validated on mRNA and protein level, respectively. Supernatants of MV-BiTE-infected cells were harvested and BiTEs were purified to enrich BiTE concentrations and to remove contaminants such as host cell-

derived proteins or nucleic acids. Notably, purification efficiency of BiTEs varied from batch to batch, which was monitored by Coomassie Blue stainings. The purification efficiency was dependent on the complexity of the culture medium. The more syncytia burst prematurely and "contaminated" the supernatant, the less efficient was the purification procedure. Therefore, indicated BiTE concentrations are not absolute but rather reflect the total protein content, including protein contaminations (estimated to 2 – 15 % contaminants by Coomassie Blue stainings).

Binding of vpBiTE to target antigen was validated by a variety of assays, including ELISAs, magnetic pull-down of BiTE-labeled cells and flow cytometry. Specificity of BiTE binding was controlled by non-relevant recombinant protein or the respective parental cell lines, which do not express the relevant tumor-associated antigen. Binding specificity was verified within the context of the selected specificity controls. Functionality of vpBiTEs was validated in LDH release assays. Therefore, vpBiTEs were added to co-cultures of immune cells and tumor cells. Tumor cells were lysed with lysis solution to assess the maximum release of LDH to define 100 % lysis. However, a limitation of the LDH release assay is the long incubation time of 24 to 48 hours. On the one side, tumor cells in the maximum LDH release control wells approximately doubled after 24 hours and doubled twice after 48 hours, respectively. On the other side, tumor cells in the experimental wells were lysed by BiTE-engaged T cells and thus, did not replicate. Expectedly, only 50 % specific lysis could be reached after 24 hours incubation time and 25 % specific lysis after 48 hours incubation time. The chromium release assay is a similar assay format to assess T cell cytotoxicity. Only the amount of chromium, which was incorporated by tumor cells in the first place can be released and measured. Thus, maximum chromium release is independent of tumor cell proliferation. On the downside, the assay setup is more elaborate and working with the radioactive chromium isotope Cr^{51} constitutes an additional safety hazard.

BiTE-mediated cytokine secretion by T cells in co-cultures with tumor cells was quantified using a cytometric bead array (CBA). In supernatants from both, murine splenocytes and human PBMCs, elevated levels of T_H1 cytokines were found. In support of these results, other studies have reported the secretion of T_H1 cytokines by BiTE-engaged T cells, as well (*34, 37, 200, 201*). T_H1 cytokines mediate pro-inflammatory effects and cellular immunity. Thus, a T_H1 polarized immune response may improve efficacy of anticancer immunotherapeutics (*202,*

203). Conclusively, this study demonstrates for the first time the feasibility to encode and express functional BiTE antibodies by negative-strand RNA viruses.

5.5. Therapeutic Efficacy of MV-BiTE

MV-BiTE treatment significantly prolonged survival of MC38-CEA-bearing mice. However, there was no significant difference between the treatment with MVs encoding the CEA-targeting and the CD20-targeting BiTE, respectively. Furthermore, MV-mCD3xCEA treatment did not significantly increase numbers, activity or cytokine expression of tumor-infiltrating lymphocytes (TILs), as compared to MV-mCD3xCD20 treatment. Apparently, the therapeutic effects resulted from MV oncolytic activity and/or from MV immunogenicity. B16-CD20-CD46 cells are more susceptible to MV infection. Thus, if the observed therapeutic effects in the MC38-CEA model resulted from MV oncolytic activity, we would expect enhanced efficacy in the B16-CD20-CD46 model. Again, MV-BiTE treatment significantly prolonged survival of B16-CD20-CD46-bearing mice. However in the B16-CD20-CD46 model, MV-mCD3xCD20 treatment significantly prolonged survival of mice, as compared to treatment with unmodified MV or MV-mCD3xCEA. Along the same lines, MV-mCD3xCD20 treatment significantly increased the number of TILs, mostly CD8+ T cells. Apparently, in the B16-CD20-CD46 model the CD20-targeting BiTE improved therapeutic efficacy of MV treatment. To further delineate the MV- and BiTE-mediated effects, we next treated B16-CD20-CD46-bearing mice with UV-inactivated MV-BiTE to abolish viral replication while the functionality of BiTE, which is present in the virus suspension, is not compromised (Figure A.9). Importantly, we did not purify the propagated recombinant MVs. The shear sensitivity and pleomorphic nature of MVs results in low recovery and purity of infectious particles after ultracentrifugation or diafiltration (*204*). For use in humans, a tangential flow filtration system (Spectrum Laboratories, Inc., CA, USA) has been developed to purify and concentrate measles viruses in accordance with good manufacturing practices (*205*). In the present study, injections of MV-BiTE always contains MV-BiTE and BiTE antibodies, which have been expressed by the MV-BiTE-infected producer cell line. Interestingly, treatment with UV-inactivated MV-mCD3xCD20 resulted in similar therapeutic effects, as compared to treatment with replication competent MV-mCD3xCD20. Thus, MV oncolytic activity is apparently not essential in the

syngeneic mouse models. Furthermore, treatment with purified mCD3xCD20 BiTE alone did not result in a meaningful therapeutic effect. Thus, the combination of the immunostimulatory effects of the replicating or non-replicating viral vector and BiTE treatment seems to recruit and activate further TILs or to stimulate local TILs to proliferate. Furthermore, MV-mCD3xCD20 treatment conferred protective antitumor immunity against the parental cell line B16. This human CD20/CD46-independent immunity indicates, that BiTE-mediated T cell cytotoxicity may lead to epitope spreading, which is supported by literature (*206, 207*).

Interestingly, the immunogenic MC38-CEA model harbors substantially higher numbers of TILs, as compared to the poorly immunogenic B16-CD20-CD46 model (mock-treated tumors: 28 % of CD3+ cells of live cells *versus* less than 1 % of CD3+ cells of live cells). Mock-treated MC38-CEA tumors developed aggressively, despite the high numbers and activation status of TILs. Apparently, the TME is highly immunosuppressive and treatment with MV-mCD3xCEA could not induce antitumor immunity. Probably, the mode of action of BiTE-mediated T cell activation is not beneficial in this model. Noteworthy, therapeutic efficacy of MVs encoding GM-CSF, anti-PD-L1 antibody or IL-12 against MC38-CEA tumors has been demonstrated in previous studies (*76, 78*). Of note, these studies used MVs retargeted to CEA (MV-anti-CEA) to establish susceptibility of MC38-CEA to MV-anti-CEA infection. Therapeutic efficacy of MV-anti-CEA encoding GM-CSF, anti-PD-L1 antibody or IL-12 was enhanced, as compared to the unmodified MV-anti-CEA encoding eGFP or the antibody constant region IgG-Fc. Thus, therapeutic efficacy must have been dependent on the mode of action of the encoded transgenes. Moreover, Veinalde *et al.* compared efficacy of CEA-targeted and non-targeted MVs encoding IL-12 (*208*). Interestingly, she obtained similar results for both viruses in terms of survival. Apparently, IL-12, as well as GM-CSF and anti-PD-L1 antibody, were able to counteract immunosuppression or T cell exhaustion and established antitumor immunity in the MC38-CEA model. In addition, considering the effects mediated by UV-inactivated MV-BiTE in the B16-CD20-CD46 model, these results support our hypothesis, that MV oncolytic activity might not be essential for therapeutic efficacy in the syngeneic mouse models.

In the patient-derived xenografts, MV-hCD3xCEA treatment with the transfer of human PBMCs prolonged survival of TSC-bearing NSG mice. Noteworthy, PBMCs were freshly isolated, neither pre-activated nor enriched for T cells. Furthermore, mice received only one transfer of PBMCs at the first day of treatment and no recombinant human cytokines were co-

administrated, which can be used to supported T cell expansion (*209, 210*). Still, MV-hCD3xCEA treatment with the transfer of PBMCs significantly prolonged survival of TSC8- and TSC23-bearing mice, as compared to MV-hCD3xCEA treatment alone. Survival of TSC17-bearing mice was prolonged as well, however statistically not significant, as compared to MV-hCD3xCEA treatment only. Of note, due to an unexpectedly low yield in PBMC isolation, TSC17-bearing mice only received 1/3 of the amount of PBMCs transferred to TSC8- and TSC23-bearing mice, respectively. Thus, the transfer of more PBMCs may have enhanced therapeutic efficacy of MV-BiTE treatment of TSC17-bearing mice.

For all three TSC xenografts, MV-BiTE treatment only delayed tumor growth, as compared to tumor growth of mock-treated mice. Interestingly, the transfer of PBMCs only increased mean tumor volumes, as compared to tumor volumes of mock-treated mice. Most likely, PBMCs did not promote tumor progression but rather caused an inflammatory swelling, which has been described for skin transplantation models in NSG mice (*211*). However, PBMC transfer with MV-BiTE treatment further delayed tumor development, as compared to MV-BiTE treatment only. This observation supports the hypothesis of a bystander effect by BiTE-mediated T cell cytotoxicity.

Interestingly, 50 % of the TSC23-bearing mice treated with the transfer of PBMCs only developed acute graft-versus-host disease (aGvHD) three to four weeks after the PBMC transfer (*212*). T cell receptors (TCRs) of human T cells do not recognize mouse MHC molecules. In GvHD-affected mice, human antigen presenting cells (APCs) probably presented mouse antigens by MHC class II molecules to CD4+ T cells (*213*). However, TSC23-bearing mice treated with PBMC transfer and MV-BiTE did not develop GvHD. Presumably, the presence of BiTEs directed the T cell activity against the tumor cells and thus prevented the development of xenogeneic GvHD. T cell activation and the release of IFNγ are known to upregulate the expression of Fas receptor and Fas ligand on both, T cells and tumor cells (*214, 215*). Thus, T cell engagement might result in activation-induced cell death (AICD) of T cells, which in turn might prevent the development of GvHD (*216*). Interestingly, TSC8- and TSC17-bearing mice, which received the transfer of PBMCs only did not show signs of acute GvHD. Median survival of TSC8-bearing mice treated with PBMCs only was 20 days after tumor implantation (= 11 days after PBMC transfer). To the contrary, median survival of TSC23-bearing mice treated with PBMCs only was 36 days after tumor implantation (= 30 days after PBMC transfer)

Considering that the development of GvHD takes about 20 to 30 days, TSC8-bearing mice reached the predefined endpoints of tumor volume or diameter before they could develop signs of GvHD. Along the same lines, median survival of TSC17-bearing mice treated with PBMCs only was 39.5 days after tumor implantation (= 22.5 days after PBMC transfer). Apparently, 50 % of the TSC17-bearing mice reached the predefined endpoints of tumor volume or diameter before they could develop signs of GvHD. The other half of the mice, which received PBMCs only, was as well sacrificed within 30 days after the transfer. Furthermore, as mentioned above, the TSC17-bearing mice only received 1/3 of the amount of PBMCs transferred to TSC8- and TSC23-bearing mice, respectively. Thus, the probability of developing GvHD may have been reduced or development of GvHD may have been delayed, as compared to TSC23-bearing mice.

5.6. Potential for Clinical Translation

Cancer immunovirotherapy has entered clinical practice with the approval of T-VEC by the FDA in 2015, an oncolytic herpes simplex virus (HSV) encoding the cytokine GM-CSF (chapter 1.3.3 and references therein). More OVs encoding immunomodulators are currently in advanced stages of clinical development and demonstrate promising results (chapter 1.4.1 and references therein). Oncolytic measles viruses offer a promising vector platform with a modular design. One or more transgenes can be inserted at various positions into the MV genome without compromising viral replication capacities or oncolytic activity (*148*). Furthermore, MV vaccines possess a proven safety record and recombinant oncolytic MVs, derived from the Edmonston vaccine strain demonstrated evidence of safety and efficacy in phase I clinical trials (*150-153*). No dose-limiting toxicities have been reported in ongoing phase I and II clinical trials to date (NCT02364713, NCT02068794, NCT00390299, NCT00450814, NCT02192775, NCT01503177, NCT01846091, NCT02700230). Furthermore, the MV H protein can be modified to ablate viral tropism for the natural cellular receptors (*217*). MVs can be retargeted to specific cellular receptors by introducing an scFv at the C-terminal end of the H protein (*218*). Thus, MV tissue specificity can be altered to enhance tumor selectivity and thereby further increase its safety profile. Additionally, tumor selectivity can be increased by introducing microRNA-target sequences into the MV genome (*219*). Thus, viral spread is

limited to tissues with an aberrant microRNA expression profile, which is often found in tumor cells (*220-224*). Considering these aspects, the MV-BiTE constructs offer a flexible vector platform in terms of tissue targeting and safety. Thus, a personalized drug can be provided, given that relevant biomarkers can be predicted or evaluated in advance to therapy. Such biomarkers would comprise tumor susceptibility to MV infection, antigen expression and miRNA expression.

The studied MV-BiTE constructs were designed in a way that the encoded scFv domains in the BiTE cassette can be exchanged by any targeting domain of choice. Thus, MV-BiTE vectors can be adapted to target any tumor surface antigen. Furthermore, several MV-BiTE vectors could be administered concurrently or sequentially, which encode for BiTEs targeting different tumor antigens to prevent outgrowth of antigen escape variants. Furthermore, the CD3-targeting domain could be exchanged by domains targeting macrophages and NK cells (*225, 226*), neutrophils and monocytes (*227*), enzymes and prodrugs (*228*), other viral vectors (*229*) or radionuclides (*230*). Thus, the MV-BiTE constructs offer a flexible vector platform for the tumor-targeted delivery of various classes of bispecific antibodies. As discussed above, BiTEs did not add meaningful therapeutic effects to MV treatment in the MC38-CEA model. However, in the B16-CD20-CD46 model, survival of mice was significantly prolonged after MV-BiTE treatment, as compared to mice treated with unmodified MV. As discussed above, these findings might result from the distinct immunological landscapes of the different tumor models. Thus, evaluating the given tumor immune contexture could serve as another biomarker to predict MV-BiTE therapeutic efficacy. Moreover, the flexible MV-BiTE vector platform can be adapted to encode the potentially most effective bispecific antibodies, as described above. Thus, MV-BiTE therapy offers the possibility for tumor-targeted delivery of personalized immunotherapy.

A major advantage of tumor-targeted expression of therapeutic transgenes is to increase drug concentrations at the tumor site while lowering systemic exposure, as compared to systemic drug administration. There are two major limitations in systemic BiTE therapy: 1.) Poor efficacy against solid tumors; 2.) Dose-limiting toxicities (chapter 1.3.4 and references therein). As discussed in chapter 1.4.2, targeted expression of BiTEs by the MV-BiTE approach has the potential to overcome both limitations. Along the same lines, we did not observe signs of MV-

BiTE-related toxicities in the *in vivo* studies. Moreover, repeated intratumoral injections of MV-BiTE did not lead to detectable systemic exposure to BiTEs (Figure 4.14 and 4.18).

Conclusively, MV-BiTE therapy offers a safe and flexible approach for personalized cancer immunotherapy. To provide informed treatment decisions, biomarkers need to be predicted or identified in advance to therapy. For biomarker analysis of tumor samples, different technologies could provide information on a 1.) Cellular level (susceptibility to MV infection, immune contexture): Inoculation of tumor material with MV, flow cytometry, enzyme-linked immunospot (ELISpot) assay with TILs, immunohistochemistry, immunosequencing; 2.) Genomic/proteomic level (IFN type I status, tumor antigens, prediction of neoantigens, clonallity of neoantigens, mutational load): application of bioinformatics to tumor samples subjected to multiplexed gene expression profiling, next generation sequencing or protein microarrays (*231-234*). The required technologies for biomarker analysis are developed and available, thus, biomarker analysis should be included in future MV-based clinical trials to determine the predictive power of the respective biomarkers. Notably, the NCT Precision Oncology Program (NCT-POP) and the DKFZ Heidelberg Center for Personalized Oncology (DKFZ-HIPO) offer a program with patient-derived tumor samples for the identification of predictive biomarkers for susceptibility to MV infection (unpublished data). Moreover, biomarker analysis will be included in a MV-based Phase I/IIa trial (CanVirex) by Ungerechts *et al.*. The CanVirex study is currently in preparation at the NCT and will investigate safety and mode of action of a combination of oncolytic MV with the anti-PD1 antibody pembrolizumab, based on results obtained by Engeland *et al.* (*92*).

5.7. Summary and Outlook

This study reports on oncolytic measles viruses, which were genetically engineered to encode bispecific T cell engagers (MV-BiTE). MVs were generated to encode BiTEs targeting human or mouse CD3 and the tumor-associated antigens human CEA and human CD20, respectively. The replication capacity and oncolytic activity of MV-BiTE was not impaired by encoding the additional transgene, as compared to the unmodified MV. MV-BiTE-infected cells expressed and secreted BiTEs and specific binding of BiTEs purified from the supernatant of MV-BiTE-infected cells was demonstrated by ELISA, magnetic pull-down of BiTE-labeled cells and flow

cytometric analyses. The potential of BiTEs to mediate T cell cytotoxicity was verified by LDH release assays with murine T cells and human PBMCs. Thus, this study demonstrates the feasibility to express functional BiTE antibodies by a negative-strand RNA virus. Therapeutic efficacy of MV-BiTE was investigated in immunocompetent and xenograft mouse models. MV-BiTE demonstrated therapeutic efficacy against the syngeneic melanoma model B16-CD20-CD46, however not against the syngeneic colon adenocarcinoma model MC38-CEA. Survival analysis of B16-CD20-CD46-bearing mice treated with UV-inactivated MV-BiTE and purified BiTE indicated that oncolytic activity might not be relevant in the murine tumor models, which is supported by work previously published by Veinalde *et al.* (*76, 208*). Thus, the BiTE-mediated mode of T cell activation seems not to be beneficial in the MC38-CEA model. Analysis of tumor-infiltrating lymphocytes indicated that the distinct immunological landscapes of the two different tumor models might determine the therapeutic benefit derived by the BiTE mode of action. Ultimately, MV-BiTE demonstrated therapeutic efficacy against three different xenografts of patient-derived colorectal cancer spheroids with the transfer of human PBMCs. No signs of MV-BiTE-related toxicities were observed and BiTE plasma levels of MV-BiTE-treated mice remained below detection limit. Thus, intratumoral MV-BiTE therapy might reduce systemic adverse events, as compared to systemic BiTE administration.

Based on the present study results, the MV-BiTE project is continued in our laboratory. The MV-BiTE repertoire will be expanded by BiTEs targeting different tumor surface antigens. An MV encoding for human high molecular weight-melanoma-associated antigen (HMWMAA)-targeting BiTE has been successfully cloned and rescued. Further potential BiTE targets could be tumor antigens, such as CD19, CD33, epidermal growth factor receptors (EGFRs), epithelial cell adhesion molecule (EpCAM) or prostate-specific membrane antigen (PSMA). Along the same lines, the panel of xenograft models of patient-derived tumor cultures could be extended by the respective BiTE-targeting tumor entities. It would be worthwhile to further investigate the mode of action of MV-BiTE treatment. Mechanistic insights could reveal prognostic markers for a given tumor immune contexture. Thus, patients who will likely benefit from the MV-BiTE therapy could be selected. Mechanistic investigations should focus on the immunomodulatory aspects of MV-BiTE therapy: What is necessary to recruit T cells to the tumor site and to what extent can T cells be recruited? Are BiTEs involved in T cell recruitment to the tumor site or does T cell recruitment rather depend on the immunogenicity of the (oncolytic) MV vector? What are the necessary preconditions to initiate/modulate an

endogenous antitumor immune response and immunological memory? How does a given immunosuppressive TME influence therapeutic outcome? Would a combination of MV-BiTE therapy with other immunomodulators, such as immune checkpoint inhibitory antibodies result in synergistic effects? These questions remain unanswered in the fields of immunotherapy and immunovirotherapy to date. To address these questions, Johannes Heidbüchel currently explores live imaging technologies to monitor MV and T cell kinetics *in vivo*. Furthermore, Johannes Heidbüchel conducts targeted transcriptome analyses of MV-BiTE-treated mice to obtain comprehensive gene expression profiles.

Conclusively, MV-BiTE therapy demonstrated therapeutic efficacy in preclinical models of solid cancers. The MV-BiTE constructs offer a modular platform, which can be adapted to target any tumor antigen of choice. Thus, MV-BiTE therapy represents a promising approach for personalized cancer immunovirotherapy, with the potential to overcome limitations of either the monotherapy with oncolytic MV or BiTE alone.

Appendix

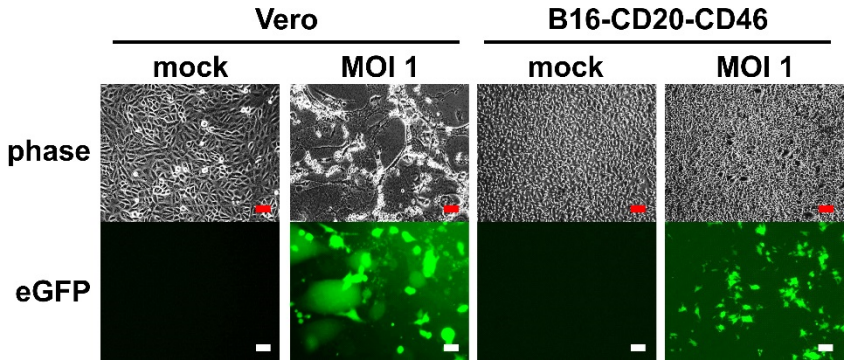

Figure A.1: Susceptibility of B16-CD20-CD46 cells to MV-BiTE infection. The susceptibility for MV-BiTE infection of B16-CD20-CD46 cells was compared to Vero cells. Cells were inoculated with MV-eGFP-mCD3xCD20 at an MOI of 1. Images were acquired 48 h post inoculation. Scale bars: 200 µm.

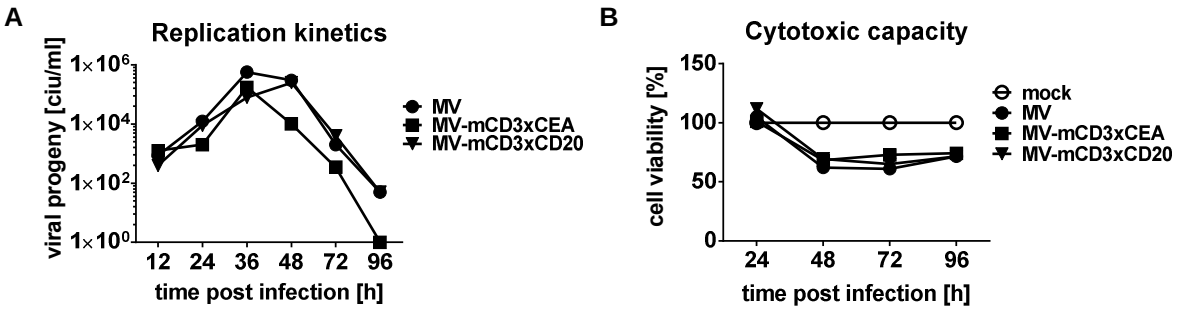

Figure A.2: Replication kinetics and cytotoxic capacity of MV-BiTE on B16-CD20-CD46 cells. B16-CD20-CD46 cells were inoculated with MV-BiTE and unmodified MV at a multiplicity of infection (MOI) of 1. (**A**) Viral progeny were determined by titration assays 12, 24, 36, 48, 72 and 96 hours post infection. Titration assays were performed in quadruplicates, which results in a detection limit of 25 cell infectious units (ciu)/ml. One-step growth curves were generated to compare MV replication kinetics in terms of viral progeny in ciu/ml. (**B**) Cell viability was determined in triplicates 24, 48, 72 and 96 hours post infection. Cell viability in % was normalized to cell viability of non-infected cells (mock), as described in chapter 3.2.3.

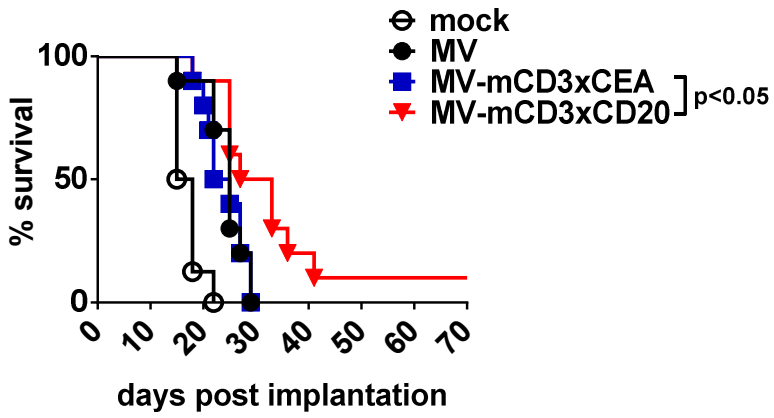

Figure A.3: Therapeutic efficacy of MV-BiTE against murine B16-CD20-CD46. $1x10^6$ B16-CD20-CD46 cells were subcutaneously implanted into the flank of C57BL/6 mice. Mice were treated with intratumoral injections of carrier fluid (mock) or $1x10^6$ cell infectious units (ciu) of indicated MV on five consecutive days (*n* = 10 mice/group). Kaplan-Meier survival analysis is shown. Log-rank (Mantel-Cox) test was performed for statistical comparison of survival curves and p values were corrected for multiple comparisons by the Bonferroni method.

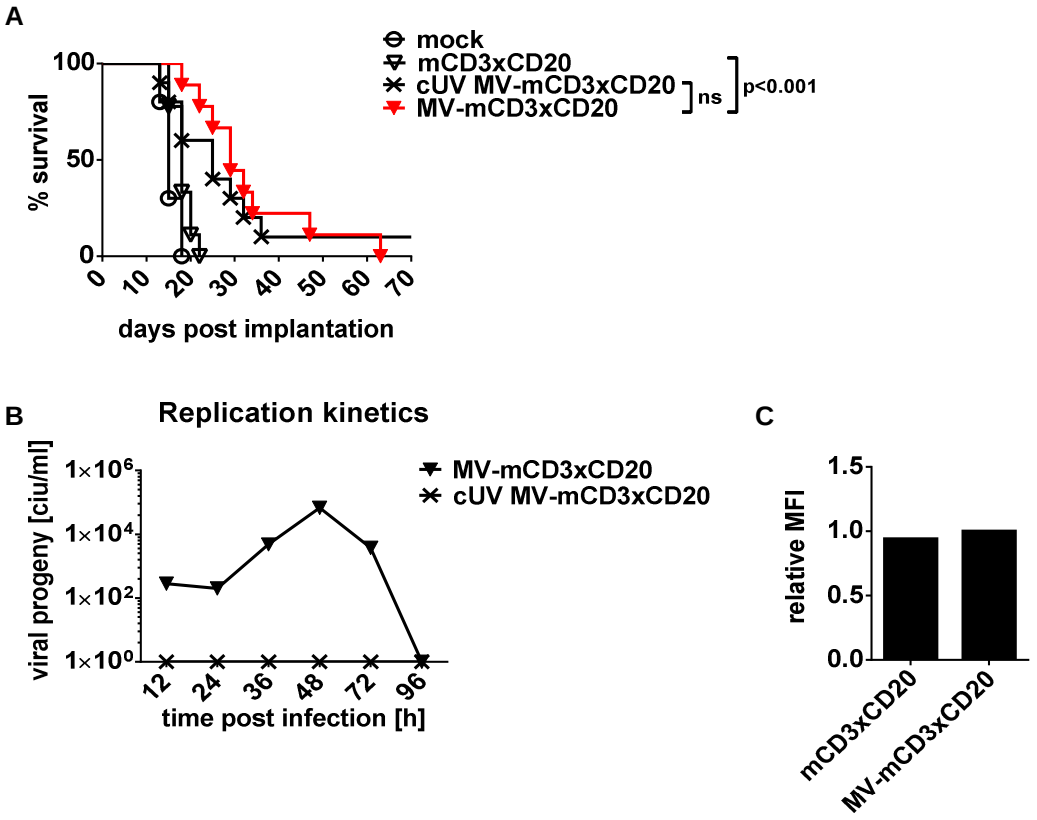

Figure A.4: Therapeutic efficacy of UV-inactivated MV-BiTE against murine B16-CD20-CD46. (**A**) 1x10^6 B16-CD20-CD46 cells were subcutaneously implanted into the flank of C57BL/6 mice. Mice were treated with intratumoral injections of carrier fluid (mock), 1x10^6 cell infectious units of MV-mCD3xCD20 or complete (c)UV-inactivated (= replication incompetent) MV-mCD3xCD20 or purified mCD3xCD20 BiTE on five consecutive days (*n* = 9-10 mice/group). Kaplan-Meier survival analysis is shown. Log-rank (Mantel-Cox) test was performed for statistical comparison of survival curves and p values were corrected for multiple comparisons by the Bonferroni method. (**B**) B16-CD20-CD46 cells were inoculated with MV-mCD3xCD20 and cUV-inactivated MV-mCD3xCD20 at a multiplicity of infection (MOI) of 1. Viral progeny were determined by titration assays 12, 24, 36, 48, 72 and 96 hours post infection. Titration assays were performed in quadruplicates, which results in a detection limit of 25 ciu/ml. One-step growth curves were generated to compare MV replication kinetics in terms of viral progeny in ciu/ml. (**C**) Relative quantification of mCD3xCD20 BiTE present in the virus suspension. Purified mCD3xCD20 BiTE was titrated on CD20-expressing Granta cells. Mean fluorescence intensity (MFI) was measured by flow cytometry. The concentration of purified mCD3xCD20 BiTE, which resulted in an equivalent MFI to MV-mCD3xCD20-stained Granta cells, was used to treat B16-CD20-CD46-bearing mice.

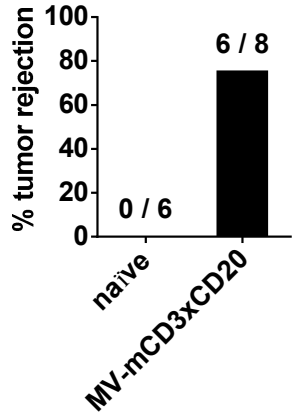

Figure A.5: Protective antitumor immunity after treatment with MV-mCD3xCD20. Mice in several experiments went into long-term remission after MV-mCD3xCD20 treatment of B16-CD20-CD46 tumors. The parental cell line B16 was implanted into the flank of naïve C57BL/6 mice and mice in long-term remission. Frequency of tumor rejection in % is shown.

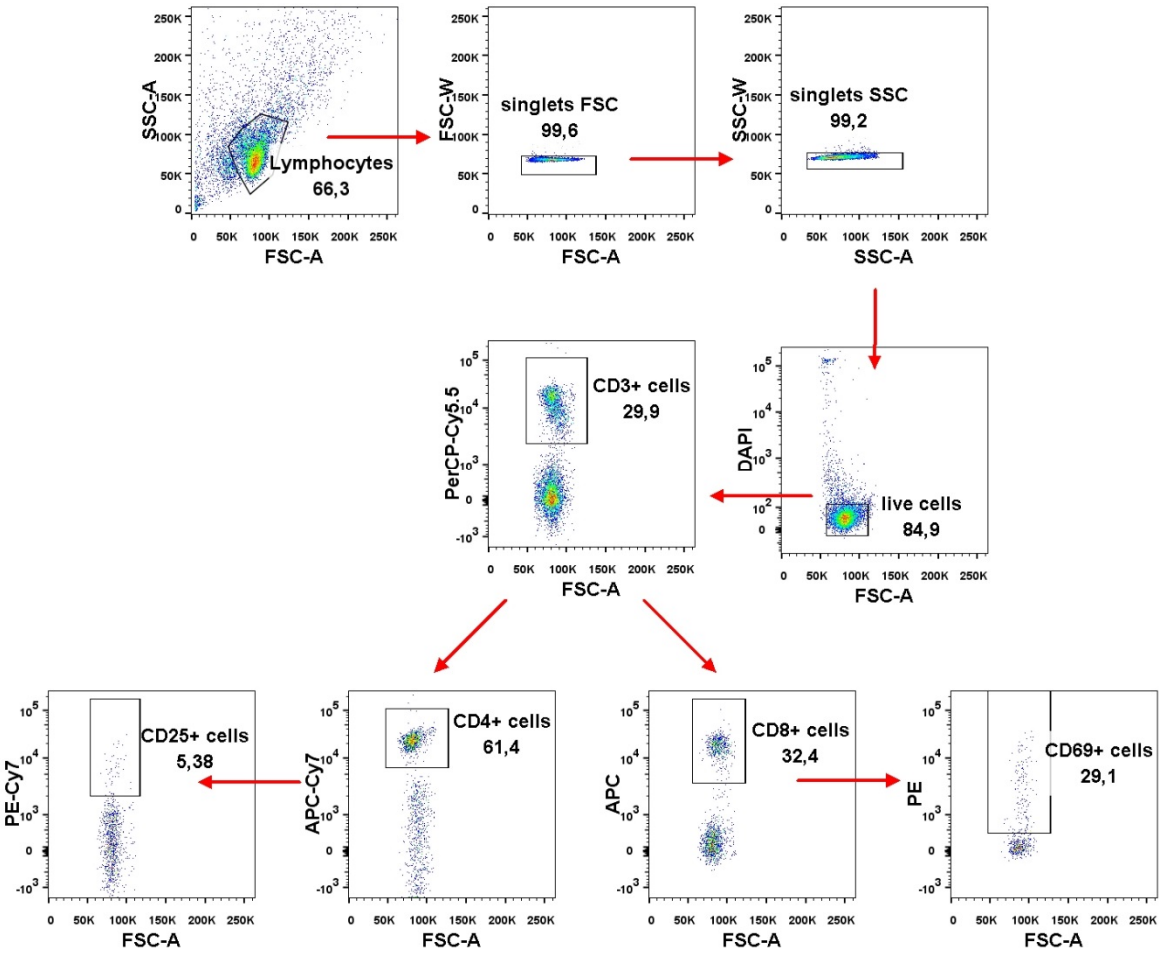

Figure A.6: Gating strategy for the analysis of tumor-infiltrating lymphocytes. Flow cytometric analysis of tumor-infiltrating lymphocytes (TILs) after MV-BiTE treatment. The first gate covers events of size (FSC) and granularity (SSC) expected for murine lymphocytes. Single cells were identified by similarities between FSC-A (area)/FSC-W (width) and SSC-A/SSC-W, respectively. Dead cells were excluded from the analysis by gating on DAPI negative events. Lymphocytes were identified by gating on CD3+ cells (PerCP-Cy5.5+ events). Next, cytotoxic T lymphocytes (CD8+ cells) and T helper cells (CD4+ cells) within the CD3+ population were identified (APC+ and APC-Cy7+ events, respectively). Activated (CD8+CD69+) and differentiated (CD4+CD25+) T cells were identified within the respective T cell fractions (PE+ and PE-Cy7+ events, respectively). Red arrows indicate the sequential gating hierarchy.

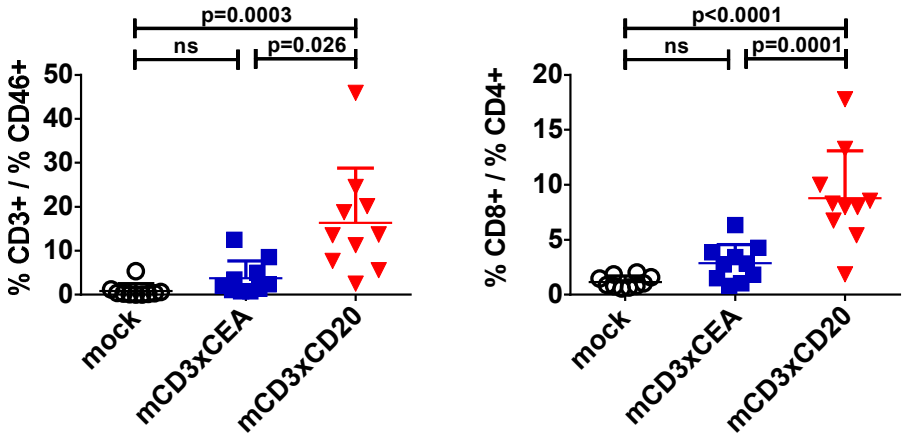

Figure A.7: Immunostimulatory effects of MV-BiTE treatment in B16-CD20-CD46-bearing mice. Analysis of tumor-infiltrating lymphocytes (TILs). B16-CD20-CD46 cells were subcutaneously implanted into the flank of C57BL/6 mice. Mice were treated with intratumoral injections of carrier fluid (mock) or the indicated MV-BiTE on five consecutive days. Tumors were explanted one day after the last treatment. Single-cell suspensions were prepared for flow cytometric analysis of TIL subpopulations (n = 10 mice/group). Mean values with standard deviation are shown. Statistical analysis was performed by one-way ANOVA and p values were adjusted for multiple comparisons by Tukey's test.

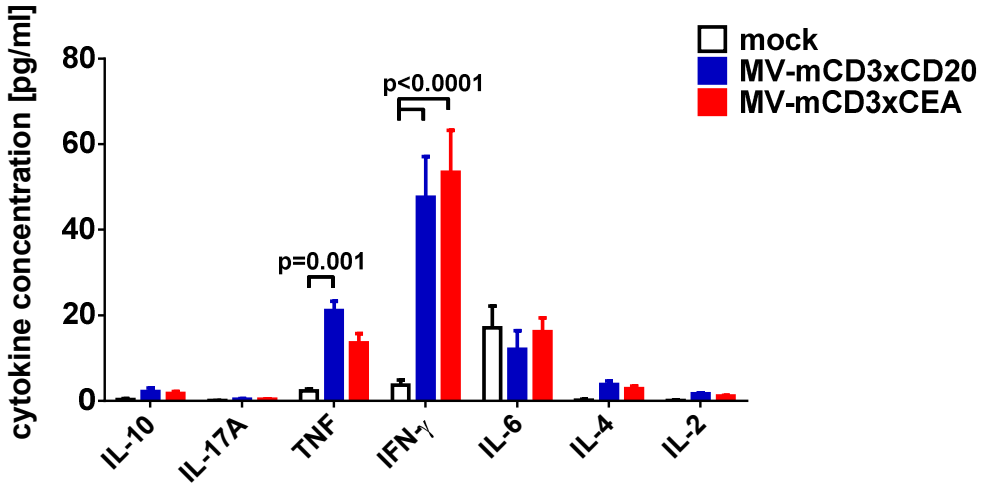

Figure A.8: Immunostimulatory effects of MV-BiTE treatment in B16-CD20-CD46-bearing mice. B16-CD20-CD46 cells were subcutaneously implanted into the flank of C57BL/6 mice. Mice were treated with intratumoral injections of carrier fluid (mock) or the indicated MV-BiTE on five consecutive days. Tumors were explanted one day after the last treatment. Cytokine profiles of MV-BiTE-treated mice. Intratumoral cytokines were quantified by cytokine bead arrays. Mean values with standard deviation are shown. Statistical analysis was performed by two-way ANOVA and p values were adjusted for multiple comparisons by Dunnett's test.

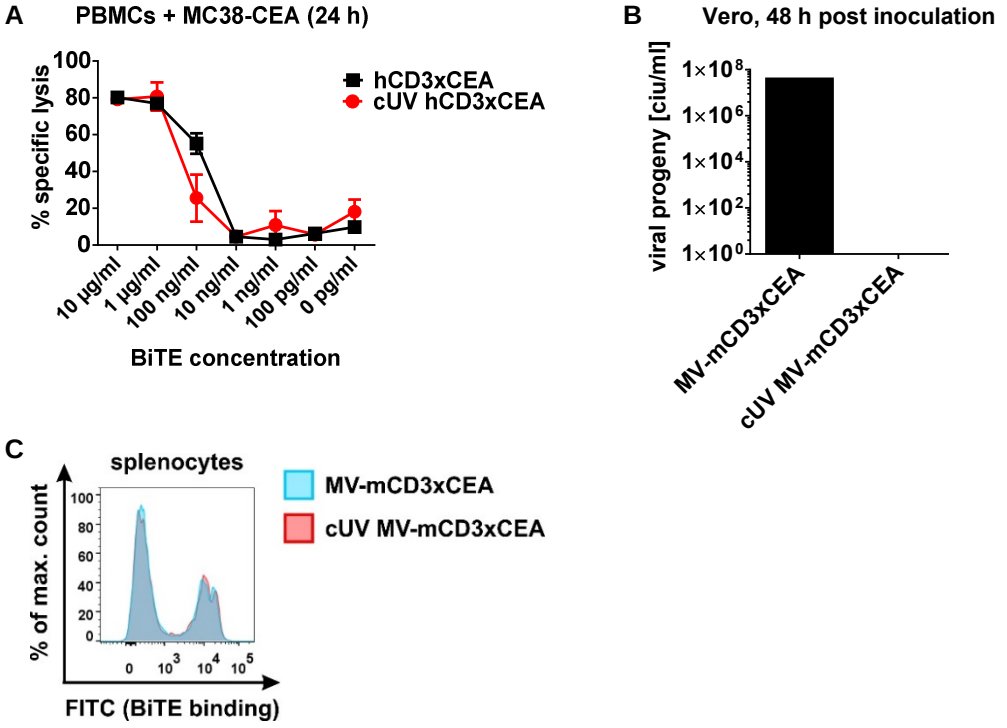

Figure A.9: Effects of UV-irradiation on BiTE functionality. (**A**) Purified hCD3xCEA BiTE was irradiated with a UV-dose of 0.75 J/cm^2. Functionality of UV-irradiated BiTE was compared to non-irradiated BiTE by using lactate dehydrogenase (LDH) release assay. Mean of triplicate samples with standard deviation is shown. (**B, C**) MV-hCD3xCEA or MV-mCD3xCEA were irradiated with a UV-dose of 0.75 J/cm^2. (**B**) Replication of UV-irradiated MV-BiTE. Vero cells were inoculated with UV-irradiated MV-hCD3xCEA and non-irradiated MV-hCD3xCEA, respectively. Viral progeny at 48 hours post inoculation were determined by titration assay. Viral progeny in cell infectious units (ciu)/ml are indicated. (**C**) BiTE binding of BiTE present in MV-BiTE suspension. Murine splenocytes were incubated with UV-irradiated MV-mCD3xCEA and non-irradiated MV-mCD3xCEA. BiTE binding to murine T cells was detected by anti-His-FITC antibody.

Bibliography

1. C. Fitzmaurice, C. Allen, R. M. Barber, L. Barregard, Z. A. Bhutta, H. Brenner, D. J. Dicker, O. Chimed-Orchir, R. Dandona, L. Dandona, T. Fleming, M. H. Forouzanfar, J. Hancock, R. J. Hay, R. Hunter-Merrill, C. Huynh, H. D. Hosgood, C. O. Johnson, J. B. Jonas, J. Khubchandani, G. A. Kumar, M. Kutz, Q. Lan, H. J. Larson, X. Liang, S. S. Lim, A. D. Lopez, M. F. MacIntyre, L. Marczak, N. Marquez, A. H. Mokdad, C. Pinho, F. Pourmalek, J. A. Salomon, J. R. Sanabria, L. Sandar, B. Sartorius, S. M. Schwartz, K. A. Shackelford, K. Shibuya, J. Stanaway, C. Steiner, J. Sun, K. Takahashi, S. E. Vollset, T. Vos, J. A. Wagner, H. Wang, R. Westerman, H. Zeeb, L. Zoeckler, F. Abd-Allah, M. B. Ahmed, S. Alabed, N. K. Alam, S. F. Aldhahri, G. Alem, M. A. Alemayohu, R. Ali, R. Al-Raddadi, A. Amare, Y. Amoako, A. Artaman, H. Asayesh, N. Atnafu, A. Awasthi, H. B. Saleem, A. Barac, N. Bedi, I. Bensenor, A. Berhane, E. Bernabe, B. Betsu, A. Binagwaho, D. Boneya, I. Campos-Nonato, C. Castaneda-Orjuela, F. Catala-Lopez, P. Chiang, C. Chibueze, A. Chitheer, J. Y. Choi, B. Cowie, S. Damtew, J. das Neves, S. Dey, S. Dharmaratne, P. Dhillon, E. Ding, T. Driscoll, D. Ekwueme, A. Y. Endries, M. Farvid, F. Farzadfar, J. Fernandes, F. Fischer, G. H. TT, A. Gebru, S. Gopalani, A. Hailu, M. Horino, N. Horita, A. Husseini, I. Huybrechts, M. Inoue, F. Islami, M. Jakovljevic, S. James, M. Javanbakht, S. H. Jee, A. Kasaeian, M. S. Kedir, Y. S. Khader, Y. H. Khang, D. Kim, J. Leigh, S. Linn, R. Lunevicius, H. M. A. El Razek, R. Malekzadeh, D. C. Malta, W. Marcenes, D. Markos, Y. A. Melaku, K. G. Meles, W. Mendoza, D. T. Mengiste, T. J. Meretoja, T. R. Miller, K. A. Mohammad, A. Mohammadi, S. Mohammed, M. Moradi-Lakeh, G. Nagel, D. Nand, Q. Le Nguyen, S. Nolte, F. A. Ogbo, K. E. Oladimeji, E. Oren, M. Pa, E. K. Park, D. M. Pereira, D. Plass, M. Qorbani, A. Radfar, A. Rafay, M. Rahman, S. M. Rana, K. Soreide, M. Satpathy, M. Sawhney, S. G. Sepanlou, M. A. Shaikh, J. She, I. Shiue, H. R. Shore, M. G. Shrime, S. So, S. Soneji, V. Stathopoulou, K. Stroumpoulis, M. B. Sufiyan, B. L. Sykes, R. Tabares-Seisdedos, F. Tadese, B. A. Tedla, G. A. Tessema, J. S. Thakur, B. X. Tran, K. N. Ukwaja, B. S. C. Uzochukwu, V. V. Vlassov, E. Weiderpass, M. Wubshet Terefe, H. G. Yebyo, H. H. Yimam, N. Yonemoto, M. Z. Younis, C. Yu, Z. Zaidi, M. E. S. Zaki, Z. M. Zenebe, C. J. L. Murray, M. Naghavi, Global, Regional, and National Cancer Incidence, Mortality, Years of Life Lost, Years Lived With Disability, and Disability-Adjusted Life-years for 32 Cancer Groups, 1990 to 2015: A Systematic Analysis for the Global Burden of Disease Study. *JAMA Oncol* **3**, 524-548 (2017).

2. M. Burnet, Cancer; a biological approach. I. The processes of control. *Br Med J* **1**, 779-786 (1957).

3. G. P. Dunn, A. T. Bruce, H. Ikeda, L. J. Old, R. D. Schreiber, Cancer immunoediting: from immunosurveillance to tumor escape. *Nat Immunol* **3**, 991-998 (2002).

4. D. Hanahan, R. A. Weinberg, Hallmarks of cancer: the next generation. *Cell* **144**, 646-674 (2011).

5. A. Bhatia, Y. Kumar, Cellular and molecular mechanisms in cancer immune escape: a comprehensive review. *Expert Rev Clin Immunol* **10**, 41-62 (2014).

6. D. S. Chen, I. Mellman, Oncology meets immunology: the cancer-immunity cycle. *Immunity* **39**, 1-10 (2013).

7. G. L. Beatty, W. L. Gladney, Immune escape mechanisms as a guide for cancer immunotherapy. *Clin Cancer Res* **21**, 687-692 (2015).

8. D. S. Chen, I. Mellman, Elements of cancer immunity and the cancer-immune set point. *Nature* **541**, 321-330 (2017).

9. B. Ebbell, *The Papyrus Ebers, the Greatest Egyptian Medical Document. Translated by B. Ebbell*. (Copenhagen; Oxford University Press: London, 1937).

10. D. B. Levine, The Hospital for the Ruptured and Crippled: William Bradley Coley, third Surgeon-in-Chief 1925-1933. *HSS J* **4**, 1-9 (2008).

11. S. A. Hoption Cann, J. P. van Netten, C. van Netten, Dr William Coley and tumour regression: a place in history or in the future. *Postgrad Med J* **79**, 672-680 (2003).

12. H. C. Nauts, G. A. Fowler, F. H. Bogatko, A review of the influence of bacterial infection and of bacterial products (Coley's toxins) on malignant tumors in man; a critical analysis of 30 inoperable cases treated by Coley's mixed toxins, in which diagnosis was confirmed by microscopic examination selected for special study. *Acta Med Scand Suppl* **276**, 1-103 (1953).

13. A. M. Engel, I. M. Svane, S. Mouritsen, J. Rygaard, J. Clausen, O. Werdelin, Methylcholanthrene-induced sarcomas in nude mice have short induction times and relatively low levels of surface MHC class I expression. *APMIS* **104**, 629-639 (1996).

14. V. Shankaran, H. Ikeda, A. T. Bruce, J. M. White, P. E. Swanson, L. J. Old, R. D. Schreiber, IFNgamma and lymphocytes prevent primary tumour development and shape tumour immunogenicity. *Nature* **410**, 1107-1111 (2001).

15. P. G. Coulie, B. J. Van den Eynde, P. van der Bruggen, T. Boon, Tumour antigens recognized by T lymphocytes: at the core of cancer immunotherapy. *Nat Rev Cancer* **14**, 135-146 (2014).

16. A. Gardner, B. Ruffell, Dendritic Cells and Cancer Immunity. *Trends Immunol* **37**, 855-865 (2016).

17. G. Kroemer, L. Galluzzi, O. Kepp, L. Zitvogel, Immunogenic cell death in cancer therapy. *Annu Rev Immunol* **31**, 51-72 (2013).

18. R. D. Schreiber, L. J. Old, M. J. Smyth, Cancer immunoediting: integrating immunity's roles in cancer suppression and promotion. *Science* **331**, 1565-1570 (2011).

19. M. D. Vesely, M. H. Kershaw, R. D. Schreiber, M. J. Smyth, Natural innate and adaptive immunity to cancer. *Annu Rev Immunol* **29**, 235-271 (2011).

20. J. M. Kirkwood, A. A. Tarhini, M. C. Panelli, S. J. Moschos, H. M. Zarour, L. H. Butterfield, H. J. Gogas, Next generation of immunotherapy for melanoma. *J Clin Oncol* **26**, 3445-3455 (2008).

21. L. Galluzzi, E. Vacchelli, J. M. Bravo-San Pedro, A. Buque, L. Senovilla, E. E. Baracco, N. Bloy, F. Castoldi, J. P. Abastado, P. Agostinis, R. N. Apte, F. Aranda, M. Ayyoub, P. Beckhove, J. Y. Blay, L. Bracci, A. Caignard, C. Castelli, F. Cavallo, E. Celis, V. Cerundolo, A. Clayton, M. P. Colombo, L. Coussens, M. V. Dhodapkar, A. M. Eggermont, D. T. Fearon, W. H. Fridman, J. Fucikova, D. I. Gabrilovich, J. Galon, A. Garg, F. Ghiringhelli, G. Giaccone, E. Gilboa, S. Gnjatic, A. Hoos, A. Hosmalin, D. Jager, P. Kalinski, K. Karre, O. Kepp, R. Kiessling, J. M. Kirkwood, E. Klein, A. Knuth, C. E. Lewis, R. Liblau, M. T. Lotze, E. Lugli, J. P. Mach, F. Mattei, D. Mavilio, I. Melero, C. J. Melief, E. A. Mittendorf, L. Moretta, A. Odunsi, H. Okada, A. K. Palucka, M. E. Peter, K. J. Pienta, A.

Porgador, G. C. Prendergast, G. A. Rabinovich, N. P. Restifo, N. Rizvi, C. Sautes-Fridman, H. Schreiber, B. Seliger, H. Shiku, B. Silva-Santos, M. J. Smyth, D. E. Speiser, R. Spisek, P. K. Srivastava, J. E. Talmadge, E. Tartour, S. H. Van Der Burg, B. J. Van Den Eynde, R. Vile, H. Wagner, J. S. Weber, T. L. Whiteside, J. D. Wolchok, L. Zitvogel, W. Zou, G. Kroemer, Classification of current anticancer immunotherapies. *Oncotarget* **5**, 12472-12508 (2014).

22. A. D. Garg, M. Vara Perez, M. Schaaf, P. Agostinis, L. Zitvogel, G. Kroemer, L. Galluzzi, Trial watch: Dendritic cell-based anticancer immunotherapy. *Oncoimmunology* **6**, e1328341 (2017).

23. C. S. Higano, E. J. Small, P. Schellhammer, U. Yasothan, S. Gubernick, P. Kirkpatrick, P. W. Kantoff, Sipuleucel-T. *Nat Rev Drug Discov* **9**, 513-514 (2010).

24. E. J. Lipson, C. G. Drake, Ipilimumab: an anti-CTLA-4 antibody for metastatic melanoma. *Clin Cancer Res* **17**, 6958-6962 (2011).

25. E. Vacchelli, J. Pol, N. Bloy, A. Eggermont, I. Cremer, W. H. Fridman, J. Galon, A. Marabelle, H. Kohrt, L. Zitvogel, G. Kroemer, L. Galluzzi, Trial watch: Tumor-targeting monoclonal antibodies for oncological indications. *Oncoimmunology* **4**, e985940 (2015).

26. S. D. Scott, Rituximab: a new therapeutic monoclonal antibody for non-Hodgkin's lymphoma. *Cancer Pract* **6**, 195-197 (1998).

27. Z. S. Guo, Z. Liu, S. Kowalsky, M. Feist, P. Kalinski, B. Lu, W. J. Storkus, D. L. Bartlett, Oncolytic Immunotherapy: Conceptual Evolution, Current Strategies, and Future Perspectives. *Front Immunol* **8**, 555 (2017).

28. J. Pol, G. Kroemer, L. Galluzzi, First oncolytic virus approved for melanoma immunotherapy. *Oncoimmunology* **5**, e1115641 (2016).

29. E. N. Baruch, A. L. Berg, M. J. Besser, J. Schachter, G. Markel, Adoptive T cell therapy: An overview of obstacles and opportunities. *Cancer* **123**, 2154-2162 (2017).

30. First-Ever CAR T-cell Therapy Approved in U.S. *Cancer Discov*, (2017).

31. T. Yuraszeck, S. Kasichayanula, J. E. Benjamin, Translation and Clinical Development of Bispecific T-cell Engaging Antibodies for Cancer Treatment. *Clin Pharmacol Ther* **101**, 634-645 (2017).

32. S. Offner, R. Hofmeister, A. Romaniuk, P. Kufer, P. A. Baeuerle, Induction of regular cytolytic T cell synapses by bispecific single-chain antibody constructs on MHC class I-negative tumor cells. *Mol Immunol* **43**, 763-771 (2006).

33. C. Haas, E. Krinner, K. Brischwein, P. Hoffmann, R. Lutterbuse, B. Schlereth, P. Kufer, P. A. Baeuerle, Mode of cytotoxic action of T cell-engaging BiTE antibody MT110. *Immunobiology* **214**, 441-453 (2009).

34. K. Brischwein, B. Schlereth, B. Guller, C. Steiger, A. Wolf, R. Lutterbuese, S. Offner, M. Locher, T. Urbig, T. Raum, P. Kleindienst, P. Wimberger, R. Kimmig, I. Fichtner, P. Kufer, R. Hofmeister, A. J. da Silva, P. A. Baeuerle, MT110: a novel bispecific single-chain antibody construct with high efficacy in eradicating established tumors. *Mol Immunol* **43**, 1129-1143 (2006).

35. A. Feldmann, C. Arndt, K. Topfer, S. Stamova, F. Krone, M. Cartellieri, S. Koristka, I. Michalk, D. Lindemann, M. Schmitz, A. Temme, M. Bornhauser, G. Ehninger, M. Bachmann, Novel humanized and highly efficient bispecific antibodies mediate killing of prostate stem cell antigen-expressing tumor cells by CD8+ and CD4+ T cells. *J Immunol* **189**, 3249-3259 (2012).

36. T. Dreier, G. Lorenczewski, C. Brandl, P. Hoffmann, U. Syring, F. Hanakam, P. Kufer, G. Riethmuller, R. Bargou, P. A. Baeuerle, Extremely potent, rapid and costimulation-independent cytotoxic T-cell response against lymphoma cells catalyzed by a single-chain bispecific antibody. *Int J Cancer* **100**, 690-697 (2002).

37. K. Brischwein, L. Parr, S. Pflanz, J. Volkland, J. Lumsden, M. Klinger, M. Locher, S. A. Hammond, P. Kiener, P. Kufer, B. Schlereth, P. A. Baeuerle, Strictly target cell-dependent activation of T cells by bispecific single-chain antibody constructs of the BiTE class. *J Immunother* **30**, 798-807 (2007).

38. B. D. Choi, P. C. Gedeon, L. Sanchez-Perez, D. D. Bigner, J. H. Sampson, Regulatory T cells are redirected to kill glioblastoma by an EGFRvIII-targeted bispecific antibody. *Oncoimmunology* **2**, e26757 (2013).

39. P. Hoffmann, R. Hofmeister, K. Brischwein, C. Brandl, S. Crommer, R. Bargou, C. Itin, N. Prang, P. A. Baeuerle, Serial killing of tumor cells by cytotoxic T cells redirected with a CD19-/CD3-bispecific single-chain antibody construct. *Int J Cancer* **115**, 98-104 (2005).

40. J. P. Van Wauwe, J. R. De Mey, J. G. Goossens, OKT3: a monoclonal anti-human T lymphocyte antibody with potent mitogenic properties. *J Immunol* **124**, 2708-2713 (1980).

41. T. Dreier, P. A. Baeuerle, I. Fichtner, M. Grun, B. Schlereth, G. Lorenczewski, P. Kufer, R. Lutterbuse, G. Riethmuller, P. Gjorstrup, R. C. Bargou, T cell costimulus-independent and very efficacious inhibition of tumor growth in mice bearing subcutaneous or leukemic human B cell lymphoma xenografts by a CD19-/CD3- bispecific single-chain antibody construct. *J Immunol* **170**, 4397-4402 (2003).

42. W. Deisting, T. Raum, P. Kufer, P. A. Baeuerle, M. Munz, Impact of Diverse Immune Evasion Mechanisms of Cancer Cells on T Cells Engaged by EpCAM/CD3-Bispecific Antibody Construct AMG 110. *PLoS One* **10**, e0141669 (2015).

43. M. Sanford, Blinatumomab: first global approval. *Drugs* **75**, 321-327 (2015).

44. N. Gokbuget, H. Dombret, J. M. Ribera, A. K. Fielding, A. Advani, R. Bassan, V. Chia, M. Doubek, S. Giebel, D. Hoelzer, N. Ifrah, A. Katz, M. Kelsh, G. Martinelli, M. Morgades, S. O'Brien, J. M. Rowe, J. Stieglmaier, M. Wadleigh, H. Kantarjian, International reference analysis of outcomes in adults with B-precursor Ph-negative relapsed/refractory acute lymphoblastic leukemia. *Haematologica* **101**, 1524-1533 (2016).

45. D. Nagorsen, P. Kufer, P. A. Baeuerle, R. Bargou, Blinatumomab: a historical perspective. *Pharmacol Ther* **136**, 334-342 (2012).

46. M. S. Topp, N. Gokbuget, G. Zugmaier, P. Klappers, M. Stelljes, S. Neumann, A. Viardot, R. Marks, H. Diedrich, C. Faul, A. Reichle, H. A. Horst, M. Bruggemann, D. Wessiepe, C. Holland, S. Alekar, N. Mergen, H. Einsele, D. Hoelzer, R. C. Bargou, Phase II trial of the anti-CD19 bispecific T cell-engager blinatumomab shows hematologic and molecular remissions in

patients with relapsed or refractory B-precursor acute lymphoblastic leukemia. *J Clin Oncol* **32**, 4134-4140 (2014).

47. H. Kantarjian, A. Stein, N. Gokbuget, A. K. Fielding, A. C. Schuh, J. M. Ribera, A. Wei, H. Dombret, R. Foa, R. Bassan, O. Arslan, M. A. Sanz, J. Bergeron, F. Demirkan, E. Lech-Maranda, A. Rambaldi, X. Thomas, H. A. Horst, M. Bruggemann, W. Klapper, B. L. Wood, A. Fleishman, D. Nagorsen, C. Holland, Z. Zimmerman, M. S. Topp, Blinatumomab versus Chemotherapy for Advanced Acute Lymphoblastic Leukemia. *N Engl J Med* **376**, 836-847 (2017).

48. M. E. Goebeler, S. Knop, A. Viardot, P. Kufer, M. S. Topp, H. Einsele, R. Noppeney, G. Hess, S. Kallert, A. Mackensen, K. Rupertus, L. Kanz, M. Libicher, D. Nagorsen, G. Zugmaier, M. Klinger, A. Wolf, B. Dorsch, B. D. Quednau, M. Schmidt, J. Scheele, P. A. Baeuerle, E. Leo, R. C. Bargou, Bispecific T-Cell Engager (BiTE) Antibody Construct Blinatumomab for the Treatment of Patients With Relapsed/Refractory Non-Hodgkin Lymphoma: Final Results From a Phase I Study. *J Clin Oncol* **34**, 1104-1111 (2016).

49. M. S. Topp, N. Gockbuget, A. S. Stein, Correction to Lancet Oncol 2015; 16: 60, 61. Safety and activity of blinatumomab for adult patients with relapsed or refractory B-precursor acute lymphoblastic leukaemia: a multi-centre, single-arm, phase 2 study. *Lancet Oncol* **16**, e158 (2015).

50. A. Viardot, M. E. Goebeler, G. Hess, S. Neumann, M. Pfreundschuh, N. Adrian, F. Zettl, M. Libicher, C. Sayehli, J. Stieglmaier, A. Zhang, D. Nagorsen, R. C. Bargou, Phase 2 study of the bispecific T-cell engager (BiTE) antibody blinatumomab in relapsed/refractory diffuse large B-cell lymphoma. *Blood* **127**, 1410-1416 (2016).

51. M. S. Topp, N. Gokbuget, A. S. Stein, G. Zugmaier, S. O'Brien, R. C. Bargou, H. Dombret, A. K. Fielding, L. Heffner, R. A. Larson, S. Neumann, R. Foa, M. Litzow, J. M. Ribera, A. Rambaldi, G. Schiller, M. Bruggemann, H. A. Horst, C. Holland, C. Jia, T. Maniar, B. Huber, D. Nagorsen, S. J. Forman, H. M. Kantarjian, Safety and activity of blinatumomab for adult patients with relapsed or refractory B-precursor acute lymphoblastic leukaemia: a multicentre, single-arm, phase 2 study. *Lancet Oncol* **16**, 57-66 (2015).

52. P. A. Baeuerle, C. Reinhardt, Bispecific T-cell engaging antibodies for cancer therapy. *Cancer Res* **69**, 4941-4944 (2009).

53. M. Pishvaian, M. A. Morse, J. McDevitt, J. D. Norton, S. Ren, G. J. Robbie, P. C. Ryan, S. Soukharev, H. Bao, C. S. Denlinger, Phase 1 Dose Escalation Study of MEDI-565, a Bispecific T-Cell Engager that Targets Human Carcinoembryonic Antigen, in Patients With Advanced Gastrointestinal Adenocarcinomas. *Clin Colorectal Cancer* **15**, 345-351 (2016).

54. M. Amann, K. Brischwein, P. Lutterbuese, L. Parr, L. Petersen, G. Lorenczewski, E. Krinner, S. Bruckmeier, S. Lippold, R. Kischel, R. Lutterbuese, P. Kufer, P. A. Baeuerle, B. Schlereth, Therapeutic window of MuS110, a single-chain antibody construct bispecific for murine EpCAM and murine CD3. *Cancer Res* **68**, 143-151 (2008).

55. M. Amann, S. D'Argouges, G. Lorenczewski, K. Brischwein, R. Kischel, R. Lutterbuese, S. Mangold, D. Rau, J. Volkland, S. Pflanz, T. Raum, M. Munz, P. Kufer, B. Schlereth, P. A. Baeuerle, M. Friedrich, Antitumor activity of an EpCAM/CD3-bispecific BiTE antibody during long-term

treatment of mice in the absence of T-cell anergy and sustained cytokine release. *J Immunother* **32**, 452-464 (2009).

56. B. Schlereth, P. Kleindienst, I. Fichtner, G. Lorenczewski, K. Brischwein, S. Lippold, A. da Silva, M. Locher, R. Kischel, R. Lutterbuse, P. Kufer, P. A. Baeuerle, Potent inhibition of local and disseminated tumor growth in immunocompetent mouse models by a bispecific antibody construct specific for Murine CD3. *Cancer Immunol Immunother* **55**, 785-796 (2006).

57. G. Fan, Z. Wang, M. Hao, J. Li, Bispecific antibodies and their applications. *J Hematol Oncol* **8**, 130 (2015).

58. D. Hendriks, G. Choi, M. de Bruyn, V. R. Wiersma, E. Bremer, Antibody-Based Cancer Therapy: Successful Agents and Novel Approaches. *Int Rev Cell Mol Biol* **331**, 289-383 (2017).

59. E. Walseng, C. G. Nelson, J. Qi, A. R. Nanna, W. R. Roush, R. K. Goswami, S. C. Sinha, T. R. Burke, Jr., C. Rader, Chemically Programmed Bispecific Antibodies in Diabody Format. *J Biol Chem* **291**, 19661-19673 (2016).

60. J. Hess, P. Ruf, H. Lindhofer, Cancer therapy with trifunctional antibodies: linking innate and adaptive immunity. *Future Oncol* **8**, 73-85 (2012).

61. U. Reusch, C. Burkhardt, I. Fucek, F. Le Gall, M. Le Gall, K. Hoffmann, S. H. Knackmuss, S. Kiprijanov, M. Little, E. A. Zhukovsky, A novel tetravalent bispecific TandAb (CD30/CD16A) efficiently recruits NK cells for the lysis of CD30+ tumor cells. *MAbs* **6**, 728-739 (2014).

62. A. C. Filley, M. Dey, Immune System, Friend or Foe of Oncolytic Virotherapy? *Front Oncol* **7**, 106 (2017).

63. Z. S. Guo, Z. Liu, D. L. Bartlett, Oncolytic Immunotherapy: Dying the Right Way is a Key to Eliciting Potent Antitumor Immunity. *Front Oncol* **4**, 74 (2014).

64. J. De Munck, A. Binks, I. A. McNeish, J. L. Aerts, Oncolytic virus-induced cell death and immunity: a match made in heaven? *J Leukoc Biol* **102**, 631-643 (2017).

65. D. Tang, R. Kang, C. B. Coyne, H. J. Zeh, M. T. Lotze, PAMPs and DAMPs: signal 0s that spur autophagy and immunity. *Immunol Rev* **249**, 158-175 (2012).

66. R. Cattaneo, T. Miest, E. V. Shashkova, M. A. Barry, Reprogrammed viruses as cancer therapeutics: targeted, armed and shielded. *Nat Rev Microbiol* **6**, 529-540 (2008).

67. M. Z. Tesfay, A. C. Kirk, E. M. Hadac, G. E. Griesmann, M. J. Federspiel, G. N. Barber, S. M. Henry, K. W. Peng, S. J. Russell, PEGylation of vesicular stomatitis virus extends virus persistence in blood circulation of passively immunized mice. *J Virol* **87**, 3752-3759 (2013).

68. C. R. O'Riordan, A. Lachapelle, C. Delgado, V. Parkes, S. C. Wadsworth, A. E. Smith, G. E. Francis, PEGylation of adenovirus with retention of infectivity and protection from neutralizing antibody in vitro and in vivo. *Hum Gene Ther* **10**, 1349-1358 (1999).

69. J. Morrison, S. S. Briggs, N. Green, K. Fisher, V. Subr, K. Ulbrich, S. Kehoe, L. W. Seymour, Virotherapy of ovarian cancer with polymer-cloaked adenovirus retargeted to the epidermal growth factor receptor. *Mol Ther* **16**, 244-251 (2008).

70. E. K. Mader, Y. Maeyama, Y. Lin, G. W. Butler, H. M. Russell, E. Galanis, S. J. Russell, A. B. Dietz, K. W. Peng, Mesenchymal stem cell carriers protect oncolytic measles viruses from antibody neutralization in an orthotopic ovarian cancer therapy model. *Clin Cancer Res* **15**, 7246-7255 (2009).

71. C. Willmon, K. Harrington, T. Kottke, R. Prestwich, A. Melcher, R. Vile, Cell carriers for oncolytic viruses: Fed Ex for cancer therapy. *Mol Ther* **17**, 1667-1676 (2009).

72. G. Fulci, L. Breymann, D. Gianni, K. Kurozomi, S. S. Rhee, J. Yu, B. Kaur, D. N. Louis, R. Weissleder, M. A. Caligiuri, E. A. Chiocca, Cyclophosphamide enhances glioma virotherapy by inhibiting innate immune responses. *Proc Natl Acad Sci U S A* **103**, 12873-12878 (2006).

73. K. Nosaki, K. Hamada, Y. Takashima, M. Sagara, Y. Matsumura, S. Miyamoto, Y. Hijikata, T. Okazaki, Y. Nakanishi, K. Tani, A novel, polymer-coated oncolytic measles virus overcomes immune suppression and induces robust antitumor activity. *Mol Ther Oncolytics* **3**, 16022 (2016).

74. E. A. Chiocca, S. D. Rabkin, Oncolytic viruses and their application to cancer immunotherapy. *Cancer Immunol Res* **2**, 295-300 (2014).

75. F. Bai, Z. Niu, H. Tian, S. Li, Z. Lv, T. Zhang, G. Ren, D. Li, Genetically engineered Newcastle disease virus expressing interleukin 2 is a potential drug candidate for cancer immunotherapy. *Immunol Lett* **159**, 36-46 (2014).

76. R. Veinalde, C. Grossardt, L. Hartmann, M. C. Bourgeois-Daigneault, J. C. Bell, D. Jager, C. von Kalle, G. Ungerechts, C. E. Engeland, Oncolytic measles virus encoding interleukin-12 mediates potent antitumor effects through T cell activation. *Oncoimmunology* **6**, e1285992 (2017).

77. M. R. Patel, B. A. Jacobson, Y. Ji, J. Drees, S. Tang, K. Xiong, H. Wang, J. E. Prigge, A. S. Dash, A. K. Kratzke, E. Mesev, R. Etchison, M. J. Federspiel, S. J. Russell, R. A. Kratzke, Vesicular stomatitis virus expressing interferon-beta is oncolytic and promotes antitumor immune responses in a syngeneic murine model of non-small cell lung cancer. *Oncotarget* **6**, 33165-33177 (2015).

78. C. Grossardt, C. E. Engeland, S. Bossow, N. Halama, K. Zaoui, M. F. Leber, C. Springfeld, D. Jaeger, C. von Kalle, G. Ungerechts, Granulocyte-macrophage colony-stimulating factor-armed oncolytic measles virus is an effective therapeutic cancer vaccine. *Hum Gene Ther* **24**, 644-654 (2013).

79. P. Wongthida, R. M. Diaz, C. Pulido, D. Rommelfanger, F. Galivo, K. Kaluza, T. Kottke, J. Thompson, A. Melcher, R. Vile, Activating systemic T-cell immunity against self tumor antigens to support oncolytic virotherapy with vesicular stomatitis virus. *Hum Gene Ther* **22**, 1343-1353 (2011).

80. Y. Q. Zhang, Y. C. Tsai, A. Monie, T. C. Wu, C. F. Hung, Enhancing the therapeutic effect against ovarian cancer through a combination of viral oncolysis and antigen-specific immunotherapy. *Mol Ther* **18**, 692-699 (2010).

81. A. Vigil, O. Martinez, M. A. Chua, A. Garcia-Sastre, Recombinant Newcastle disease virus as a vaccine vector for cancer therapy. *Mol Ther* **16**, 1883-1890 (2008).

82. P. Castelo-Branco, B. J. Passer, J. S. Buhrman, S. Antoszczyk, M. Marinelli, C. Zaupa, S. D. Rabkin, R. L. Martuza, Oncolytic herpes simplex virus armed with xenogeneic homologue of prostatic acid phosphatase enhances antitumor efficacy in prostate cancer. *Gene Ther* **17**, 805-810 (2010).

83. B. W. Bridle, J. E. Boudreau, B. D. Lichty, J. Brunelliere, K. Stephenson, S. Koshy, J. L. Bramson, Y. Wan, Vesicular stomatitis virus as a novel cancer vaccine vector to prime antitumor immunity amenable to rapid boosting with adenovirus. *Mol Ther* **17**, 1814-1821 (2009).

84. J. G. Pol, L. Zhang, B. W. Bridle, K. B. Stephenson, J. Resseguier, S. Hanson, L. Chen, N. Kazdhan, J. L. Bramson, D. F. Stojdl, Y. Wan, B. D. Lichty, Maraba virus as a potent oncolytic vaccine vector. *Mol Ther* **22**, 420-429 (2014).

85. S. C. Azoury, D. M. Straughan, V. Shukla, Immune Checkpoint Inhibitors for Cancer Therapy: Clinical Efficacy and Safety. *Curr Cancer Drug Targets* **15**, 452-462 (2015).

86. Z. Liu, R. Ravindranathan, P. Kalinski, Z. S. Guo, D. L. Bartlett, Rational combination of oncolytic vaccinia virus and PD-L1 blockade works synergistically to enhance therapeutic efficacy. *Nat Commun* **8**, 14754 (2017).

87. C. Y. Chen, P. Y. Wang, B. Hutzen, L. Sprague, H. M. Swain, J. K. Love, J. R. Stanek, L. Boon, J. Conner, T. P. Cripe, Cooperation of Oncolytic Herpes Virotherapy and PD-1 Blockade in Murine Rhabdomyosarcoma Models. *Sci Rep* **7**, 2396 (2017).

88. N. Woller, E. Gurlevik, B. Fleischmann-Mundt, A. Schumacher, S. Knocke, A. M. Kloos, M. Saborowski, R. Geffers, M. P. Manns, T. C. Wirth, S. Kubicka, F. Kuhnel, Viral Infection of Tumors Overcomes Resistance to PD-1-immunotherapy by Broadening Neoantigenome-directed T-cell Responses. *Mol Ther* **23**, 1630-1640 (2015).

89. W. Shen, M. M. Patnaik, A. Ruiz, S. J. Russell, K. W. Peng, Immunovirotherapy with vesicular stomatitis virus and PD-L1 blockade enhances therapeutic outcome in murine acute myeloid leukemia. *Blood* **127**, 1449-1458 (2016).

90. D. Zamarin, R. B. Holmgaard, S. K. Subudhi, J. S. Park, M. Mansour, P. Palese, T. Merghoub, J. D. Wolchok, J. P. Allison, Localized oncolytic virotherapy overcomes systemic tumor resistance to immune checkpoint blockade immunotherapy. *Sci Transl Med* **6**, 226ra232 (2014).

91. T. Du, G. Shi, Y. M. Li, J. F. Zhang, H. W. Tian, Y. Q. Wei, H. Deng, D. C. Yu, Tumor-specific oncolytic adenoviruses expressing granulocyte macrophage colony-stimulating factor or anti-CTLA4 antibody for the treatment of cancers. *Cancer Gene Ther* **21**, 340-348 (2014).

92. C. E. Engeland, C. Grossardt, R. Veinalde, S. Bossow, D. Lutz, J. K. Kaufmann, I. Shevchenko, V. Umansky, D. M. Nettelbeck, W. Weichert, D. Jager, C. von Kalle, G. Ungerechts, CTLA-4 and PD-L1 checkpoint blockade enhances oncolytic measles virus therapy. *Mol Ther* **22**, 1949-1959 (2014).

93. J. A. Chesney, I. Puzanov, M. I. Ross, F. A. Collichio, M. M. Milhem, L. Chen, J. J. Kim, C. Garbe, A. Hauschild, R. H. I. Andtbacka, Primary results from a randomized (1:1), open-label phase II study of talimogene laherparepvec (T) and ipilimumab (I) vs I alone in unresected stage IIIB- IV melanoma. *Journal of Clinical Oncology* **35**, 9509-9509 (2017).

94. A. Ribas, R. Dummer, I. Puzanov, A. VanderWalde, R. H. I. Andtbacka, O. Michielin, A. J. Olszanski, J. Malvehy, J. Cebon, E. Fernandez, J. M. Kirkwood, T. F. Gajewski, L. Chen, K. S. Gorski, A. A. Anderson, S. J. Diede, M. E. Lassman, J. Gansert, F. S. Hodi, G. V. Long, Oncolytic Virotherapy Promotes Intratumoral T Cell Infiltration and Improves Anti-PD-1 Immunotherapy. *Cell* **170**, 1109-1119 e1110 (2017).

95. C. Grigg, Z. Blake, R. Gartrell, A. Sacher, B. Taback, Y. Saenger, Talimogene laherparepvec (T-Vec) for the treatment of melanoma and other cancers. *Semin Oncol* **43**, 638-646 (2016).

96. R. H. Andtbacka, M. Ross, I. Puzanov, M. Milhem, F. Collichio, K. A. Delman, T. Amatruda, J. S. Zager, L. Cranmer, E. Hsueh, L. Chen, M. Shilkrut, H. L. Kaufman, Patterns of Clinical Response with Talimogene Laherparepvec (T-VEC) in Patients with Melanoma Treated in the OPTiM Phase III Clinical Trial. *Ann Surg Oncol* **23**, 4169-4177 (2016).

97. I. Puzanov, M. M. Milhem, D. Minor, O. Hamid, A. Li, L. Chen, M. Chastain, K. S. Gorski, A. Anderson, J. Chou, H. L. Kaufman, R. H. Andtbacka, Talimogene Laherparepvec in Combination With Ipilimumab in Previously Untreated, Unresectable Stage IIIB-IV Melanoma. *J Clin Oncol* **34**, 2619-2626 (2016).

98. H. L. Kaufman, F. J. Kohlhapp, A. Zloza, Oncolytic viruses: a new class of immunotherapy drugs. *Nat Rev Drug Discov* **14**, 642-662 (2015).

99. A. Marchini, E. M. Scott, J. Rommelaere, Overcoming Barriers in Oncolytic Virotherapy with HDAC Inhibitors and Immune Checkpoint Blockade. *Viruses* **8**, (2016).

100. F. J. Warnders, S. J. Waaijer, M. Pool, M. N. Lub-de Hooge, M. Friedrich, A. G. Terwisscha van Scheltinga, P. Deegen, S. K. Stienen, P. C. Pieslor, H. K. Cheung, J. G. Kosterink, E. G. de Vries, Biodistribution and PET Imaging of Labeled Bispecific T Cell-Engaging Antibody Targeting EpCAM. *J Nucl Med* **57**, 812-817 (2016).

101. F. Yu, X. Wang, Z. S. Guo, D. L. Bartlett, S. M. Gottschalk, X. T. Song, T-cell engager-armed oncolytic vaccinia virus significantly enhances antitumor therapy. *Mol Ther* **22**, 102-111 (2014).

102. C. A. Fajardo, S. Guedan, L. A. Rojas, R. Moreno, M. Arias-Badia, J. de Sostoa, C. H. June, R. Alemany, Oncolytic Adenoviral Delivery of an EGFR-Targeting T-cell Engager Improves Antitumor Efficacy. *Cancer Res* **77**, 2052-2063 (2017).

103. J. D. Freedman, J. Hagel, E. M. Scott, I. Psallidas, A. Gupta, L. Spiers, P. Miller, N. Kanellakis, R. Ashfield, K. D. Fisher, M. R. Duffy, L. W. Seymour, Oncolytic adenovirus expressing bispecific antibody targets T-cell cytotoxicity in cancer biopsies. *EMBO Mol Med* **9**, 1067-1087 (2017).

104. B. N. Fields, D. M. Knipe, P. M. Howley, *Fields virology*. (Wolters Kluwer Health/Lippincott Williams & Wilkins, Philadelphia, 2013).

105. P. Plattet, L. Alves, M. Herren, H. C. Aguilar, Measles Virus Fusion Protein: Structure, Function and Inhibition. *Viruses* **8**, 112 (2016).

106. M. Ludlow, L. J. Rennick, S. Sarlang, G. Skibinski, S. McQuaid, T. Moore, R. L. de Swart, W. P. Duprex, Wild-type measles virus infection of primary epithelial cells occurs via the basolateral surface without syncytium formation or release of infectious virus. *J Gen Virol* **91**, 971-979 (2010).

107. T. F. Wild, E. Malvoisin, R. Buckland, Measles virus: both the haemagglutinin and fusion glycoproteins are required for fusion. *J Gen Virol* **72 (Pt 2)**, 439-442 (1991).

108. T. Cathomen, B. Mrkic, D. Spehner, R. Drillien, R. Naef, J. Pavlovic, A. Aguzzi, M. A. Billeter, R. Cattaneo, A matrix-less measles virus is infectious and elicits extensive cell fusion: consequences for propagation in the brain. *EMBO J* **17**, 3899-3908 (1998).

109. T. Cathomen, H. Y. Naim, R. Cattaneo, Measles viruses with altered envelope protein cytoplasmic tails gain cell fusion competence. *J Virol* **72**, 1224-1234 (1998).

110. X. Yu, S. Shahriari, H. M. Li, R. Ghildyal, Measles Virus Matrix Protein Inhibits Host Cell Transcription. *PLoS One* **11**, e0161360 (2016).

111. A. Hirano, M. Ayata, A. H. Wang, T. C. Wong, Functional analysis of matrix proteins expressed from cloned genes of measles virus variants that cause subacute sclerosing panencephalitis reveals a common defect in nucleocapsid binding. *J Virol* **67**, 1848-1853 (1993).

112. P. Calain, L. Roux, The rule of six, a basic feature for efficient replication of Sendai virus defective interfering RNA. *J Virol* **67**, 4822-4830 (1993).

113. S. Delpeut, R. S. Noyce, R. W. Siu, C. D. Richardson, Host factors and measles virus replication. *Curr Opin Virol* **2**, 773-783 (2012).

114. W. J. Moss, D. E. Griffin, Measles. *Lancet* **379**, 153-164 (2012).

115. D. Normile, Animal science. Rinderpest, deadly for cattle, joins smallpox as a vanquished disease. *Science* **330**, 435 (2010).

116. Y. Furuse, A. Suzuki, H. Oshitani, Origin of measles virus: divergence from rinderpest virus between the 11th and 12th centuries. *Virol J* **7**, 52 (2010).

117. H. Tatsuo, N. Ono, K. Tanaka, Y. Yanagi, SLAM (CDw150) is a cellular receptor for measles virus. *Nature* **406**, 893-897 (2000).

118. R. E. Dorig, A. Marcil, A. Chopra, C. D. Richardson, The human CD46 molecule is a receptor for measles virus (Edmonston strain). *Cell* **75**, 295-305 (1993).

119. D. Naniche, G. Varior-Krishnan, F. Cervoni, T. F. Wild, B. Rossi, C. Rabourdin-Combe, D. Gerlier, Human membrane cofactor protein (CD46) acts as a cellular receptor for measles virus. *J Virol* **67**, 6025-6032 (1993).

120. M. D. Muhlebach, M. Mateo, P. L. Sinn, S. Prufer, K. M. Uhlig, V. H. Leonard, C. K. Navaratnarajah, M. Frenzke, X. X. Wong, B. Sawatsky, S. Ramachandran, P. B. McCray, Jr., K. Cichutek, V. von Messling, M. Lopez, R. Cattaneo, Adherens junction protein nectin-4 is the epithelial receptor for measles virus. *Nature* **480**, 530-533 (2011).

121. R. S. Noyce, D. G. Bondre, M. N. Ha, L. T. Lin, G. Sisson, M. S. Tsao, C. D. Richardson, Tumor cell marker PVRL4 (nectin 4) is an epithelial cell receptor for measles virus. *PLoS Pathog* **7**, e1002240 (2011).

122. K. Lemon, R. D. de Vries, A. W. Mesman, S. McQuaid, G. van Amerongen, S. Yuksel, M. Ludlow, L. J. Rennick, T. Kuiken, B. K. Rima, T. B. Geijtenbeek, A. D. Osterhaus, W. P. Duprex, R. L. de Swart, Early target cells of measles virus after aerosol infection of non-human primates. *PLoS Pathog* **7**, e1001263 (2011).

123. L. de Witte, R. D. de Vries, M. van der Vlist, S. Yuksel, M. Litjens, R. L. de Swart, T. B. Geijtenbeek, DC-SIGN and CD150 have distinct roles in transmission of measles virus from dendritic cells to T-lymphocytes. *PLoS Pathog* **4**, e1000049 (2008).

124. R. S. Noyce, C. D. Richardson, Nectin 4 is the epithelial cell receptor for measles virus. *Trends Microbiol* **20**, 429-439 (2012).

125. M. K. Patel, M. Gacic-Dobo, P. M. Strebel, A. Dabbagh, M. N. Mulders, J. M. Okwo-Bele, L. Dumolard, P. A. Rota, K. Kretsinger, J. L. Goodson, Progress Toward Regional Measles Elimination - Worldwide, 2000-2015. *MMWR Morb Mortal Wkly Rep* **65**, 1228-1233 (2016).

126. J. F. Enders, T. C. Peebles, Propagation in tissue cultures of cytopathogenic agents from patients with measles. *Proc Soc Exp Biol Med* **86**, 277-286 (1954).

127. B. Bankamp, M. Takeda, Y. Zhang, W. Xu, P. A. Rota, Genetic characterization of measles vaccine strains. *J Infect Dis* **204 Suppl 1**, S533-548 (2011).

128. J. F. Enders, S. L. Katz, M. V. Milovanovic, A. Holloway, Studies on an attenuated measles-virus vaccine. I. Development and preparations of the vaccine: technics for assay of effects of vaccination. *N Engl J Med* **263**, 153-159 (1960).

129. G. Pasquinucci, Possible effect of measles on leukaemia. *Lancet* **1**, 136 (1971).

130. S. Gross, Measles and leukaemia. *Lancet* **1**, 397-398 (1971).

131. Z. Zygiert, Hodgkin's disease: remissions after measles. *Lancet* **1**, 593 (1971).

132. A. Z. Bluming, J. L. Ziegler, Regression of Burkitt's lymphoma in association with measles infection. *Lancet* **2**, 105-106 (1971).

133. T. Mori, K. Sasaki, H. Hashimoto, S. Makino, Molecular cloning and complete nucleotide sequence of genomic RNA of the AIK-C strain of attenuated measles virus. *Virus Genes* **7**, 67-81 (1993).

134. Safety of high-titre measles vaccine. *Lancet* **338**, 920 (1991).

135. F. Radecke, P. Spielhofer, H. Schneider, K. Kaelin, M. Huber, C. Dotsch, G. Christiansen, M. A. Billeter, Rescue of measles viruses from cloned DNA. *EMBO J* **14**, 5773-5784 (1995).

136. K. W. Peng, G. J. Ahmann, L. Pham, P. R. Greipp, R. Cattaneo, S. J. Russell, Systemic therapy of myeloma xenografts by an attenuated measles virus. *Blood* **98**, 2002-2007 (2001).

137. K. W. Peng, S. Facteau, T. Wegman, D. O'Kane, S. J. Russell, Non-invasive in vivo monitoring of trackable viruses expressing soluble marker peptides. *Nat Med* **8**, 527-531 (2002).

138. L. K. Phuong, C. Allen, K. W. Peng, C. Giannini, S. Greiner, C. J. TenEyck, P. K. Mishra, S. I. Macura, S. J. Russell, E. C. Galanis, Use of a vaccine strain of measles virus genetically engineered to produce carcinoembryonic antigen as a novel therapeutic agent against glioblastoma multiforme. *Cancer Res* **63**, 2462-2469 (2003).

139. D. Grote, S. J. Russell, T. I. Cornu, R. Cattaneo, R. Vile, G. A. Poland, A. K. Fielding, Live attenuated measles virus induces regression of human lymphoma xenografts in immunodeficient mice. *Blood* **97**, 3746-3754 (2001).

140. E. A. Chiocca, Oncolytic viruses. *Nat Rev Cancer* **2**, 938-950 (2002).

141. C. Erlenhofer, W. P. Duprex, B. K. Rima, V. ter Meulen, J. Schneider-Schaulies, Analysis of receptor (CD46, CD150) usage by measles virus. *J Gen Virol* **83**, 1431-1436 (2002).

142. M. Tahara, M. Takeda, F. Seki, T. Hashiguchi, Y. Yanagi, Multiple amino acid substitutions in hemagglutinin are necessary for wild-type measles virus to acquire the ability to use receptor CD46 efficiently. *J Virol* **81**, 2564-2572 (2007).

143. L. T. Lin, C. D. Richardson, The Host Cell Receptors for Measles Virus and Their Interaction with the Viral Hemagglutinin (H) Protein. *Viruses* **8**, (2016).

144. M. K. Liszewski, J. P. Atkinson, Complement regulator CD46: genetic variants and disease associations. *Hum Genomics* **9**, 7 (2015).

145. Z. Fishelson, N. Donin, S. Zell, S. Schultz, M. Kirschfink, Obstacles to cancer immunotherapy: expression of membrane complement regulatory proteins (mCRPs) in tumors. *Mol Immunol* **40**, 109-123 (2003).

146. B. D. Anderson, T. Nakamura, S. J. Russell, K. W. Peng, High CD46 receptor density determines preferential killing of tumor cells by oncolytic measles virus. *Cancer Res* **64**, 4919-4926 (2004).

147. S. Aref, K. Bailey, A. Fielding, Measles to the Rescue: A Review of Oncolytic Measles Virus. *Viruses* **8**, (2016).

148. M. A. Billeter, H. Y. Naim, S. A. Udem, Reverse genetics of measles virus and resulting multivalent recombinant vaccines: applications of recombinant measles viruses. *Curr Top Microbiol Immunol* **329**, 129-162 (2009).

149. B. K. Rima, W. P. Duprex, The measles virus replication cycle. *Curr Top Microbiol Immunol* **329**, 77-102 (2009).

150. L. Heinzerling, V. Kunzi, P. A. Oberholzer, T. Kundig, H. Naim, R. Dummer, Oncolytic measles virus in cutaneous T-cell lymphomas mounts antitumor immune responses in vivo and targets interferon-resistant tumor cells. *Blood* **106**, 2287-2294 (2005).

151. E. Galanis, L. C. Hartmann, W. A. Cliby, H. J. Long, P. P. Peethambaram, B. A. Barrette, J. S. Kaur, P. J. Haluska, Jr., I. Aderca, P. J. Zollman, J. A. Sloan, G. Keeney, P. J. Atherton, K. C. Podratz, S. C. Dowdy, C. R. Stanhope, T. O. Wilson, M. J. Federspiel, K. W. Peng, S. J. Russell, Phase I trial of intraperitoneal administration of an oncolytic measles virus strain engineered to express carcinoembryonic antigen for recurrent ovarian cancer. *Cancer Res* **70**, 875-882 (2010).

152. E. Galanis, P. J. Atherton, M. J. Maurer, K. L. Knutson, S. C. Dowdy, W. A. Cliby, P. Haluska, Jr., H. J. Long, A. Oberg, I. Aderca, M. S. Block, J. Bakkum-Gamez, M. J. Federspiel, S. J. Russell, K. R. Kalli, G. Keeney, K. W. Peng, L. C. Hartmann, Oncolytic measles virus expressing the sodium iodide symporter to treat drug-resistant ovarian cancer. *Cancer Res* **75**, 22-30 (2015).

153. S. J. Russell, M. J. Federspiel, K. W. Peng, C. Tong, D. Dingli, W. G. Morice, V. Lowe, M. K. O'Connor, R. A. Kyle, N. Leung, F. K. Buadi, S. V. Rajkumar, M. A. Gertz, M. Q. Lacy, A. Dispenzieri, Remission of disseminated cancer after systemic oncolytic virotherapy. *Mayo Clin Proc* **89**, 926-933 (2014).

154. C. Yanisch-Perron, J. Vieira, J. Messing, Improved M13 phage cloning vectors and host strains: nucleotide sequences of the M13mp18 and pUC19 vectors. *Gene* **33**, 103-119 (1985).

155. M. Tanaka, W. Herr, Differential transcriptional activation by Oct-1 and Oct-2: interdependent activation domains induce Oct-2 phosphorylation. *Cell* **60**, 375-386 (1990).

156. A. Martin, P. Staeheli, U. Schneider, RNA polymerase II-controlled expression of antigenomic RNA enhances the rescue efficacies of two different members of the Mononegavirales independently of the site of viral genome replication. *J Virol* **80**, 5708-5715 (2006).

157. D. Müller, R. E. Kontermann, in *Bispecific Antibodies,* R. E. Kontermann, Ed. (Springer Berlin Heidelberg, Berlin, Heidelberg, 2011), pp. 83-100.

158. K. D. Miller, R. L. Siegel, C. C. Lin, A. B. Mariotto, J. L. Kramer, J. H. Rowland, K. D. Stein, R. Alteri, A. Jemal, Cancer treatment and survivorship statistics, 2016. *CA Cancer J Clin* **66**, 271-289 (2016).

159. M. O. Palumbo, P. Kavan, W. H. Miller, Jr., L. Panasci, S. Assouline, N. Johnson, V. Cohen, F. Patenaude, M. Pollak, R. T. Jagoe, G. Batist, Systemic cancer therapy: achievements and challenges that lie ahead. *Front Pharmacol* **4**, 57 (2013).

160. S. A. Rosenberg, Decade in review-cancer immunotherapy: entering the mainstream of cancer treatment. *Nat Rev Clin Oncol* **11**, 630-632 (2014).

161. G. G. Au, L. G. Beagley, E. S. Haley, R. D. Barry, D. R. Shafren, Oncolysis of malignant human melanoma tumors by Coxsackieviruses A13, A15 and A18. *Virol J* **8**, 22 (2011).

162. M. M. Zulkifli, R. Ibrahim, A. M. Ali, I. Aini, H. Jaafar, S. S. Hilda, N. B. Alitheen, J. M. Abdullah, Newcastle diseases virus strain V4UPM displayed oncolytic ability against experimental human malignant glioma. *Neurol Res* **31**, 3-10 (2009).

163. K. Geletneky, J. P. Nuesch, A. Angelova, I. Kiprianova, J. Rommelaere, Double-faceted mechanism of parvoviral oncosuppression. *Curr Opin Virol* **13**, 17-24 (2015).

164. C. J. Breitbach, R. Arulanandam, N. De Silva, S. H. Thorne, R. Patt, M. Daneshmand, A. Moon, C. Ilkow, J. Burke, T. H. Hwang, J. Heo, M. Cho, H. Chen, F. A. Angarita, C. Addison, J. A. McCart, J. C. Bell, D. H. Kirn, Oncolytic vaccinia virus disrupts tumor-associated vasculature in humans. *Cancer Res* **73**, 1265-1275 (2013).

165. G. Chang, S. Xu, M. Watanabe, H. R. Jayakar, M. A. Whitt, J. R. Gingrich, Enhanced oncolytic activity of vesicular stomatitis virus encoding SV5-F protein against prostate cancer. *J Urol* **183**, 1611-1618 (2010).

166. B. D. Lichty, C. J. Breitbach, D. F. Stojdl, J. C. Bell, Going viral with cancer immunotherapy. *Nat Rev Cancer* **14**, 559-567 (2014).

167. A. M. Waters, J. M. Johnston, A. T. Reddy, J. Fiveash, A. Madan-Swain, K. Kachurak, A. K. Bag, G. Y. Gillespie, J. M. Markert, G. K. Friedman, Rationale and Design of a Phase 1 Clinical Trial to Evaluate HSV G207 Alone or with a Single Radiation Dose in Children with Progressive or Recurrent Malignant Supratentorial Brain Tumors. *Hum Gene Ther Clin Dev* **28**, 7-16 (2017).

168. H. Kasuya, Y. Kodera, A. Nakao, K. Yamamura, T. Gewen, W. Zhiwen, Y. Hotta, S. Yamada, T. Fujii, S. Fukuda, N. Tsurumaru, T. Kuwahara, T. Kikumori, Y. Koide, Y. Fujimoto, T. Nakashima, Y. Hirooka, H. Shiku, M. Tanaka, K. Takesako, T. Kondo, B. Aleksic, H. Kawashima, H. Goto, Y. Nishiyama, Phase I Dose-escalation Clinical Trial of HF10 Oncolytic Herpes Virus in 17 Japanese Patients with Advanced Cancer. *Hepatogastroenterology* **61**, 599-605 (2014).

169. V. T. Packiam, D. L. Lamm, D. A. Barocas, A. Trainer, B. Fand, R. L. Davis, 3rd, W. Clark, M. Kroeger, I. Dumbadze, K. Chamie, A. K. Kader, D. Curran, J. Gutheil, A. Kuan, A. W. Yeung, G. D. Steinberg, An open label, single-arm, phase II multicenter study of the safety and efficacy of CG0070 oncolytic vector regimen in patients with BCG-unresponsive non-muscle-invasive bladder cancer: Interim results. *Urol Oncol*, (2017).

170. N. Martinez-Velez, E. Xipell, B. Vera, A. Acanda de la Rocha, M. Zalacain, L. Marrodan, M. Gonzalez-Huarriz, G. Toledo, M. Cascallo, R. Alemany, A. Patino, M. M. Alonso, The Oncolytic Adenovirus VCN-01 as Therapeutic Approach Against Pediatric Osteosarcoma. *Clin Cancer Res* **22**, 2217-2225 (2016).

171. S. Tejada, M. Alonso, A. Patino, J. Fueyo, C. Gomez-Manzano, R. Diez-Valle, Phase I Trial of DNX-2401 for Diffuse Intrinsic Pontine Glioma Newly Diagnosed in Pediatric Patients. *Neurosurgery*, (2017).

172. R. Garcia-Carbonero, R. Salazar, I. Duran, I. Osman-Garcia, L. Paz-Ares, J. M. Bozada, V. Boni, C. Blanc, L. Seymour, J. Beadle, S. Alvis, B. Champion, E. Calvo, K. Fisher, Phase 1 study of intravenous administration of the chimeric adenovirus enadenotucirev in patients undergoing primary tumor resection. *J Immunother Cancer* **5**, 71 (2017).

173. A. Dispenzieri, C. Tong, B. LaPlant, M. Q. Lacy, K. Laumann, D. Dingli, Y. Zhou, M. J. Federspiel, M. A. Gertz, S. Hayman, F. Buadi, M. O'Connor, V. J. Lowe, K. W. Peng, S. J. Russell, Phase I trial of systemic administration of Edmonston strain of measles virus genetically engineered to express the sodium iodide symporter in patients with recurrent or refractory multiple myeloma. *Leukemia*, (2017).

174. C. J. Breitbach, A. Moon, J. Burke, T. H. Hwang, D. H. Kirn, A Phase 2, Open-Label, Randomized Study of Pexa-Vec (JX-594) Administered by Intratumoral Injection in Patients with Unresectable Primary Hepatocellular Carcinoma. *Methods Mol Biol* **1317**, 343-357 (2015).

175. C. R. Heery, C. Palena, S. McMahon, R. N. Donahue, L. M. Lepone, I. Grenga, U. Dirmeier, L. Cordes, J. Marte, W. Dahut, H. Singh, R. A. Madan, R. I. Fernando, D. H. Hamilton, J. Schlom, J.

L. Gulley, Phase I Study of a Poxviral TRICOM-Based Vaccine Directed Against the Transcription Factor Brachyury. *Clin Cancer Res* **23**, 6833-6845 (2017).

176. D. E. Cohn, M. W. Sill, J. L. Walker, D. O'Malley, C. I. Nagel, T. L. Rutledge, W. Bradley, D. L. Richardson, K. M. Moxley, C. Aghajanian, Randomized phase IIB evaluation of weekly paclitaxel versus weekly paclitaxel with oncolytic reovirus (Reolysin(R)) in recurrent ovarian, tubal, or peritoneal cancer: An NRG Oncology/Gynecologic Oncology Group study. *Gynecol Oncol* **146**, 477-483 (2017).

177. I. V. Dolzhikova, O. V. Zubkova, A. I. Tukhvatulin, A. S. Dzharullaeva, N. M. Tukhvatulina, D. V. Shcheblyakov, M. M. Shmarov, E. A. Tokarskaya, Y. V. Simakova, D. A. Egorova, D. N. Scherbinin, I. L. Tutykhina, A. A. Lysenko, A. V. Kostarnoy, P. G. Gancheva, T. A. Ozharovskaya, B. V. Belugin, L. V. Kolobukhina, V. B. Pantyukhov, S. I. Syromyatnikova, I. V. Shatokhina, T. V. Sizikova, I. G. Rumyantseva, A. F. Andrus, N. V. Boyarskaya, A. N. Voytyuk, V. F. Babira, S. V. Volchikhina, D. A. Kutaev, A. N. Bel'skih, K. V. Zhdanov, S. M. Zakharenko, S. V. Borisevich, D. Y. Logunov, B. S. Naroditsky, A. L. Gintsburg, Safety and immunogenicity of GamEvac-Combi, a heterologous VSV- and Ad5-vectored Ebola vaccine: An open phase I/II trial in healthy adults in Russia. *Hum Vaccin Immunother* **13**, 613-620 (2017).

178. J. Hajda, M. Lehmann, O. Krebs, M. Kieser, K. Geletneky, D. Jager, M. Dahm, B. Huber, T. Schoning, O. Sedlaczek, A. Stenzinger, N. Halama, V. Daniel, B. Leuchs, A. Angelova, J. Rommelaere, C. E. Engeland, C. Springfeld, G. Ungerechts, A non-controlled, single arm, open label, phase II study of intravenous and intratumoral administration of ParvOryx in patients with metastatic, inoperable pancreatic cancer: ParvOryx02 protocol. *BMC Cancer* **17**, 576 (2017).

179. T. F. Cloughesy, J. Landolfi, D. J. Hogan, S. Bloomfield, B. Carter, C. C. Chen, J. B. Elder, S. N. Kalkanis, S. Kesari, A. Lai, I. Y. Lee, L. M. Liau, T. Mikkelsen, P. L. Nghiemphu, D. Piccioni, T. Walbert, A. Chu, A. Das, O. R. Diago, D. Gammon, H. E. Gruber, M. Hanna, D. J. Jolly, N. Kasahara, D. McCarthy, L. Mitchell, D. Ostertag, J. M. Robbins, M. Rodriguez-Aguirre, M. A. Vogelbaum, Phase 1 trial of vocimagene amiretrorepvec and 5-fluorocytosine for recurrent high-grade glioma. *Sci Transl Med* **8**, 341ra375 (2016).

180. R. H. I. Andtbacka, B. D. Curti, S. Hallmeyer, Z. Feng, C. Paustian, C. Bifulco, B. Fox, M. Grose, D. Shafren, Phase II calm extension study: Coxsackievirus A21 delivered intratumorally to patients with advanced melanoma induces immune-cell infiltration in the tumor microenvironment. *Journal for Immunotherapy of Cancer* **3**, P343-P343 (2015).

181. A. Gauvrit, S. Brandler, C. Sapede-Peroz, N. Boisgerault, F. Tangy, M. Gregoire, Measles virus induces oncolysis of mesothelioma cells and allows dendritic cells to cross-prime tumor-specific CD8 response. *Cancer Res* **68**, 4882-4892 (2008).

182. J. B. Guillerme, N. Boisgerault, D. Roulois, J. Menager, C. Combredet, F. Tangy, J. F. Fonteneau, M. Gregoire, Measles virus vaccine-infected tumor cells induce tumor antigen cross-presentation by human plasmacytoid dendritic cells. *Clin Cancer Res* **19**, 1147-1158 (2013).

183. O. G. Donnelly, F. Errington-Mais, L. Steele, E. Hadac, V. Jennings, K. Scott, H. Peach, R. M. Phillips, J. Bond, H. Pandha, K. Harrington, R. Vile, S. Russell, P. Selby, A. A. Melcher, Measles virus causes immunogenic cell death in human melanoma. *Gene Ther* **20**, 7-15 (2013).

184. A. Baldo, E. Galanis, F. Tangy, P. Herman, Biosafety considerations for attenuated measles virus vectors used in virotherapy and vaccination. *Hum Vaccin Immunother* **12**, 1102-1116 (2016).

185. C. Combredet, V. Labrousse, L. Mollet, C. Lorin, F. Delebecque, B. Hurtrel, H. McClure, M. B. Feinberg, M. Brahic, F. Tangy, A molecularly cloned Schwarz strain of measles virus vaccine induces strong immune responses in macaques and transgenic mice. *J Virol* **77**, 11546-11554 (2003).

186. F. Allagui, C. Achard, C. Panterne, C. Combredet, N. Labarriere, B. Dreno, A. B. Elgaaied, D. Pouliquen, F. Tangy, J. F. Fonteneau, M. Gregoire, N. Boisgerault, Modulation of the Type I Interferon Response Defines the Sensitivity of Human Melanoma Cells to Oncolytic Measles Virus. *Curr Gene Ther* **16**, 419-428 (2017).

187. R. Cattaneo, G. Rebmann, A. Schmid, K. Baczko, V. ter Meulen, M. A. Billeter, Altered transcription of a defective measles virus genome derived from a diseased human brain. *EMBO J* **6**, 681-688 (1987).

188. S. Bossow, C. Grossardt, A. Temme, M. F. Leber, S. Sawall, E. P. Rieber, R. Cattaneo, C. von Kalle, G. Ungerechts, Armed and targeted measles virus for chemovirotherapy of pancreatic cancer. *Cancer Gene Ther* **18**, 598-608 (2011).

189. J. K. Kaufmann, S. Bossow, C. Grossardt, S. Sawall, J. Kupsch, P. Erbs, J. C. Hassel, C. von Kalle, A. H. Enk, D. M. Nettelbeck, G. Ungerechts, Chemovirotherapy of malignant melanoma with a targeted and armed oncolytic measles virus. *J Invest Dermatol* **133**, 1034-1042 (2013).

190. K. Zaoui, S. Bossow, C. Grossardt, M. F. Leber, C. Springfeld, P. K. Plinkert, C. Kalle, G. Ungerechts, Chemovirotherapy for head and neck squamous cell carcinoma with EGFR-targeted and CD/UPRT-armed oncolytic measles virus. *Cancer Gene Ther* **19**, 181-191 (2012).

191. S. J. Russell, K. W. Peng, J. C. Bell, Oncolytic virotherapy. *Nat Biotechnol* **30**, 658-670 (2012).

192. J. Mercer, A. Helenius, Virus entry by macropinocytosis. *Nat Cell Biol* **11**, 510-520 (2009).

193. S. Vincent, D. Spehner, S. Manie, R. Delorme, R. Drillien, D. Gerlier, Inefficient measles virus budding in murine L.CD46 fibroblasts. *Virology* **265**, 185-195 (1999).

194. S. Vincent, I. Tigaud, H. Schneider, C. J. Buchholz, Y. Yanagi, D. Gerlier, Restriction of measles virus RNA synthesis by a mouse host cell line: trans-complementation by polymerase components or a human cellular factor(s). *J Virol* **76**, 6121-6130 (2002).

195. Y. Yanagi, M. Takeda, S. Ohno, Measles virus: cellular receptors, tropism and pathogenesis. *J Gen Virol* **87**, 2767-2779 (2006).

196. T. H. Corbett, D. P. Griswold, Jr., B. J. Roberts, J. C. Peckham, F. M. Schabel, Jr., Tumor induction relationships in development of transplantable cancers of the colon in mice for chemotherapy assays, with a note on carcinogen structure. *Cancer Res* **35**, 2434-2439 (1975).

197. B. J. M. L. Roscoe, *Handbook on genetically standardized Jax mice*. (Roscoe B. Jackson Memorial Laboratory, Bar Harbor, Me., 1962).

198. M. G. Lechner, S. S. Karimi, K. Barry-Holson, T. E. Angell, K. A. Murphy, C. H. Church, J. R. Ohlfest, P. Hu, A. L. Epstein, Immunogenicity of murine solid tumor models as a defining feature of in vivo behavior and response to immunotherapy. *J Immunother* **36**, 477-489 (2013).

199. E. Becht, N. A. Giraldo, M. C. Dieu-Nosjean, C. Sautes-Fridman, W. H. Fridman, Cancer immune contexture and immunotherapy. *Curr Opin Immunol* **39**, 7-13 (2016).

200. R. Lutterbuese, T. Raum, R. Kischel, P. Hoffmann, S. Mangold, B. Rattel, M. Friedrich, O. Thomas, G. Lorenczewski, D. Rau, E. Schaller, I. Herrmann, A. Wolf, T. Urbig, P. A. Baeuerle, P. Kufer, T cell-engaging BiTE antibodies specific for EGFR potently eliminate KRAS- and BRAF-mutated colorectal cancer cells. *Proc Natl Acad Sci U S A* **107**, 12605-12610 (2010).

201. M. Friedrich, A. Henn, T. Raum, M. Bajtus, K. Matthes, L. Hendrich, J. Wahl, P. Hoffmann, R. Kischel, M. Kvesic, J. W. Slootstra, P. A. Baeuerle, P. Kufer, B. Rattel, Preclinical characterization of AMG 330, a CD3/CD33-bispecific T-cell-engaging antibody with potential for treatment of acute myelogenous leukemia. *Mol Cancer Ther* **13**, 1549-1557 (2014).

202. O. A. Haabeth, B. Bogen, A. Corthay, A model for cancer-suppressive inflammation. *Oncoimmunology* **1**, 1146-1155 (2012).

203. W. Zhang, Y. Pan, P. Gou, C. Zhou, L. Ma, Q. Liu, Y. Du, J. Yang, Q. Wang, Effect of xanthohumol on Th1/Th2 balance in a breast cancer mouse model. *Oncol Rep* **39**, 280-288 (2018).

204. D. Sviben, D. Forcic, T. Kurtovic, B. Halassy, M. Brgles, Stability, biophysical properties and effect of ultracentrifugation and diafiltration on measles virus and mumps virus. *Arch Virol* **161**, 1455-1467 (2016).

205. K. K. Langfield, H. J. Walker, L. C. Gregory, M. J. Federspiel, Manufacture of measles viruses. *Methods Mol Biol* **737**, 345-366 (2011).

206. T. Dao, D. Pankov, A. Scott, T. Korontsvit, V. Zakhaleva, Y. Xu, J. Xiang, S. Yan, M. D. de Morais Guerreiro, N. Veomett, L. Dubrovsky, M. Curcio, E. Doubrovina, V. Ponomarev, C. Liu, R. J. O'Reilly, D. A. Scheinberg, Therapeutic bispecific T-cell engager antibody targeting the intracellular oncoprotein WT1. *Nat Biotechnol* **33**, 1079-1086 (2015).

207. N. Eissler, P. Ruf, J. Mysliwietz, H. Lindhofer, R. Mocikat, Trifunctional bispecific antibodies induce tumor-specific T cells and elicit a vaccination effect. *Cancer Res* **72**, 3958-3966 (2012).

208. R. Veinalde, Unraveling Determinants of Efficacy in Measles Immunovirotherapy, PhD Thesis, Ruprecht-Karls University, Heidelberg (2017).

209. S. Abraham, H. Guo, J. G. Choi, C. Ye, M. B. Thomas, N. Ortega, A. Dwivedi, N. Manjunath, G. Yi, P. Shankar, Combination of IL-10 and IL-2 induces oligoclonal human CD4 T cell expansion during xenogeneic and allogeneic GVHD in humanized mice. *Heliyon* **3**, e00276 (2017).

210. A. Sun, H. Wei, R. Sun, W. Xiao, Y. Yang, Z. Tian, Human interleukin-15 improves engraftment of human T cells in NOD-SCID mice. *Clin Vaccine Immunol* **13**, 227-234 (2006).

211. W. J. Racki, L. Covassin, M. Brehm, S. Pino, R. Ignotz, R. Dunn, J. Laning, S. K. Graves, A. A. Rossini, L. D. Shultz, D. L. Greiner, NOD-scid IL2rgamma(null) mouse model of human skin transplantation and allograft rejection. *Transplantation* **89**, 527-536 (2010).

212. R. Ito, I. Katano, K. Kawai, H. Hirata, T. Ogura, T. Kamisako, T. Eto, M. Ito, Highly sensitive model for xenogenic GVHD using severe immunodeficient NOG mice. *Transplantation* **87**, 1654-1658 (2009).

213. P. J. Lucas, G. M. Shearer, S. Neudorf, R. E. Gress, The human antimurine xenogeneic cytotoxic response. I. Dependence on responder antigen-presenting cells. *J Immunol* **144**, 4548-4554 (1990).

214. A. Mullbacher, M. Lobigs, R. T. Hla, T. Tran, T. Stehle, M. M. Simon, Antigen-dependent release of IFN-gamma by cytotoxic T cells up-regulates Fas on target cells and facilitates exocytosis-independent specific target cell lysis. *J Immunol* **169**, 145-150 (2002).

215. R. Arakaki, A. Yamada, Y. Kudo, Y. Hayashi, N. Ishimaru, Mechanism of activation-induced cell death of T cells and regulation of FasL expression. *Crit Rev Immunol* **34**, 301-314 (2014).

216. P. R. Walker, P. Saas, P. Y. Dietrich, Role of Fas ligand (CD95L) in immune escape: the tumor cell strikes back. *J Immunol* **158**, 4521-4524 (1997).

217. E. M. Hadac, K. W. Peng, T. Nakamura, S. J. Russell, Reengineering paramyxovirus tropism. *Virology* **329**, 217-225 (2004).

218. T. Nakamura, K. W. Peng, M. Harvey, S. Greiner, I. A. Lorimer, C. D. James, S. J. Russell, Rescue and propagation of fully retargeted oncolytic measles viruses. *Nat Biotechnol* **23**, 209-214 (2005).

219. M. F. Leber, S. Bossow, V. H. Leonard, K. Zaoui, C. Grossardt, M. Frenzke, T. Miest, S. Sawall, R. Cattaneo, C. von Kalle, G. Ungerechts, MicroRNA-sensitive oncolytic measles viruses for cancer-specific vector tropism. *Mol Ther* **19**, 1097-1106 (2011).

220. G. O. Chong, H. S. Jeon, H. S. Han, J. W. Son, Y. H. Lee, D. G. Hong, Y. S. Lee, Y. L. Cho, Differential MicroRNA Expression Profiles in Primary and Recurrent Epithelial Ovarian Cancer. *Anticancer Res* **35**, 2611-2617 (2015).

221. H. Yoshino, N. Seki, T. Itesako, T. Chiyomaru, M. Nakagawa, H. Enokida, Aberrant expression of microRNAs in bladder cancer. *Nat Rev Urol* **10**, 396-404 (2013).

222. X. L. Lai, Y. H. Huang, Y. S. Li, G. N. Li, L. P. Wang, R. Sun, Y. S. Ma, S. Y. Feng, Z. Y. Chang, X. H. Wang, D. Fu, X. Han, X. L. Cong, W. P. Li, Differential expression profiling of microRNAs in para-carcinoma, carcinoma and relapse human pancreatic cancer. *Clin Transl Oncol* **17**, 398-408 (2015).

223. H. Y. Lee, S. S. Han, H. Rhee, J. H. Park, J. S. Lee, Y. M. Oh, S. S. Choi, S. H. Shin, W. J. Kim, Differential expression of microRNAs and their target genes in non-small-cell lung cancer. *Mol Med Rep* **11**, 2034-2040 (2015).

224. S. Shrestha, S. D. Hsu, W. Y. Huang, H. Y. Huang, W. Chen, S. L. Weng, H. D. Huang, A systematic review of microRNA expression profiling studies in human gastric cancer. *Cancer Med* **3**, 878-888 (2014).

225. F. Hartmann, C. Renner, W. Jung, C. Deisting, M. Juwana, B. Eichentopf, M. Kloft, M. Pfreundschuh, Treatment of refractory Hodgkin's disease with an anti-CD16/CD30 bispecific antibody. *Blood* **89**, 2042-2047 (1997).

226. M. K. Gleason, J. A. Ross, E. D. Warlick, T. C. Lund, M. R. Verneris, A. Wiernik, S. Spellman, M. D. Haagenson, A. J. Lenvik, M. R. Litzow, P. K. Epling-Burnette, B. R. Blazar, L. M. Weiner, D. J. Weisdorf, D. A. Vallera, J. S. Miller, CD16xCD33 bispecific killer cell engager (BiKE) activates NK cells against primary MDS and MDSC CD33+ targets. *Blood* **123**, 3016-3026 (2014).

227. N. D. James, P. J. Atherton, J. Jones, A. J. Howie, S. Tchekmedyian, R. T. Curnow, A phase II study of the bispecific antibody MDX-H210 (anti-HER2 x CD64) with GM-CSF in HER2+ advanced prostate cancer. *Br J Cancer* **85**, 152-156 (2001).

228. S. Müller-Brüsselbach, T. Korn, T. Völkel, R. Müller, R. Kontermann, *Enzyme recruitment and tumor cell killing in vitro by a secreted bispecific single-chain diabody*. (1999), vol. 4, pp. 115-123.

229. T. Korn, D. M. Nettelbeck, T. Volkel, R. Muller, R. E. Kontermann, Recombinant bispecific antibodies for the targeting of adenoviruses to CEA-expressing tumour cells: a comparative analysis of bacterially expressed single-chain diabody and tandem scFv. *J Gene Med* **6**, 642-651 (2004).

230. D. G. DeNardo, C. Y. Xiong, X. B. Shi, G. L. DeNardo, S. J. DeNardo, Anti-HLA-DR/anti-DOTA diabody construction in a modular gene design platform: bispecific antibodies for pretargeted radioimmunotherapy. *Cancer Biother Radiopharm* **16**, 525-535 (2001).

231. G. V. Masucci, A. Cesano, R. Hawtin, S. Janetzki, J. Zhang, I. Kirsch, K. K. Dobbin, J. Alvarez, P. B. Robbins, S. R. Selvan, H. Z. Streicher, L. H. Butterfield, M. Thurin, Validation of biomarkers to predict response to immunotherapy in cancer: Volume I - pre-analytical and analytical validation. *J Immunother Cancer* **4**, 76 (2016).

232. N. McGranahan, A. J. Furness, R. Rosenthal, S. Ramskov, R. Lyngaa, S. K. Saini, M. Jamal-Hanjani, G. A. Wilson, N. J. Birkbak, C. T. Hiley, T. B. Watkins, S. Shafi, N. Murugaesu, R. Mitter, A. U. Akarca, J. Linares, T. Marafioti, J. Y. Henry, E. M. Van Allen, D. Miao, B. Schilling, D. Schadendorf, L. A. Garraway, V. Makarov, N. A. Rizvi, A. Snyder, M. D. Hellmann, T. Merghoub, J. D. Wolchok, S. A. Shukla, C. J. Wu, K. S. Peggs, T. A. Chan, S. R. Hadrup, S. A. Quezada, C. Swanton, Clonal neoantigens elicit T cell immunoreactivity and sensitivity to immune checkpoint blockade. *Science* **351**, 1463-1469 (2016).

233. S. Gnjatic, V. Bronte, L. R. Brunet, M. O. Butler, M. L. Disis, J. Galon, L. G. Hakansson, B. A. Hanks, V. Karanikas, S. N. Khleif, J. M. Kirkwood, L. D. Miller, D. J. Schendel, I. Tanneau, J. M. Wigginton, L. H. Butterfield, Identifying baseline immune-related biomarkers to predict clinical outcome of immunotherapy. *J Immunother Cancer* **5**, 44 (2017).

234. J. Yuan, P. S. Hegde, R. Clynes, P. G. Foukas, A. Harari, T. O. Kleen, P. Kvistborg, C. Maccalli, H. T. Maecker, D. B. Page, H. Robins, W. Song, E. C. Stack, E. Wang, T. L. Whiteside, Y. Zhao, H. Zwierzina, L. H. Butterfield, B. A. Fox, Novel technologies and emerging biomarkers for personalized cancer immunotherapy. *J Immunother Cancer* **4**, 3 (2016).

List of Publications

Speck T[*], Heidbüchel JPW[*], Veinalde R, Jäger D, von Kalle C, Ball CR, Ungerechts G, Engeland CE. **Targeted BiTE expression by an oncolytic vector augments therapeutic efficacy against solid tumors.** Clinical Cancer Research (under revision).[†]

Khandelwal N, Breinig M, **Speck T**, Michels T, Kreutzer C, Sorrentino A, Sharma AK, Umansky L, Conrad H, Poschke I, Offringa R, König R, Bernhard H, Machlenkin A, Boutros M, Beckhove P. **High-throughput RNAi screen identifies novel breast cancer antigens that mediate immune escape by inhibiting cytotoxic T-cell responses.** EMBO Molecular Medicine. 2015. 7, 450-463

Weiss J, Theile D, Rüppell MA, **Speck T**, Spalwisz A, Haefeli WE. **Interaction profile of macitentan, a new non-selective endothelin-1 receptor antagonist, in vitro.** European Journal of Pharmacology. 2013. 70, 168–175

Dinkel H, Van Roey K, Michael S, Davey NE, Weatheritt RJ, Born D, **Speck T**, Krüger D, Grebnev G, Kuban M, Strumillo M, Uyar B, Budd A, Altenberg B, Seiler M, Chemes LB, Glavina J, Sánchez IE, Diella F, Gibson TJ. **The eukaryotic linear motif resource ELM: 10 years and counting. Nucleic Acids Research.** 2013. 42, 259–266

[*]Shared first authorship
[†] Main results of the present thesis are summarized in this publication

Congress Contributions and Awards

25th Annual Meeting of the European Society for Gene and Cell Therapy (**ESGCT**)

T. Speck, J. Heidbüchel, R. Veinalde, D. Jäger, C. Ball, C. von Kalle, G. Ungerechts, C. E. Engeland

Berlin, Germany, 17th-20th October 2017, selected abstract for **oral presentation**

3rd **CRI-CIMT-EATI-AACR** International Cancer Immunotherapy Conference

T. Speck, J. Heidbüchel, R. Veinalde, D. Jäger, C. Ball, C. von Kalle, G. Ungerechts, C. E. Engeland

Mainz, Germany, 06th-09th September 2017, selected abstract for **poster presentation**

20th Annual Meeting of the American Society for Gene and Cell Therapy (**ASGCT**)

T. Speck, J. Heidbüchel, D. Jäger, C. von Kalle, G. Ungerechts, C. E. Engeland

Washington, DC, 10th-13th May 2017, selected abstract for **oral presentation**

Awarded a **Meritorious Abstract Travel Award of $ 600** by the Abstract Reviewer Committee.

1st EMBL – Cancer Core Europe Conference - **Cancer Immunotherapy**

T. Speck, J. Heidbüchel, D. Jäger, C. von Kalle, G. Ungerechts, C. E. Engeland

Heidelberg, Germany, 02nd-04th February 2016, selected abstract for **poster presentation**

10th International Meeting on Replicating Oncolytic Virus Therapeutics (**OVC**)

T. Speck, J. Heidbüchel, D. Jäger, C. von Kalle, G. Ungerechts, C. E. Engeland

Vancouver, BC, Canada, 01st-04th October 2016, selected abstract for **poster presentation**

22th Annual Meeting of the German Society for Gene Therapy (**DG-GT**)

T. Speck, J. Heidbüchel, D. Jäger, C. von Kalle, G. Ungerechts, C. E. Engeland

Heidelberg, Germany, 14th-16th September 2016, selected abstract for **poster presentation**

21th Annual Meeting of the German Society for Gene Therapy (**DG-GT**)

T. Speck, C. E. Engeland, D. Jäger, C. von Kalle, G. Ungerechts

Vienna, Austria, 26th-28th February 2015, selected abstract for **poster presentation**

Acknowledgements

When all is said and done, I would like to express my deep gratitude to all the people who supported me during the past four years:

First, I would like to express my very great appreciation to Prof. Dr. Dr. Guy Ungerechts for giving me the opportunity to join his lab and to work on this great PhD project. Although he was in Canada for three years during my PhD, he still managed to support my work through mailing, phone calls and skype sessions.
Especially, I am grateful for the support given by Dr. Dr. Christine E. Engeland. Christine helped to develop this project to the most ambitious extent with her excellent scientific supervision. Also, Christine's support in private regards deserves more than words could tell.
I wish to acknowledge my TAC members and thesis examiners Prof. Dr. Ralf Bartenschlager (first referee), Prof. Dr. Christof von Kalle (second referee), Prof. Dr. Michael Kirschfink, PD Dr. Karin Müller-Decker and apl. Prof. Dr. Martin Müller.
Special thanks are extended to my PhD and MD colleagues. In particular, I would like to thank Johannes Heidbüchel (Hanno) and Dr. Rūta Veinalde, who from time to time sacrificed day and night and weekend to support my work.
Furthermore, I wish to thank our technicians Jessica Albert (Jessi) and Birgit Hoyler. Both made huge contributions to this work. Loads of thanks also for enduring my pranks and humor for such a long time.
Moreover, I was very pleased to receive support from colleagues beyond our working group. First, I would like to thank Dr. Claudia Ball for sharing the TSCs. Thankfully, Nina Hofmann maintained and expanded the TSCs for this study. Furthermore, I would like to thank Prof. Dr. Stefan Eichmüller and Antonino Pane for sharing the murine CTLs.
I would like to offer special thanks to Deutsche Bahn. We had some difficulties from time to time, but at the bottom line, I managed to commute between Bretten and Heidelberg for four years to work on this study.
Last but not least, a loving note of thanks goes to my family and friends. They accompanied me through ups and downs, joys and desperations, tragedies and miracles. I wish to thank especially Jana Borger, who backed me up whenever it was necessary. Special thanks also go to my sister Isabel Speck, Martin Loos and Margarete Loos who provided me a haven for finishing this work.

Thesis Declaration

I hereby declare that I have written the submitted dissertation myself and in this process I have used no other sources or materials than those expressly indicated. I hereby declare that I have not applied to be examined at any other institution, nor have I used the dissertation in this or any other form at any other institution as an examination paper, nor submitted it to any other faculty as a dissertation.

Heidelberg, December 19th 2017 Tobias Speck